Role of cyclase-associated protein 2 in platelet function and description of an inherited macrothrombocytopenia

Rolle von cyclase-associated protein 2 in der Thrombozytenfunktion und Beschreibung einer erblich bedingten Makrothrombozytopenie

Doctoral thesis for a medical doctoral degree
at the Graduate School of Life Sciences,
Julius-Maximilians-Universität Würzburg,
Section Biomedicine

submitted by

Johannes Heck

from

Heilbronn

Würzburg, 2018

Submitted on:

……

Office stamp

Members of the *Promotionskomitee*:

Chairperson: Prof. Dr. Wolfgang Kastenmüller

Primary Supervisor: Prof. Dr. Bernhard Nieswandt

Supervisor (Second): Prof. Dr. Harald Schulze

Supervisor (Third): Prof. Dr. Carsten Hoffmann

Date of Public Defense:

9 May 2019

Date of Receipt of Certificates:

……

Table of contents

Table of figures

Table of abbreviations

A	Ampere
aa	Amino acid
ABC	ATP-binding cassette
ABP	Actin-binding protein
ADAM	A Disintegrin And Metalloproteinase
ADF	Actin-depolymerizing factor
ADF-H	ADF homology
ADP	Adenosine diphosphate
AIP1	Actin-interacting protein 1
APS	Ammonium persulfate
Arp	Actin-related protein
ATP	Adenosine triphosphate
AZ	Arizona
BEACH	Beige and Chediak–Higashi syndrome
BM	Bone marrow
bp	Base pair
BSA	Bovine serum albumin
BSS	Bernard–Soulier syndrome
c	Centi (10^{-2})
CA	California
cAMP	Cyclic adenosine monophosphate
CAMT	Congenital amegakaryocytic thrombocytopenia
CAP	Cyclase-associated protein
CARP	Cyclase-associated protein and X-linked retinitis pigmentosa 2 gene product
CD	Cluster of differentiation
Cdc42	Cell division cycle 42
CLEC-2	C-type lectin-like type II transmembrane receptor
CML	Chronic myeloid leukemia
CRP	Collagen-related peptide
d	Day
Da	Dalton
DAPI	4',6-diamidino-2-phenylindole
DCM	Dilated cardiomyopathy
DIC	Differential interference contrast
DNA	Deoxyribonucleic acid
dNTP	Deoxynucleotide triphosphate
DTS	Dense tubular system
ECL	Enhanced chemiluminescence
ECM	Extracellular matrix
EDTA	Ethylenediaminetetraacetic acid
e.g.	From Latin: *exempli gratia*, "for example"
EGTA	Ethylene glycol tetraacetic acid
ERK	Extracellular signal-regulated kinase

et al.	From Latin: *et alii*, "and others"
Fab	Fragment antigen-binding
FACS	Fluorescence-activated cell sorting
F-actin	Filamentous actin
FITC	Fluorescein isothiocyanate
Fc	Fragment crystallizable
FcRγ	Fc receptor-γ
FPD/AML	Familial platelet disorder with predisposition to acute myeloid leukemia
FRT	Flippase recognition target site
FSC	Forward scatter
g	Gram Acceleration of gravity (9.8 m/s²)
G-actin	Globular actin
GAPDH	Glyceraldehyde 3-phosphate dehydrogenase
GFI1B	Growth factor-independent 1B
GP	Glycoprotein Glykoprotein
GPCR	G protein-coupled receptor
GPS	Gray platelet syndrome
GSLS	Graduate School of Life Sciences
gt	Gene-trap
GT	Glanzmann thrombasthenia
GvHD	Graft-versus-host disease
h	Hour
Hb	Hemoglobin concentration
HCC	Hepatocellular carcinoma
HCT	Hematocrit
H&E	Hematoxylin and eosin
HEPES	4-(2-hydroxyethyl)-1-piperazineethanesulfonic acid
HFD	Helical folded domain
HIV	Human immunodeficiency virus
HLA	Human leukocyte antigen
HRP	Horseradish peroxidase
HSC	Hematopoietic stem cell
HSCT	Hematopoietic stem cell transplantation
5-HT	5-hydroxytryptamine/serotonin
i.e.	From Latin: *id est*, "that is to say"
IL	Interleukin
IMS	Invaginated membrane system
IMT	Inherited macrothrombocytopenia
IP	Immunoprecipitation
IT	Inherited thrombocytopenia
ITAM	Immunoreceptor tyrosine-based activation motif
JBS	Jacobsen syndrome
k	Kilo (10^3)
KO	Knockout

L	Litre
lacZ	β-galactosidase gene
LN	Lymph node
loxP	Locus of X-over P1
µ	Micro (10^{-6})
m	Meter
	Milli (10^{-3})
M	Molar (mol/L)
MA	Massachusetts
MAPK	Mitogen-activated protein kinase
MCV	Mean corpuscular volume
MD	Maryland
	Medical Doctor/medical doctoral
MFI	Mean fluorescence intensity
min	Minute
MK	Megakaryocyte
MMP	Matrix metalloprotease
MPV	Mean platelet volume
mRNA	Messenger RNA
MYH	Myosin heavy chain
MYH9-RD	Myosin heavy chain 9-related disease
NBEAL2	Neurobeachin-like protein 2
Neo	Neomycin phosphotransferase gene
NES	Nuclear export signal
NLS	Nuclear localization signal
NMMHC IIA	Nonmuscle myosin heavy chain IIA
NMMHC IIB	Nonmuscle myosin heavy chain IIB
NP-40	Nonidet P-40
NSAID	Non-steroidal antiinflammatory drug
OCS	Open canalicular system
OR	Oregon
orph	Orphan
pA	Polyadenylation site
PA	Pennsylvania
PAGE	Polyacrylamide gel electrophoresis
PBS	Phosphate-buffered saline
PCR	Polymerase chain reaction
PDGF	Platelet-derived growth factor
PDW	Platelet distribution width
PFA	Paraformaldehyde
PGI_2	Prostaglandin I_2/Prostacyclin
pH	Potentia Hydrogenii
PI3K	Phosphatidylinositide 3-kinase
PIP_2	Phosphatidylinositol 4,5-bisphosphate
PIPES	Piperazine-N,N'-bis(2-ethanesulfonic acid)
PKA	Protein kinase A
PKC	Protein kinase C

PMA	Phorbol 12-myristate 13-acetate
polyP	Polyphosphate
PP_i	Pyrophosphate
PRP	Platelet-rich plasma
PVDF	Polyvinylidene difluoride
RIPA	Ristocetin-induced platelet aggregation
RNA	Ribonucleic acid
p	P-value
PE	Phycoerythrin
®	Registered trademark
Rac1	RAS-related C3 botulinum substrate 1
RAS	Rat sarcoma
RBC	Red blood cell
rpm	Rotations per minute
RT	Room temperature
s	Second
SD	Standard deviation
SDS	Sodium dodecyl sulfate
SH3	Src homology 3
sog.	sogenannt
Src	Sarcoma
TCPT	Paris–Trousseau thrombocytopenia
TEM	Transmission electron microscopy
TEMED	Tetramethylethylenediamine
Thr	Thrombin
TGF	Transforming growth factor
TLR	Toll-like receptor
™	Trademark
THPO	Thrombopoietin
TRAP	Thrombin receptor-activating peptide
TRIS	Tris(hydroxymethyl)aminomethane
TXA_2	Thromboxane A_2
U	Unit
U46	U46619
UK	United Kingdom
USA	United States of America
UV	Ultra-violet
V	Volt
vs.	Versus
vWF	Von Willebrand factor
WAS	Wiskott–Aldrich syndrome
WASP	Wiskott–Aldrich syndrome protein
WAVE	WASP family verprolin-homologous protein
WBC	White blood cell
WH2	WASP homology 2
WIP	WASP-interacting protein

WT	Wild-type Wildtyp

1 Introduction

1.1 Megakaryocytes

Megakaryocytes (MKs) are large (30–100 µm), polyploid cells that primarily reside in the bone marrow (BM) of vertebrates,[1] but also in the yolk sac, liver, and spleen during fetal development.[2] Originally, MKs differentiate from hematopoietic stem cells (HSCs)[3] under the influence of a myriad of cytokines (e.g. interleukin-(IL-)1, IL-3, IL-6, IL-11, and c-kit ligand),[4] but predominantly thrombopoietin (THPO) which binds to the MK-specific receptor c-Mpl.[5] Engagement of THPO with c-Mpl leads to receptor dimerization and subsequent activation of various intracellular signaling cascades including the phosphatidylinositide 3-kinase (PI3K), Akt, MAPK, and ERK1/ERK2 pathways.[6] In the course of THPO-stimulated differentiation and maturation, MKs increase in size and repeatedly undergo deoxyribonucleic acid (DNA) replication without terminal cell division (so-called endomitosis), resulting in a DNA content of up to 128n in a single multilobulated nucleus. Polyploidy is thought to be required for large-scale thrombopoiesis, allowing MKs to generate huge quantities of messenger ribonucleic acid (mRNA) and protein that are packed into granules which are distributed to nascent platelets.[7] Additionally, MKs develop a highly tortuous invaginated membrane system (IMS) which serves as a membrane reservoir for the 2,000–5,000 platelets that can evolve from a single MK.[8]

1.2 Thrombopoiesis

Stegner *et al.* have recently shown that the majority of MKs is located in close proximity to sinusoidal BM vessels.[9] Upon contact with the subendothelial basement membrane of these sinusoids, MKs are thought to form podosomes, dot-like membrane evaginations with degradative capacity (**Fig. 1**).

Podosomes consist of an actin filament-rich core which is supported by the core proteins Arp2/3 complex, WASP (Wiskott–Aldrich syndrome protein), and cortactin, and which is surrounded by a ring structure containing integrins, vinculin, talin, paxillin, and myosin IIA.[10] Podosomes presumably allow MKs to adhere to and degrade the subendothelial basement membrane by secreted and/or membrane-resident matrix metalloproteases (MMPs).[11] However, their *in vivo* relevance is still under debate.[12] Penetration of the basement membrane is followed by the protrusion of long cytoplasmic extensions designated proplatelets into the lumen of BM sinusoids. Proplatelet extension is an essentially microtubule- and dynein-driven process.[13,14] Microtubules are polarized (containing a plus and a minus end) cytoskeletal polymers consisting of α- and β-tubulin heterodimers, while dynein is an adenosine triphosphate (ATP)-dependent minus-end molecular motor protein which enables microtubules to slide past each other.[14] Microtubule bundles running along the proplatelet shaft show a mixed polarity and serve as tracks for the transport of granules and organelles into nascent platelets. At the distal end of the shaft, the microtubules make a loop and re-enter the shaft, thereby forming a tennis racket-shaped structure from which larger fragments (termed preplatelets) are shed into the vessel lumen by shear forces within the bloodstream.[15] Whereas mature human platelets are 2–3 µm in diameter, preplatelets are 3–10 µm across. In the vasculature, preplatelets adopt a barbell shape that ultimately matures into separate platelets. Thus, final platelet maturation takes place in the circulation.[13]

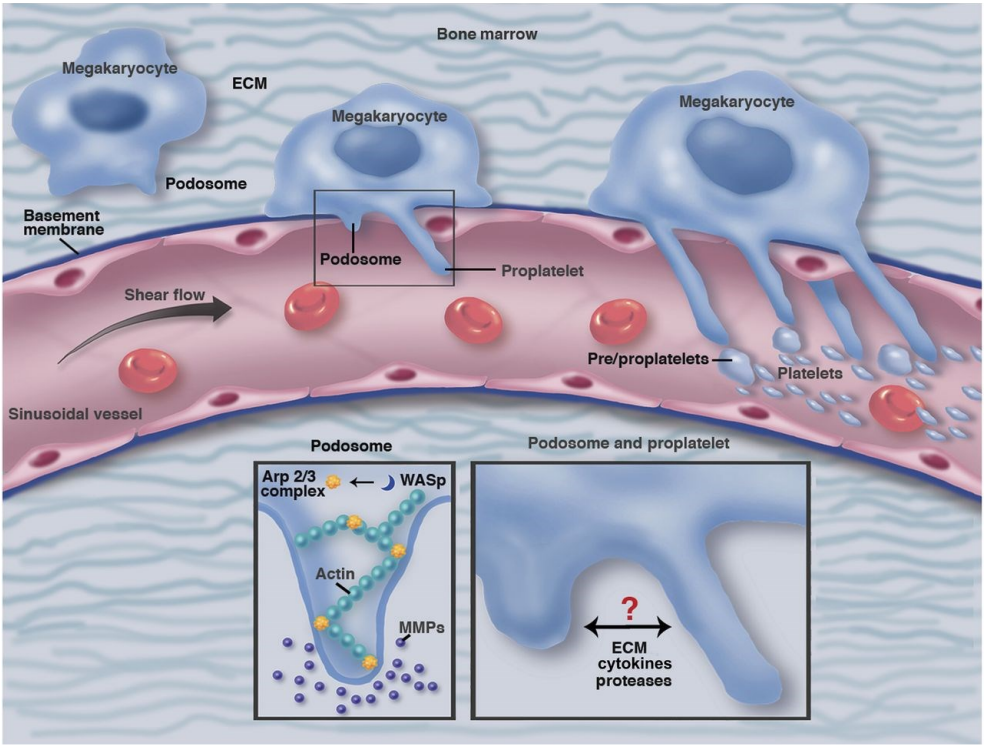

Fig. 1: Current model of platelet biogenesis

In the BM, MKs are predominantly located adjacent to the subendothelial basement membrane of sinusoids.[9] To surmount this barrier MKs are thought to form podosomes, dot-like matrix contacts with degradative capacity.[10] After penetration of the basement membrane, MKs extend long cytoplasmic protrusions termed proplatelets into the lumen of sinusoidal BM vessels. At the distal end of the proplatelet shaft, immature preplatelets are released into the circulation by shear forces within the bloodstream.[15] The reorganization of the actin cytoskeleton plays a pivotal role during both podosome and proplatelet formation. The precise molecular interplay between podosomes and proplatelets, however, needs yet to be elucidated. ECM, extracellular matrix; WASp, Wiskott–Aldrich syndrome protein; MMPs, matrix metalloproteases. (Image is reproduced with permission from French.[11])

1.3 Platelet morphology

Platelets are discoid, anucleate cell fragments whose main biologic function is the surveillance of vascular integrity. Besides, they play roles in diverse processes such as inflammation and immunity, angiogenesis, and cancer progression. In healthy human individuals, platelet counts range from 150 to

450 × 10^9 L^{-1}, and platelets have an average lifespan of 8–10 days.[1] Platelet counts in mice, by contrast, are four times those of humans (up to 1,000 × 10^9 L^{-1}), whereas platelet diameter and lifespan are halved as compared with their human counterparts (1–3 µm and 5 days, respectively).[16] Aged platelets are removed from the circulation by macrophages of the reticulo-endothelial system located in the spleen and liver.

Platelets feature a spectrin-based membrane skeleton, an actin-based cytoskeleton, various organelles (e.g. mitochondria, peroxisomes, and glycogen stores) as well as different types of granules.[1] α-granules are most abundant (50–80 per platelet) and are 200–500 nm in diameter, hence comprising ~10% of the total platelet volume. α-granules harbor both membrane-bound (e.g. integrins αIIbβ3, α6β1, GPVI, and P-selectin) and hundreds of soluble proteins such as von Willebrand factor (vWF), fibrinogen, fibronectin, the coagulation factors V and VIII as well as platelet-derived growth factor (PDGF) and transforming growth factor (TGF)-β. Additionally, α-granules provide an appreciable membrane reservoir for platelet spreading.[17,18]

Dense or δ-granules are smaller (~150 nm) and less abundant (3–8 per platelet).[19] They embody membrane transporters, Ca^{2+} ions, adenosine diphosphate (ADP) and ATP, serotonin/5-hydroxytryptamine (5-HT), pyrophosphate (PP_i), and inorganic polyphosphates (polyP).[15,20]

Lysosomes are sparse (0–3 per platelet) with an intermediate size between α- and δ-granules (200–250 nm).[21] They have an acidic intraluminal pH and store hydrolytic enzymes involved in carbohydrate, protein and lipid degradation.[15,19]

Recently, a fourth granule type has been identified, the T granule. T granules contain the eponymous toll-like receptor (TLR) 9 as well as the protein disulfid isomerase.[22]

In addition to their delimited cell membrane, platelets possess two specialized membrane compartments, the dense tubular system (DTS) and the open canalicular system (OCS). The DTS is a closed-tunnel network derived from the endoplasmic reticulum which — among other functions — acts as a Ca^{2+} store. The OCS, on the other hand, is an elaborate system of plasma membrane invaginations retaining contact to the extracellular environment.[1] Together with α-granules which may fuse with the cell membrane upon platelet stimulation, the OCS serves as a membrane reservoir capable of increasing the platelet surface area by 2–4-fold during spreading.[17]

1.4 Hemostasis

The regulation of hemostasis at sites of vascular injury is the primary task of platelets. Damage of the vessel wall exposes the subendothelial ECM which mainly consists of adhesive macromolecules such as collagens, laminin, fibronectin, and vWF to circulating platelets in the bloodstream.[23] Under conditions of high shear forces prevailing in small arteries and arterioles, the initial tethering of platelets to the ECM is controlled by the interaction between platelet receptor glycoprotein (GP)Ibα, the major functional subunit of the GPIb–IX–V complex, and vWF which is immobilized on exposed collagen I fibrils[24] (**Fig. 2**). The GPIbα–vWF interaction, however, has a rapid dissociation rate and therefore does not allow firm adhesion of platelets to the underlying substrate. It rather acts as a molecular brake, decelerating platelets and enabling their translocation on the ECM in a "stop-and-go" manner, a process known as "rolling".

"Rolling" platelets can bind to collagen directly via their immunoglobulin superfamily receptor GPVI. Ligation of GPVI — though unable to mediate firm platelet adhesion — triggers an intracellular phosphorylation cascade starting from the immunoreceptor tyrosine-based activation motif (ITAM) of

GPVI's signal transducing subunit, the Fc (fragment crystallizable) receptor-γ (FcRγ) chain, and results in a sharp elevation of the cytosolic Ca^{2+} concentration.[25] Thus, the GPVI–ITAM signaling cascade is able to induce the reorganization of the actin and tubulin cytoskeleton followed by a transition of platelets from discoid to spheric shape, the shift of platelet integrins — most notably integrins α2β1 and αIIbβ3 — from a low- to a high-affinity state ("inside-out" signaling)[23] as well as the release of the secondary mediators ADP, thromboxane A_2 (TXA_2), 5-HT, and epinephrine/adrenaline. In conjunction with locally produced thrombin, these soluble agonists bind to the G protein-coupled receptors (GPCRs) PAR1/4 (thrombin), $P2Y_1$ and $P2Y_{12}$ (ADP), TPα/β (TXA_2), $5\text{-}HT_{2A}$ (5-HT), and α_{2A} (epinephrine). GPCR signaling in platelets involves the heterotrimeric G proteins G_q, $G_{12/13}$, and $G_{i/z}$ whose synergistic interplay results in full platelet activation.[26] Firm platelet adhesion is eventually achieved by binding of high-affinity β1 integrins (α2β1, α5β1, and α6β1) to their respective adhesive ECM ligands (collagen, fibronectin, and laminin), followed by "outside-in" signaling cascades which further sustain platelet activation.[23]

Additional platelets are recruited into the nascent thrombus by two molecular mechanisms: initial interplatelet contacts are established through cross-bridging of vWF by GPIbα and αIIbβ3 of two neighboring platelets, while stable platelet aggregates are formed by binding of αIIbβ3 integrins to fibrinogen.[16] Moreover, the thrombus is proposed to be stabilized through the hemITAM-coupled C-type lectin-like receptor 2 (CLEC-2) and a so far unknown intravascular ligand.[27]

The development of a platelet plug at the site of vascular injury is termed primary hemostasis. Under physiologic circumstances, primary hemostasis is accompanied by the activation of the coagulation cascade, a well-orches-

trated sequence of multitudinous clotting factors culminating in the conversion of soluble fibrinogen molecules into insoluble fibrin strands via the serine protease thrombin. The newly formed fibrin strands permeate the platelet plug and entrap red blood cells in the growing thrombus (secondary hemostasis). The resulting blood clot — consisting of platelets, fibrin, and red blood cells — finally seals the vessel leak, and further blood loss is prevented.[28]

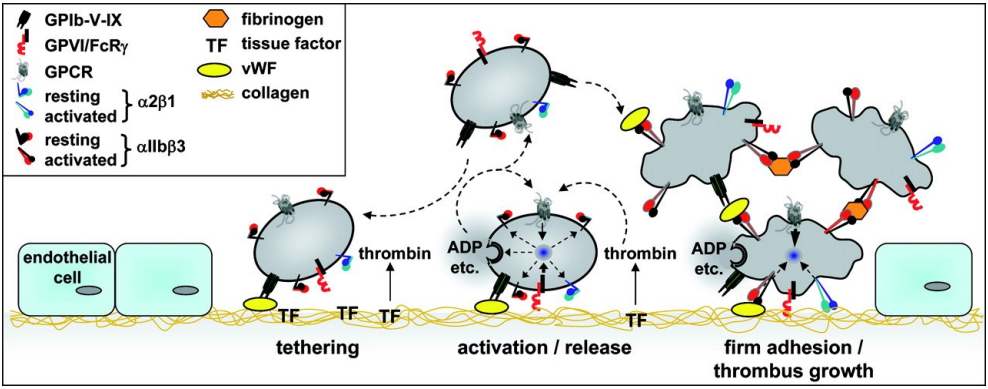

Fig. 2: The role of platelets in hemostasis

The formation of a hemostatic plug by platelets upon vascular injury can be divided into three major stages: initial tethering to the exposed subendothelial ECM, full activation accompanied by granule release, and firm adhesion/thrombus growth. Tethering to and "rolling" on the ECM are mediated by GPIbα–vWF interactions, while full platelet activation is achieved via GPVI signaling upon ligation of collagen. This triggers platelet shape change, the transition of integrins to a high-affinity state, and the release of secondary mediators (ADP etc.). Thrombin is generated locally by tissue factor (TF) and contributes to sustained platelet activation. While firm adhesion of platelets to the ECM is enabled by high-affinity integrins (mainly α2β1 and αIIbβ3), thrombus growth is established through cross-bridging of vWF and fibrinogen molecules by neighboring platelets. (Image is reproduced with permission from Varga-Szabo *et al.*.[23])

1.5 The actin cytoskeleton

Both human and animal cells feature a sophisticated and highly specialized cytoskeleton that consists of three polymeric proteins: microtubules that separate chromosomes during mitosis and that serve as tracks for long-

range intracellular transport of large particles; intermediate filaments which can be considered as intracellular ligaments or tendons exerting resistance to mechanical forces; and actin filaments that play a key role in a myriad of biological functions, e.g. in cytokinesis, locomotion, endo- and exocytosis, the formation of cellular protrusions, and which serve as tracks for short-range movement of intracellular cargo in cooperation with myosin motor proteins.[29]

Actin and myosin were discovered in the 1940s in muscle tissue and belong to the evolutionarily best conserved proteins. The molecular origin of actin for instance dates back ~3 billion years when a common ancestor of today's species featured an archaic actin-encoding gene among its ~400 genes.[30] In humans, there are six functional actin genes which encode three actin isoforms: α-, β-, and γ-actin. In platelets, β- and γ-actin are present and their combined cellular concentration (500 µM) makes up 15–20% of the total platelet protein.[25] Besides, platelets possess myosin II ("conventional myosin") which comprises two light chains and one heavy chain. Myosin II's heavy chain hydrolyzes ATP and interacts with actin, hence providing the force necessary for contractile events in the course of platelet activation.[31]

Actin exists in two distinct forms: monomeric globular (G-)actin and polymeric filamentous (F-)actin (**Fig. 3 B**). The latter is an extended bipolar double helix with a barbed (plus) end where polymerization of actin monomers takes place, and a pointed (minus) end where depolymerization mainly occurs. In order to maintain its tertiary conformation, G-actin must keep either ADP or ATP in its adenine nucleotide pocket. ATP-bound G-actin has a 10-fold higher affinity for polymerization into actin filaments at the barbed end than ADP–G-actin. Upon incorporation of ATP–G-actin bricks into F-actin and as the filament ages, ATP is gradually hydrolyzed, leading from an intermediate

ADP–P_i-bound actin form to ADP–G-actin. ADP–G-actin eventually depolymerizes from the pointed end, is "recharged" with fresh ATP, a process facilitated by adenine nucleotide exchange factors, and thus becomes ready for another round of polymerization at the barbed end. This permanent actin turnover — assembly at the barbed end and disassembly at the pointed end — is called "treadmilling".[25,29]

1.6 Actin-binding proteins

Eukaryotic cells take advantage of more than 100 accessory proteins to interact with actin.[29] These so-called actin-binding proteins can be divided into two categories depending on their affinity to either G- or F-actin.

F-actin-binding proteins are much more numerous than G-actin-binding proteins. They restrict the length of actin filaments by shielding the barbed end from further polymerization (capping proteins) or by cleaving actin filaments into smaller fragments (severing proteins). Furthermore, they are able to cross-link actin filaments into bundles or networks.

G-actin-binding proteins, on the other hand, maintain a large cellular pool of monomeric actin (sequestering proteins), promote the exchange from ADP to ATP on G-actin (adenine nucleotide exchange factors), and enhance polymerization or depolymerization of actin filaments.[32] They interact with G-actin through three different protein motifs: via the profilin, the ADF-H (actin-depolymerizing factor homology), or the WH2 (Wiskott–Aldrich syndrome protein homology 2) domain. In the course of evolution, six conserved actin monomer-binding protein families have evolved: profilin, twinfilin, ADF/cofilin, WASP/WAVE (WASP family verprolin-homologous protein), verprolin/WIP (WASP-interacting protein), and Srv2/CAP (cyclase-associated protein).[33]

1.7 Cyclase-associated proteins

In 1990, cyclase-associated protein was discovered in budding yeast (*Saccharomyces cerevisiae*) as a component of the adenylyl cyclase complex[34] — an enzyme catalyzing the production of cyclic adenosine monophosphate (cAMP) — and also as a suppressor of hyperactive RAS2 (RAS^{Val19}),[35] which explains its yeast name Srv2. It is important to mention that CAP and Srv2 are identical and commonly referred to as Srv2/CAP.

CAP consists of ~450–550 amino acid (aa) residues[36] and is a predominantly hydrophilic protein composed of α-helices and a small region rich in β-sheets close to its carboxyl-(C-)terminus.[32] The protein structure of CAP is evolutionarily highly conserved from yeast to mammals and contains three domains (**Fig. 3 A**): the amino-(N-)terminal domain is comprised of a coiled coil region enabling association with adenylyl cyclase in yeast and a helical folded domain (HFD) that promotes severing of F-actin. The N-domain is followed by a proline-rich stretch which separates it from the C-domain and allows binding of SH3 (Src homology 3) domain-containing proteins such as profilin, the cytoplasmic tyrosine kinase Abl, and the F-actin-binding protein ABP1 (actin-binding protein 1). The proline-rich stretch can be further divided into regions P1 (highly conserved) and P2 (less well-conserved). The WH2 domain, located between P1 and P2, is responsible for sequestration of G-actin, nucleotide exchange on actin monomers, and severing of actin filaments. The C-domain consists of an extraordinary β-helical structure whose core unit is designated CARP (cyclase-associated protein and X-linked retinitis pigmentosa 2 gene product) domain, and a dimerization motif. The CARP domain allows binding to actin monomers independently of the WH2 domain and promotes nucleotide exchange on G-actin.

The dimerization motif — together with the N-terminal coiled coil region and the HFD — is implicated in self-association of CAP.[36] CAPs have the potential to form dimers, trimers,[37] and even hexamers resembling a *shuriken*, the traditional throwing star of Japanese *Ninja*.[38] CAP is able to bind to G-actin in both monomeric and oligomeric form.

CAP has three main actin-regulatory functions (**Fig. 3 B**): first, it sequesters G-actin and thus prevents actin polymerization. Second, it severs ADF/cofilin-bound actin filaments into smaller pieces in a similar manner to AIP1 (actin-interacting protein 1), hence generating new barbed ends. Third, CAP's probably most important function might be its adenine nucleotide exchange activity. CAP promotes the exchange from ADP to ATP on G-actin in a similar fashion to profilin and antagonistically to ADF/cofilin and twinfilin (which suppress adenine nucleotide exchange).[36] In plants, CAP even is the only known nucleotide exchanger for G-actin since plant profilin lacks this activity.[39]

CAP's cellular concentration has not yet been determined and little is known about its regulation. Abl and the PDGF signaling pathway have been suggested to activate CAP. Phosphatidylinositol 4,5-bisphosphate (PIP_2), on the other hand, is a negative regulator since it induces the release of G-actin from CAP and consequently promotes F-actin assembly. This finding is in agreement with PIP_2's activatory function on WASP which eventually leads to actin nucleation by the Arp2/3 complex. PIP_2 may also regulate the interaction between CAP's N- and C-termini which interact with each other as well as with themselves, thus forming antiparallel or parallel CAP dimers, respectively.[32] Oligomerization of CAP enhances both its G-actin-binding and its F-actin-severing activity.[36] In *Saccharomyces cerevisiae*, ABP1 binds to the poly-proline domain of Srv2/CAP, thus localizing it to cortical actin patches.[32]

Protists, fungi, and many invertebrates only have a single CAP gene, whereas plants such as *Oryza sativa* (rice) possess up to four CAP isoforms. Vertebrates have two CAP isoforms, CAP1 and CAP2, which share ~60% identity in their aa sequences.[36] Mouse CAP1 can be phosphorylated[36] and is intracellularly degraded by a matrix metalloproteinase.[40] CAP's actin-binding motifs are highly homologous in all species investigated so far, suggesting evolutionarily well-conserved actin-regulatory functions of CAP homologs. Even though the N-domain does contain a homologous leucine-rich stretch called RLE (arginine–leucine–glutamate) motif or "CAP signature" allowing interaction with adenylyl cyclase in yeast, it has functionally diverged during evolution and does not feature this activity in higher eukaryotes anymore. Nevertheless, the RLE motif might be critical for CAP function in all organisms; therefore, CAP is regarded as a bifunctional protein linking cell signaling processes (via its N-domain) to cytoskeletal reorganization (through its C-domain).[32]

CAPs play a pivotal role in a plethora of actin-dependent cellular processes such as endocytosis, vesicle trafficking, the establishment of cell polarity, cytokinesis, locomotion, plant and animal development, sarcomere organization in striated muscle tissue, neuronal growth, and cancer progression.[33,36]

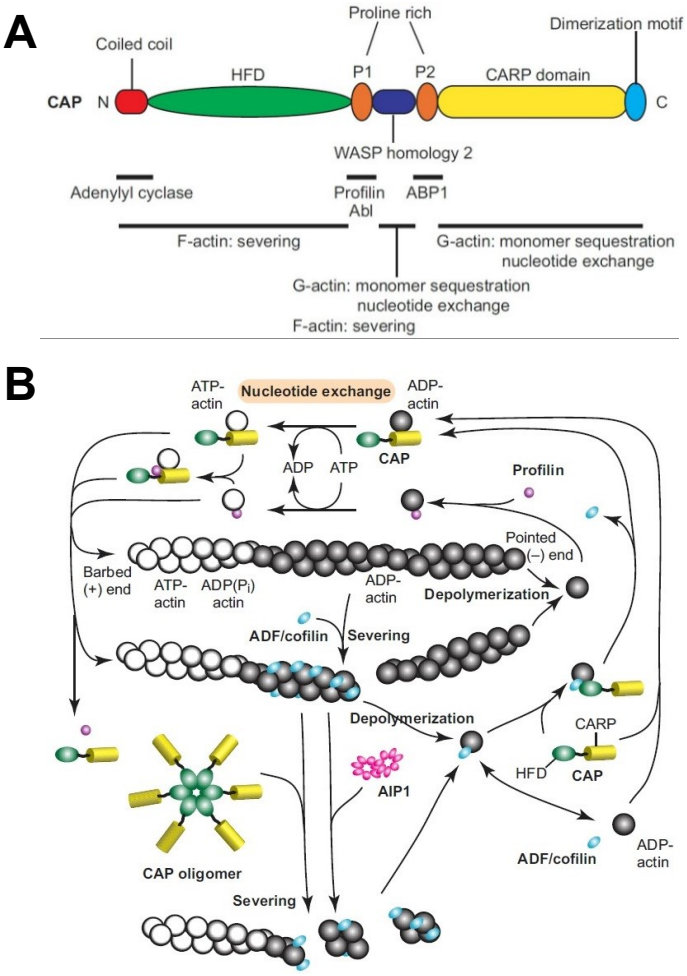

Fig. 3: Structure and actin-regulatory functions of cyclase-associated protein

CAP consists of an N-terminal coiled coil region and a helical folded domain (HFD), a centrally located proline-rich stretch (whose P1 and P2 motifs surround a Wiskott–Aldrich syndrome protein homology 2 (WH2) domain), and a C-terminal cyclase-associated protein and X-linked retinitis pigmentosa 2 gene product (CARP) domain followed by a dimerization motif. The actin-regulatory functions and binding partners of CAP are denoted below the respective domains/motifs to which they belong **(A)**. CAP promotes nucleotide exchange on G-actin and severs ADF/cofilin-bound F-actin, thus exerting functions related to that of profilin and actin-interacting protein 1 (AIP1), respectively. Besides, CAP competes with ADF/cofilin for binding to monomeric actin (G-actin-sequestering function).[36] CAP oligomers have been suggested to resemble hexameric *shurikens*, a throwing weapon of Japanese *Ninja*[38] **(B)**. (Image is adapted with permission from Ono.[36])

1.8 Cyclase-associated protein 2

Vertebrates possess two CAP isoforms, CAP1 and CAP2, which share 62% identity and 76% similarity on the aa level in mice. Both CAP isoforms from several mammalian species including *Homo sapiens*, *Mus musculus*, and *Rattus norvegicus* are 93–96% (CAP1) and 88–93% (CAP2) identical among each other.[41] While mouse and human CAP1 consist of 474 and 475 aa residues, respectively, CAP2 from both species comprises 476 aa residues.[32] CAP1 is expressed ubiquitously in mice (except for skeletal muscle), whereas CAP2 expression is limited to brain, heart, skeletal muscle, skin, and testis. These are tissues with no or reduced CAP1 expression, suggesting a complementary distribution pattern of both isoforms.[41]

The subcellular distribution of CAP1 and CAP2 differs, too. In PAM212 cells, a mouse keratinocyte cell line co-expressing both CAP isoforms, CAP1 is present in the cytosol where it localizes to dynamic regions of the cortical actin cytoskeleton such as lamellipodia. CAP2, on the other hand, is predominantly found in the nucleus, its presence in the cytosol rather being weak and diffuse. CAP2 is also present in the nucleus of undifferentiated myoblasts but it leaves this cellular compartment upon differentiation into myotubes. In the latter, CAP2 is enriched at the M-line of sarcomeres, the basic contractile units of striated muscle cells.[41] CAP2 has been proposed as a conserved regulator of striated muscle development because its knockdown in zebrafish (*Danio rerio*) and mice leads to a short-body phenotype with pericardial edema[42] and dilated cardiomyopathy (DCM), respectively. DCM in CAP2-deficient mice affects all four chambers of the heart and is accompanied by a pronounced reduction in basal heart rate, prolongations in atrioventricular (PQ) and intraventricular (QRS and QT) conduction times, the development of cardiac fibrosis with increased apoptosis, and disarrayed sarcomeres in both cardiac and skeletal muscle cells.

Affected sarcomeres are shorter and lack the characteristic A-band, the zone of overlapping actin and myosin molecules. Moreover, the overall number of myofibrils drops off dramatically and aggregate formation of desmin and troponin-I can be observed.

Additionally, CAP2-null mice display a decrease in body weight of ~40% and a reduced survival rate: 13% of female and 60% of male mice have died 70 days after birth — mainly because of sudden cardiac death — compared to only 1% deceased wild-type (WT) littermates. Yet, mutant mice do not die during embryogenesis and do not exhibit upregulation of CAP1 which has proapoptotic properties.[37,43] Together, these findings suggest that CAP2 deficiency manifests shortly after birth.

In human skin, CAP2 is expressed in keratinocytes of the living layers of the epidermis — *stratum basale* and *stratum spinosum* — and it is present in the nucleus and at cell–cell borders in these cells. Upon skin injury, by contrast, CAP2 is upregulated and shifts from the nucleus to the cytosol.[44] It is currently unknown how exactly CAP2 enters or leaves the nucleus since it neither harbors a nuclear localization signal (NLS) nor a nuclear export signal (NES).[41]

CAP2 is also upregulated in various human cancers such as bladder (transitional cell carcinoma level III), colon (adenocarcinoma well-differentiated), thyroid (adenocarcinoma), kidney (clear cell carcinoma), brain[41] and liver cancer. Liver cancer/hepatocellular carcinoma (HCC) displays a multistage process of tumor progession, a pathologic process in which the accumulation of mutations leads to dedifferentiation and increased aggressiveness of tumor cells. CAP2 presumably contributes to multistage hepatocarcinogenesis because its cellular concentration increases in parallel to cancer development: CAP2 levels are low in noncancerous liver tissue, elevated in the early, and highest in the progressed component of nodule-in-nodule type

HCCs.[45] Although the precise pathomechanism remains unknown, CAP2 up-regulation is associated with tumor size, portal vein invasion and intrahepatic metastasis in HCC.[42]

Similar to CAPs from nonmammalian species, mammalian CAP2 consists of an N- and a C-terminal domain which are separated by a proline-rich stretch. The function of the N-terminal domain has not yet been elucidated, the proline-rich stretch has been proposed to allow binding of SH3 domain-containing proteins, and the C-terminal domain is responsible for the actin-regulatory functions of CAP2. Regulation of actin dynamics by CAP2 is mainly mediated through its WH2 domain which is part of the C-terminal domain. The WH2 domain consists of ~25 aa residues and contains an N-terminal helix as well as a conserved LRHV (leucine–arginine–histidine–valine) motif.[46] It is intrinsically disordered, adopting an α-helical shape only upon binding to actin.[47] The WH2 domain sequesters G-actin, thus removing it from the G-/F-actin equilibrium and preventing actin polymerization. Furthermore, the WH2 domain is able to cut actin filaments into smaller fragments (F-actin-severing function). In contrast to CAP1, CAP2 can also sever F-actin in the absence of ADF/cofilin and at a neutral pH.[37] In addition to the WH2 motif, the C-terminal domain of murine CAP2 features two CARP domains in tandem repeats (aa residues 358–395 and 396–433). Although the CARP domain has been demonstrated to bind to G-actin independently of the WH2 motif, its *in vivo* relevance for mammalian CAP2 remains elusive so far.[36]

CAP2 is encoded by the *Cap2*/*CAP2* gene which is located on chromosomes 13 and 6 in mice and humans, respectively. The human gene codes for at least six different proteins. Whereas fourteen intron–exon boundaries are canonical, three are reported to be "fuzzy", resulting in a variable use of four exons. CAP2 transcripts are further diversified by virtue of 3' truncations,

variable promoter usage, and alternative splicing. All these transcriptional modifications ultimately yield a unique biological versatility of CAP2 proteins in mammals.[48,49]

1.9 The role of actin-binding proteins in resting and activated platelets

Platelets embody a large cellular pool of G-actin as well as two F-actin compartments. Resting platelets harbor 300–350 µM of monomeric actin accounting for up to 70% of total actin and exceeding the critical concentration for barbed-end polymerization (the concentration at which G-actin molecules start to assemble into F-actin) by ~1,500-fold.[25,50] To maintain such plentiful G-actin resources and to prevent random actin polymerization in the absence of adequate platelet stimuli, a large array of G-actin-sequestering proteins is required. The vast majority of monomeric actin in platelets is bound to thymosin β4 via formation of a nonpolymerizable 1:1 complex, but profilin1 and ASP-56 also contribute to actin sequestration. ASP-56 was isolated in 1992 from pig platelets and sequence analyses have later shown that it is identical to porcine CAP1.[36,51]

The first of the two F-actin compartments in platelets consists of ~2,000 long actin filaments which radiate from the platelet center to its periphery, resembling the spokes of a wheel. These actin filaments with an average length of ~1.1 µm are bundled by vasoactive-stimulated phosphoprotein (VASP), protecting them from degradation. Additionally, the filaments are cross-linked by α-actinin, tropomyosin, and caldesmon. 95% of cytoplasmic actin filaments are capped by CapZ (the most important capping protein in platelets), gCAP39, gelsolin, and flightless 1. Of note, CapZ and gCAP39 do not belong to the family of cyclase-associated proteins, although their names might

suggest otherwise. Capping of F-actin prevents barbed-end elongation under resting conditions.[25]

The second F-actin compartment constitutes a submembranous lattice of short actin filaments designated membrane skeleton which coats the platelet plasma membrane, thus providing contour, stability, and the proper distribution of surface receptors. The membrane skeleton is rich in spectrin, filamin A, and dystrophin-related protein (DRP) which cross-link the short actin filaments. Moreover, the membrane skeleton contains talin, moesin, protein 4.1, and skelemin. All these cytoskeletal proteins link membrane GPs to the underlying actin filament network.[31] In this respect, the axes GPIbα–filamin A–F-actin and αIIbβ3–talin–F-actin deserve particular attention as they are critical for proper platelet sizing.[52]

Resting platelets circulate in the bloodstream as non-adhesive "disks". Upon activation by exposed subendothelial ECM proteins or by soluble agonists in the course of vascular injury, however, platelets undergo a tremendous shape change and greatly increase their propensity to aggregate. Platelet shape change is accompanied by an extensive remodeling of the actin cytoskeleton and can be divided into four activation stages: (i) rounding, (ii) filopodia projection, (iii) lamellipodia extension, and (iv) formation of adhesion plaques/full spreading (see also **3.2.8.1**).

Immediately after stimulation, the platelet becomes spherical. Ca^{2+} enters the cell and activates gelsolin, an F-actin-severing protein which cuts the long cytoplasmic as well as the short submembranous actin filaments into smaller fragments. Myosin II pulls the severed actin filaments into the platelet center where a contractile actin–myosin ring structure forms. This contractile ring accumulates the platelet granules into a dome of central cytoplasm termed hyalomere. Here, degranulation of α- and δ-granules into the OCS occurs, followed by the release of procoagulant proteins and soluble agonists into

the extracellular space. Furthermore, the Ca^{2+}-activated protease calpain digests spectrin, filamin A as well as numerous other membrane skeletal proteins so that the plasma membrane loses its rigidity and becomes much more easily malleable.[25]

The second activation stage is characterized by a burst of filopodia from the platelet surface, long digitate membrane evaginations that dynamically extend and retract, and ultimately lead to a spiny morphology of the platelet. Filopodia projection involves new rounds of actin polymerization triggered by the Arp2/3 complex.[53] The Arp2/3 complex is composed of Arp2, Arp3, and five other proteins (ARC1–5).[54] It induces actin nucleation at the pointed end and binds to the barbed end where it acts as a Y adaptor, allowing actin polymerization from both arms of the Y. Besides, the Arp2/3 complex attaches laterally to existing filaments, evoking branched actin assembly at an angle of ~70°.[55] Profilin1 and ADF/cofilin promote rapid actin reorganization by replenishing G-actin with ATP and by accelerating actin monomer loss from the pointed end, respectively. CapZ, by contrast, releases barbed ends in a process called uncapping, thus determining hotspots for barbed-end elongation.[25] In activated platelets, the G-/F-actin ratio is turned upside down, with F-actin now accounting for 70% of total actin.[56] VASP and other cross-linking proteins associate with the newly formed filaments and distribute them into the nascent filopodia.

Third, lamellipodia arise from the plasma membrane between two discrete filopodia or directly from the sides of filopodia. Lamellipodia extend as sheets of short actin filaments nucleated by kaptin and the Arp2/3 complex. Forward movement of lamellipodia is much slower than filopodia extension, but — in contrast to filopodia — lamellipodia rarely retract.

Fourth, and finally, platelets proceed towards full spreading. They establish firm contacts with the underlying substate (so-called adhesion plaques)

which are characterized by the presence of the cytoskeletal attachment proteins VASP, zyxin, vinculin, talin, and α-actinin.[25] α-actinin stabilizes filamentous actin in adhesion plaques, connects the cytoplasmic tail of surface receptors to F-actin,[57] and serves as a scaffolding protein for signaling molecules, allowing them to transmit signals regarding cell attachment to the interior of the platelet.[25]

1.10 Thrombocytopenia

The human body produces 10^{11} platelets per day to maintain the integrity of the vascular system.[58] Thrombopoiesis is an elaborate and finely tuned process, perturbations of which can cause lower-than-average platelet counts that may become clinically relevant. Thrombocytopenia is defined as a peripheral platelet count below 150×10^9 L^{-1}. Affected individuals may suffer from easy bruising, petechiae (pinhead-sized bleedings into skin and mucosae), epistaxis (nosebleed), bleeding gums, or hypermenorrhea (excessive blood loss during menstruation). A drop of platelet counts below 10 to 20×10^9 L^{-1} poses a high risk for spontaneous, potentially life-threatening bleeding, and should therefore prompt emergency treatment.

Thrombocytopenias can be classified into acquired and inherited forms. Acquired causes for low platelet counts are myriad and include such diverse conditions as vitamin B_{12} or folic acid deficiency, chemotherapy, dengue fever, human immunodeficiency virus (HIV) infection, and surgery.[15,59]

Inherited thrombocytopenias (ITs) can be further divided into three subgroups according to the size of platelets encountered in peripheral blood. First, in microthrombocytopenias platelets are smaller than usual. A well-known example is Wiskott–Aldrich syndrome (WAS), an X-linked recessive hereditary disease characterized by a triad of few and small platelets, immune deficiency, and eczema.[60] Second, the arguably best understood IT

with normal-sized platelets is congenital amegakaryocytic thrombocytopenia (CAMT), an autosomal recessive condition evoked by mutations in *MPL*, the gene encoding the THPO receptor c-Mpl. Affected individuals have no or only small numbers of BM MKs, and develop a lethal BM aplasia within the first years of life.[61] Third, macrothrombocytopenias encompass a multitude of clinically variegated diseases with large or even giant platelets.

1.11 Inherited macrothrombocytopenias

Inherited macrothrombocytopenias (IMTs) constitute a heterogeneous group of genetic hematologic disorders which share three common hallmarks: large/giant platelets, a low platelet count from birth, and bleeding tendencies of variable severity. IMTs can be divided into conditions affecting the platelet cytoskeleton (e.g. myosin heavy chain 9-related diseases), platelet surface receptors (e.g. Bernard–Soulier syndrome), the formation of platelet granules (e.g. gray platelet syndrome), and transcription factors of the hematopoietic system (e.g. Paris–Trousseau thrombocytopenia; reviewed in [62]). However, in approximately half of the IMT cases the precise molecular origin remains unknown.[58,63]

2 Aim of the study

The aim of this study is to elucidate the role of CAP2 in murine platelet function. Furthermore, a new form of inherited macrothrombocytopenia in mice is characterized.

3 Materials and methods

3.1 Materials

3.1.1 Chemicals and reagents

Chemical/reagent	Company
Acetic acid	Roth (Karlsruhe, Germany)
ADP	Sigma-Aldrich (Steinheim, Germany)
Agarose	Roth (Karlsruhe, Germany), BioFroxx (Pfungstadt, Germany)
Alexa Fluor® 488	Molecular Probes (Eugene, OR, USA)
Amersham Hyperfilm™ ECL	GE Healthcare (Little Chalfont, UK)
Ammonium persulfate (APS)	Roth (Karlsruhe, Germany)
Apyrase (grade III)	Sigma-Aldrich (Steinheim, Germany)
β-mercaptoethanol	Roth (Karlsruhe, Germany)
Botrocetin	Pentapharm (Basel, Switzerland)
Bovine serum albumin (BSA)	AppliChem (Darmstadt, Germany)
Bromophenol blue (3',3",5',5"-tetra-bromophenolsulfonphthalein)	AppliChem (Darmstadt, Germany)
Cacodylate buffer, 50 mM (pH 7.2)	AppliChem (Darmstadt, Germany)
Calcium chloride ($CaCl_2$)	Roth (Karlsruhe, Germany)
Cryo-Gel®	(Leica Biosystems, Nussloch, Germany)
Cy3	Jackson ImmunoResearch (West Grove, PA, USA)
4',6-Diamidino-2-phenylindole (DAPI)	Invitrogen (Karlsruhe, Germany)
Disodium hydrogen phosphate	Roth (Karlsruhe, Germany)
DreamTaq Green PCR MasterMix (2x)	Life Technologies (Carlsbad, CA, USA)
Dry milk, fat-free	Roth (Karlsruhe, Germany)

Chemical/reagent	Company
Deoxynucleotide triphosphates (dNTP) mix	Fermentas (St. Leon-Rot, Germany)
EMbed 812	Electron Microscopy Sciences (Hatfield, PA, USA)
Ethylenediaminetetraacetic acid (EDTA)	AppliChem (Darmstadt, Germany)
Ethylene glycol tetraacetic acid (EGTA)	Sigma-Aldrich (Steinheim, Germany)
Eukitt® quick-hardening mounting medium	Sigma-Aldrich (Steinheim, Germany)
Eosin	Roth (Karlsruhe, Germany)
Ethanol	Roth (Karlsruhe, Germany)
Fluorescein isothiocyanate (FITC)	Molecular Probes (Eugene, OR, USA)
Fluoroshield™	Sigma-Aldrich (Steinheim, Germany)
GeneRuler Mix	Fermentas (St. Leon-Rot, Germany)
Giemsa stock solution	Roth (Karlsruhe, Germany)
Glucose	Roth (Karlsruhe, Germany)
Glutaraldehyde	Merck (Darmstadt, Germany), Electron Microscopy Sciences (Hatfield, PA, USA)
Glycerine	Roth (Karlsruhe, Germany)
Glycine	AppliChem (Darmstadt, Germany)
Hematoxylin	Sigma-Aldrich (Steinheim, Germany)
Heparin sodium	Ratiopharm (Ulm, Germany)
Human fibrinogen	Sigma-Aldrich (Steinheim, Germany)
Hydrogen chloride (HCl)	Roth (Karlsruhe, Germany)
4-(2-Hydroxyethyl)-1-piperazine-ethanesulfonic acid (HEPES)	Roth (Karlsruhe, Germany)
IGEPAL® CA-630	Sigma-Aldrich (Steinheim, Germany)
Integrilin® (eptifibatide)	Millennium Pharmaceuticals (Cambridge, MA, USA)
Isofluran CP®	cp-pharma (Burgdorf, Germany)

Chemical/reagent	Company
Isopropanol	Roth (Karlsruhe, Germany)
Lead citrate	Electron Microscopy Sciences (Hatfield, PA, USA)
Loading dye solution, 6x	Fermentas (St. Leon-Rot, Germany)
Magnesium chloride ($MgCl_2$)	Roth (Karlsruhe, Germany)
May–Grünwald's solution	Roth (Karlsruhe, Germany)
Methanol	Roth (Karlsruhe, Germany)
Midori Green Advanced DNA Stain	Nippon Genetics Europe (Düren, Germany)
Nonidet P-40 (NP-40)	Roche Diagnostics (Mannheim, Germany)
Osmium tetroxide (OsO_4)	Merck (Darmstadt, Germany)
PageRuler® prestained protein ladder	Fermentas (St. Leon-Rot, Germany)
Paraformaldehyde (PFA)	AppliChem (Darmstadt, Germany)
Phalloidin-ATTO 647N	Sigma-Aldrich (Steinheim, Germany)
Phenol/chloroform/isoamyl alcohol	Roth (Karlsruhe, Germany)
Piperazine-N,N'-bis(2-ethanesulfonic acid) (PIPES)	AppliChem (Darmstadt, Germany)
Polyclonal rabbit anti-human von Willebrand factor	Dako (Hamburg, Germany)
Potassium chloride (KCl)	Roth (Karlsruhe, Germany)
Potassium dihydrogen phosphate (KH_2PO_4)	Roth (Karlsruhe, Germany)
Propylene oxide	Sigma-Aldrich (Steinheim, Germany)
Prostacyclin (PGI_2)	Sigma-Aldrich (Steinheim, Germany)
Protease inhibitor cocktail (100x)	Sigma-Aldrich (Steinheim, Germany)
Proteinase K	Fermentas (St. Leon-Rot, Germany)
R-phycoerythrin (PE)	EUROPA (Cambridge, UK)
Rotiphorese® Gel A 30% Acrylamide solution	Roth (Karlsruhe, Germany)
Sodium azide (NaN_3)	Roth (Karlsruhe, Germany)
Sodium chloride (NaCl)	Roth (Karlsruhe, Germany)

Chemical/reagent	Company
Sodium dihydrogen phosphate (NaH_2PO_4)	Roth (Karlsruhe, Germany)
Sodium dodecyl sulfate (SDS)	Sigma-Aldrich (Steinheim, Germany)
Sodium hydrogen carbonate ($NaHCO_3$)	Roth (Karlsruhe, Germany)
Sodium hydrogen phosphate (Na_2HPO_4)	Roth (Karlsruhe, Germany)
Sucrose	Sigma-Aldrich (Steinheim, Germany)
Taq buffer (+KCl, -$MgCl_2$), 10x	Fermentas (St. Leon-Rot, Germany)
Taq polymerase	Fermentas (St. Leon-Rot, Germany)
Tetramethylethylenediamine (TEMED)	Roth (Karlsruhe, Germany)
Thrombin	Roche Diagnostics (Mannheim, Germany)
Tris(hydroxymethyl)aminomethane (TRIS)	Roth (Karlsruhe, Germany)
Triton® X-100	VWR International (Darmstadt, Germany)
Tween 20®	Roth (Karlsruhe, Germany)
U46619	Enzo Lifesciences (Lörrach, Germany)
Uranyl acetate	Electron Microscopy Sciences (Hatfield, PA, USA)
Water, nuclease-free	Life Technologies (Carlsbad, CA, USA)
Western Lightning™ Plus-ECL Enhanced Chemiluminescence Substrate	PerkinElmer (Waltham, MA, USA)

All non-listed chemicals/reagents were purchased from AppliChem (Darmstadt, Germany), Sigma-Aldrich (Steinheim, Germany), or Roth (Karlsruhe, Germany). Collagen-related peptide (CRP) was generously provided by Prof. Dr. Steve Watson (University of Birmingham, UK). Rhodocytin was a kind gift from Prof. Dr. Johannes Eble (University Hospital Frankfurt, Germany).

3.1.2 Kits

Kit	Company
Reticulin silver plating kit according to Gordon & Sweets	Merck (Darmstadt, Germany)

3.1.3 Antibodies

3.1.3.1 Antibodies used for flow cytometry

Antibody	Clone	Isotype	Antigen	Company/ description
p0p4	15E2	IgG2b	GPIbα	[64]
DOM2	89H11	IgG2a	GPV	[64]
p0p6	56F8	IgG2b	GPIX	[64]
MWReg30	5D7	IgG1	GPIIb	[65]
EDL-1	57B10	IgG2a	GPIIIa	[64]
JON6	14A3	IgG2b	GPIIbIIIa	unpublished
JON/A	4H5	IgG2b	GPIIbIIIa	Emfret Analytics (Eibelstadt, Germany)
-	12C6	IgG2b	α2	unpublished
BAR-1	25B11	IgG1	α5	[66]
Anti-β1(CD29)-FITC	9EG7	IgG2a	β1	BD Bio-sciences (Heidelberg, Germany)
JAQ1	98A3	IgG2a	GPVI	[67]
INU1	11E9	IgG1	CLEC-2	[27]
ULF1	96H10	IgG2a	CD9	[64]
JER1	10B6	IgG2a	CD84	[68]
WUG1.9	5C8	IgG1	P-selectin	unpublished
	12H10		P-selectin	unpublished
Anti-fibrinogen-Fab			Fibrinogen	
Anti-fibronectin			Fibronectin	
Anti-vWF	polyclonal	-	vWF	Dako (Hamburg, Germany)

Unless indicated otherwise, all antibodies used for flow cytometry experiments were purified in our laboratory and labeled with fluorescein isothiocyanate (FITC) or phycoerythrin (PE) by standard methods.[69]

3.1.3.2 Antibodies used for immunoblotting

Antibody	Company/description
Rabbit anti-CAP1	Sigma-Aldrich (Steinheim, Germany)
Rabbit anti-CAP2	kindly provided by Dr. Vivek Peche (Institute for Biochemistry I, University of Cologne, Germany)
Mouse anti-Rac1	BD Biosciences (Heidelberg, Germany)
Mouse anti-Cdc42	BD Biosciences (Heidelberg, Germany)
Rabbit anti-β-actin	Cell Signaling Technology (Cambridge, UK)
Rat anti-α-tubulin	EMD Millipore (Temecula, CA, USA)
Rat anti-β3 integrin HRP	[64]
Rabbit anti-GAPDH	Sigma-Aldrich (Steinheim, Germany)
Polyclonal rabbit anti-mouse IgG HRP	Dako (Hamburg, Germany)
Donkey anti-rabbit IgG HRP	Dianova (Hamburg, Germany)
Donkey anti-rat IgG HRP	Dianova (Hamburg, Germany)

3.1.3.3 Antibodies used for immunofluorescence staining

Antibody	Fluorophore conjugation	Company/description
Anti-α-tubulin	Alexa Fluor® 488	Invitrogen (Karlsruhe, Germany)
Anti-CD105/endoglin	Alexa Fluor® 647	BioLegend (San Diego, CA, USA)
Anti-GPIb (7A9)	Alexa Fluor® 488	[64]

3.1.4 Buffers and media

Blocking buffer (for Western blot)

Washing buffer/TBS-T	
Fat-free dry milk	5%

Coating buffer (for spreading assay on vWF), pH 9.6

$NaHCO_3$	50 mM

Decalcification buffer, pH 7.4

PBS	
EDTA	10%

IP buffer

NaCl	155 mM
TRIS/HCl (pH 8.0)	15 mM
EDTA	1 mM
NaN_3	0.005%

Laemmli buffer (for SDS-PAGE)

TRIS	40 mM
Glycine	0.95 M
SDS	0.5%

Lysis buffer (for DNA isolation), pH 7.2

NaCl	200 mM
TRIS	100 mM
EDTA	5 mM
SDS	0.2%
Proteinase K (added immediately before usage)	100 µg/mL

PBS/EDTA (for platelet lysates)

PBS	
EDTA	5 mM

PHEM, pH 6.9

PIPES	60 mM
HEPES	25 mM
EGTA	10 mM
$MgCl_2$	2 mM

PHEM complete buffer, pH 7.2

PHEM	
PFA	4%
NP-40	1%

PHEM fixative

PHEM	
PFA	4%
Glutaraldehyde	0.05%
Triton® X-100	0.05%

Phosphate-buffered saline (PBS), pH 7.14

NaCl	137 mM
KCl	2.7 mM
Na_2HPO_4	8 mM
KH_2PO_4	1.5 mM

Separating gel buffer (for Western blot), pH 8.8

TRIS/HCl	1.5 M

SDS sample buffer, 4x

β-mercaptoethanol (generates reducing conditions)	20%
TRIS (1 M), pH 6.8	20%
Glycerine	40%
SDS	4%
Bromophenol blue (3',3",5',5"-tetrabromophenolsulfon-phthalein)	0.04%

Sörensen phosphate buffer, pH 6.8–7.0

Na_2HPO_4	0.06 M
KH_2PO_4	0.04 M

Stacking gel buffer (for Western blot), pH 6.8

TRIS/HCl	0.5 M

Stripping buffer (for Western blot), pH 2.0

PBS	
Glycine	25 mM
SDS	1%

TAE buffer, 50x, pH 8.0

TRIS	0.2 M
Acetic acid	5.7%
EDTA	50 mM

TBS (TRIS-buffered saline), pH 7.3

NaCl	137 mM
TRIS/HCl	20 mM

TBS-T

TBS	
Tween 20®	0.1%

TE buffer, pH 8.0

TRIS	10 mM
EDTA	1 mM

Transfer buffer (for semi-dry Western blot)

TRIS ultra pure	50 mM
Glycine	40 mM
Methanol	20%

Tyrode's buffer ± Ca^{2+}, pH 7.3

NaCl	137 mM
KCl	2.7 mM
$NaHCO_3$	12 mM
NaH_2PO_4	0.43 mM
$CaCl_2$	0 or 2 mM
$MgCl_2$	1 mM
HEPES	5 mM
BSA	0.35%
(added immediately before usage)	
Glucose	0.1%
(added immediately before usage)	

All buffers were prepared and diluted in deionized water obtained from a Milli-Q® Water Purification System (Merck Millipore, Billerica, MA, USA).

3.2 Methods

3.2.1 Genetically modified mice

Constitutive CAP2 knockout (*Cap2*$^{gt/gt}$, gt: gene-trap) mice were kindly provided by Dr. Vivek Peche (Institute for Biochemistry I, University of Cologne, Germany). The generation of the *Cap2*$^{gt/gt}$ mouse model is described in detail in [37]. Briefly, a knockout vector containing a gene-trap cassette was inserted into intron 2 of the murine *Cap2* gene in embryonic stem cells (**Fig. 4**). Alternative splicing of the *Cap2*^{gt} allele results in a new transcript which encodes a dysfunctional fusion protein (exon 2 + lacZ) comprising only the first 40 aa residues of full-length CAP2. Finally, mating of *Cap2*$^{+/gt}$ males and *Cap2*$^{+/gt}$ females yielded *Cap2*$^{gt/gt}$ mice.

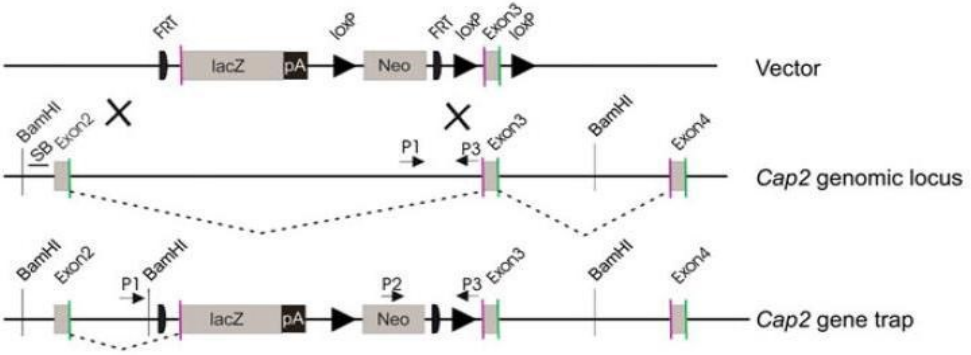

Fig. 4: Targeting strategy of the *Cap2* locus

The knockout vector contains a β-galactosidase gene (lacZ) and a neomycin phosphotransferase gene (Neo). The genomic locus of the *Cap2* gene on chromosome 13 depicts exons 2, 3, and 4. P1, P2, and P3 denote the polymerase chain reaction (PCR) primers used for genotyping of mice (CAP2_forw, CAP2_GT, and CAP2_rev, respectively; see **3.2.2.2**). Green and purple vertical dashes denote splice donor and splice acceptor, respectively. FRT, flippase recognition target site; pA, polyadenylation site; loxP, locus of X-over P1. (Image is reproduced with permission from Peche *et al.*.[37])

An IMT phenotype preliminarily termed orphan (orph) was discovered among the mouse population designated for the study of CAP2 function in platelets.

We could not detect any correlation between the occurrence of the phenotype of orph mice and a specific CAP2 genotype, meaning that orph mice could (genetically) be *Cap2*$^{+/+}$, *Cap2*$^{+/gt}$, or *Cap2*$^{gt/gt}$. In order to exclude any influence of the *Cap2*^{gt} allele on our studies of the phenotype of orph mice, the respective mice were backcrossed on a *Cap2*$^{+/+}$ background (C57BL/6J), and phenotyped according to the definition outlined in **3.2.3**.

3.2.2 Genotyping of mice

3.2.2.1 Isolation of murine genomic DNA

(Semi)circular pieces of mouse ear were obtained during earmarking and dissolved overnight in 500 µL lysis buffer at 55 °C and 900 rpm in a Thermomixer comfort (Eppendorf, Hamburg, Germany). The following day, 500 µL phenol/chloroform/isoamylalcohol (ratio 25:24:1) were added and samples were shaken vigorously. Centrifugation for 10 min at 10,000 rpm at room temperature (RT) in an Eppendorf Centrifuge 5417 R yielded biphasic samples. The aqueous upper phase which contained DNA/RNA was collected and transferred into a new tube previously supplied with 500 µL isopropanol. Afterwards, the precipitating nucleic acids were spun down by centrifugation for 10 min at 14,000 rpm and 4 °C. The supernatant was discarded and the remaining pellet was washed and dehydrated by addition of 500 µL 70% ethanol and centrifugation for 10 min at 14,000 rpm and 4 °C. Subsequently, the ethanol was discarded and samples were allowed to dry in a Thermomixer comfort for approximately half an hour at 37 °C. Finally, 60–80 µL TE buffer were added and the pellet was dissolved by gentle shaking (450 rpm) for ~30 min at 37 °C. 2 µL of the resulting DNA solution were used for all PCR reactions.

3.2.2.2 Polymerase chain reaction

Two distinct genotyping strategies were applied: first, a CAP2 PCR with pooled primers (two separate forward primers and one common reverse

primer) was performed as described in [37]. Second, the obtained result was confirmed by means of three further PCRs: another CAP2 PCR displaying the presence of a CAP2 WT allele, a gene-trap PCR revealing the existence of a gene-trap cassette, and a Neo PCR identifying the occurrence of a neomycin phosphotransferase gene. The constellation of the results of these overall four PCRs with regard to the respective CAP2 genotype is depicted in the following table (+, band present; -, band absent):

	CAP2 PCR with pooled primers according to [37]	**CAP2 PCR**	**Gene-trap PCR**	**Neo PCR**
***Cap2*$^{+/+}$**	only WT band	+	-	-
***Cap2*$^{+/gt}$**	both WT and *Cap2*^{gt} band	+	+	+
***Cap2*$^{gt/gt}$**	only *Cap2*^{gt} band	-	+	+

CAP2 PCR with pooled primers

Primers[37]:

CAP2_forw	5' GTGCTTCACTGATGGGCTTG 3'
CAP2_GT	5' GCCGCTCCCGATTCGCAG 3'
CAP2_rev	5' TCACCCCACATTTACGATGG 3'

Pipetting scheme:

Genomic DNA	2 µL
DreamTaq Green PCR MasterMix (2x)	10 µL
CAP2_forw (1 µg/µL)	0.03 µL
CAP2_GT (1 µg/µL)	0.07 µL
CAP2_rev (1 µg/µL)	0.10 µL
Water, nuclease-free	7.7 µL

PCR program:

94 °C	120 s	
94 °C	45 s	36 cycles
62 °C	45 s	
72 °C	90 s	
72 °C	10 min	
22 °C	stop	

Results (expected band sizes[37]):

Cap2$^{+/+}$	~550 bp
Cap2$^{+/gt}$	~550 bp and ~800 bp
Cap2$^{gt/gt}$	~800 bp

CAP2 PCR

Primers:

CAP2_for_new	5' CGGCATCAGGCAGCAACATTG 3'
CAP2_rev_new	5' CAGCTGCTCCAGCCGGATG 3'

Pipetting scheme:

Genomic DNA	2 µL
Taq buffer (+KCl, -$MgCl_2$), 10x	2 µL
$MgCl_2$ (25 mM)	1.2 µL
dNTPs (10 mM)	0.4 µL
CAP2_for_new (1 µg/µL)	0.10 µL
CAP2_rev_new (1 µg/µL)	0.10 µL
Taq polymerase (5 U/µL)	0.125 µL
H_2O	14.075 µL

PCR program:

94 °C	120 s	
94 °C	45 s	
58.4 °C	45 s	36 cycles
72 °C	90 s	
72 °C	10 min	
22 °C	stop	

Results (expected band sizes):

Cap2$^{+/+}$	523 bp
Cap2$^{+/gt}$	523 bp
Cap2$^{gt/gt}$	-

Gene-trap PCR

Primers:

Gentrap For	5' TTATCGATGAGCGTGGTGGTTATG 3'
Gentrap Rev	5' GCGCGTACATCGGGCAAATAATAT 3'

Pipetting scheme:

Genomic DNA	2 µL
Taq buffer (+KCl, -$MgCl_2$), 10x	2.5 µL
$MgCl_2$ (25 mM)	2.5 µL
dNTPs (10 mM)	0.5 µL
Gentrap For (1 µg/µL)	0.05 µL
Gentrap Rev (1 µg/µL)	0.05 µL
Taq polymerase (5 U/µL)	0.25 µL
H_2O	18.15 µL

PCR program:

96 °C	180 s	
94 °C	30 s	
51.4 °C	30 s	40 cycles
72 °C	60 s	
72 °C	5 min	
22 °C	stop	

Results (expected band sizes):

Cap2$^{+/+}$	-
Cap2$^{+/gt}$	680 bp
Cap2$^{gt/gt}$	680 bp

Neo PCR

Primers:

RIAM NeoInF	5' TTCGGCTATGACTGGGCACAACAG 3'
RIAM NeoInR	5' TACTTTCTCGGCAGGAGCAAGGTG 3'

Pipetting scheme:

Genomic DNA	2 µL
Taq buffer (+KCl, -$MgCl_2$), 10x	2 µL
$MgCl_2$ (25 mM)	1.2 µL
dNTPs (10 mM)	0.4 µL
RIAM NeoInF (1 µg/µL)	0.10 µL
RIAM NeoInR (1 µg/µL)	0.10 µL
Taq polymerase (5 U/µL)	0.125 µL
H_2O	14.075 µL

PCR program:

96 °C	180 s	
94 °C	30 s	
66.9 °C	30 s	35 cycles
72 °C	30 s	
72 °C	180 s	
22 °C	stop	

Results (expected band sizes):

Cap2$^{+/+}$	-
Cap2$^{+/gt}$	282 bp
Cap2$^{gt/gt}$	282 bp

Primers for both CAP2 PCRs as well as the gene-trap PCR were purchased from biomers.net (Ulm, Germany), while primers for the Neo PCR were obtained from Eurofins Genomics (Ebersberg, Germany). All PCRs were run on a FlexCycler (Analytik Jena, Jena, Germany).

3.2.2.3 Agarose gel electrophoresis

For the separation and size determination of PCR products, 1% agarose gels of different volumes were used. Therefore, appropriate amounts of agarose and TAE buffer were mixed in a conical (Erlenmeyer) flask and dissolution of the agarose was achieved by boiling the suspension in a microwave. The agarose solution was allowed to cool down to ~60 °C and Midori Advanced DNA Stain was added (5 µL per 100 mL agarose solution). The fluid was cast into a tray containing a variable number of combs and (after solidification of the gel) the tray was transferred into an electrophoresis chamber (neoLab, Heidelberg, Germany) filled with 1x TAE buffer. Then, all combs were removed. PCR products were mixed with 6x loading dye solution and loaded into the slots of the gel. In order to determine the size of the PCR products, a GeneRuler Mix (range 100–10,000 bp) was run in parallel. After running

the gels for ~30 min at 120–160 V (power supply: Biometra, Göttingen, Germany), DNA bands were visualized by UV light and pictures were taken with a camera (Herolab, Wiesloch, Germany).

3.2.3 Phenotyping of mice

50 µL of blood were withdrawn from the retroorbital plexus of anesthetized mice with capillary pipettes (A. Hartenstein, Würzburg, Germany) into 300 µL heparin (20 U/mL), and 650 µL PBS or Tyrode's buffer without Ca^{2+} were added. Subsequently, 50 µL of diluted, heparinized blood were incubated with 20 µL of a 1:1 mixture of fluorophore-labeled antibodies directed against two prominent platelet surface molecules (89H11-FITC directed against GPV; 14A3-PE directed against GPIIbIIIa) for 15 min at RT. The incubation period was terminated by the addition of 500 µL PBS prior to sample analysis on a BD FACSCalibur™ Flow Cytometer (BD Biosciences, San Jose, CA, USA) using Cell Quest™ software (BD Biosciences, Heidelberg, Germany). Platelet size as determined by forward scatter (FSC) and platelet count (events s^{-1}) were measured and evaluated. Mice displaying both an FSC value larger than 500 and a platelet count below 200 events s^{-1} were defined as orph mice.

3.2.4 Western blotting with platelet lysates

Mice were bled under isoflurane anesthesia from the retroorbital plexus with heparinized micro-hematocrit-tubes (Assistent®/Glaswarenfabrik Karl Hecht, Sondheim, Germany). 700 µL of blood were withdrawn into 300 µL heparin (20 U/mL) and another 300 µL heparin were added. Samples were centrifuged for 6 min at 800 rpm in an Eppendorf Centrifuge 5415 C and the upper phase including the buffy coat and some erythrocytes was transferred into a new tube containing 300 µL heparin. Another cycle of centrifugation for 6 min at 800 rpm yielded platelet-rich plasma (PRP) which was collected

into a new tube previously supplied with apyrase and PGI_2 (final concentrations of 0.02 U/mL and 0.1 µg/mL, respectively). The PRP was centrifuged for 5 min at 2,800 rpm in an Eppendorf Centrifuge 5424 and the supernatant was removed from the resulting platelet pellet.

Platelet pellets were washed in 1 mL 5 mM EDTA in PBS and platelet counts were determined on a Sysmex KX-21N automated hematology analyzer (Sysmex, Kobe, Japan). Platelet concentrations were adjusted to 0.5×10^6 platelets μL^{-1} by addition of appropriate volumes of IP buffer previously supplied with 1% NP-40 and 1x protease inhibitors. Samples were incubated on ice for 20 min and subsequently centrifuged for 10 min at 14,000 rpm and 4 °C in an Eppendorf Centrifuge 5417 R. Afterwards, supernatants were collected, mixed with suitable volumes of 4x SDS sample buffer, and boiled for 5 min at 95 °C in a Thermomixer comfort. Platelet lysates were either used immediately or stored at -20 °C.

Proteins within the platelet lysates were separated by sodium dodecyl sulfate polyacrylamide gel electrophoresis (SDS-PAGE). Therefore, 10 µL of platelet lysate were loaded into the slots of a polyacrylamide gel comprised of a 4% stacking part and a 10% separating part. A PageRuler® prestained protein ladder was loaded into a separate slot and served as a marker. The gel was mounted into an electrophoresis chamber (Biometra, Göttingen, Germany) filled with Laemmli buffer and run at 10–15 mA in the stacking part and at 20–25 mA in the separating part for ~90 min in total. Thereafter, the stacking part of the gel was cut off and discarded, and the protein-containing separating part was subjected to Western blotting. Proteins were transmitted onto a polyvinylidene difluoride (PVDF) membrane using a semi-dry blotting system (0.8 mA/cm^2 for 60 min). Subsequently, the membrane was blocked for 1 h at RT in blocking buffer under gentle rotation, rinsed with TBS-T, and incubated overnight at 4 °C with the desired primary antibody (anti-CAP1

(1:300), anti-CAP2 (1:5,000), anti-Rac1 (1:500), anti-Cdc42 (1:500), or anti-GAPDH antibody (1:5,000)) under smooth agitation. The next day, the membrane was washed three times for 10 min in TBS-T, incubated for 1 h at RT with the corresponding horseradish peroxidase (HRP)-conjugated secondary antibodies, and again washed thrice. For visualization of the proteins, enhanced chemiluminescence (ECL) solution and developing films (Amersham Hyperfilm™ ECL) were employed. Stripping of the membranes was achieved by incubation in stripping buffer for 20 min at RT under vigorous shaking. Afterwards, membranes were washed three times for 10 min in TBS-T, blocked for 30 min in blocking buffer, rinsed, and reprobed with a different primary antibody.

3.2.5 Platelet purification

Platelet pellets were prepared as described in **3.2.4**, resuspended in 1 mL of Tyrode's buffer without Ca^{2+} containing apyrase (0.02 U/mL) and PGI_2 (0.1 µg/mL), and allowed to rest for 5 min at 37 °C in a Thermomixer comfort. Platelet concentrations were determined on a Sysmex KX-21N automated hematology analyzer, samples were centrifuged for 5 min at 2,800 rpm, supernatants were removed, and the platelet pellets were resuspended in adequate volumes of Tyrode's buffer without Ca^{2+} previously supplied with apyrase (0.02 U/mL) to achieve the desired platelet concentration. Platelet suspensions (hereon referred to as washed platelets) were kept at 37 °C for 15 min prior to the experiments.

3.2.6 Flow cytometric analyses of platelets

3.2.6.1 Determination of platelet size and count

Platelet size (FSC) and platelet count (events s^{-1}) were determined as outlined in **3.2.3**.

3.2.6.2 Investigation of GP expression levels and platelet activation responses

50 µL of blood were withdrawn from the retroorbital plexus of anesthetized mice with capillary pipettes into 300 µL heparin (20 U/mL), and 650 µL Tyrode's buffer without Ca^{2+} were added. 50 µL of this diluted, heparinized blood were incubated for 15 min at RT with 10 µL of FITC-labeled antibodies in order to analyze the expression level of prominent platelet surface molecules. The incubation was terminated by addition of 500 µL PBS, and samples were measured immediately on a BD FACSCalibur™ Flow Cytometer using Cell Quest™ software.

To inquire platelet activation responses, the remaining heparinized blood samples were washed (5 min at 2,800 rpm) in 1 mL of Tyrode's buffer without Ca^{2+} and resuspended in suitable volumes of Tyrode's buffer containing 2 mM Ca^{2+}. 50 µL of washed blood per condition were incubated for 7 min at 37 °C followed by 7 min at RT with 20 µL of a 1:1 mixture of fluorophore-labeled antibodies (4H5-PE directed against active GPIIbIIIa; 5C8-FITC directed against P-selectin) in the presence of adequately diluted agonists (ADP, the stable TXA_2 analog U46619, a combination of both, thrombin, CRP, and the snake venom toxin rhodocytin). The addition of 500 µL PBS stopped the incubation and samples were measured as described above for the GP expression analysis.

3.2.6.3 Assessment of α-granule content

10 µL of washed platelets (0.5×10^6 platelets μL^{-1}) were fixed with 0.5% PFA in PBS for 30 min at RT and subsequently washed with 2 mL PBS by centrifugation for 5 min at 1,800 rpm. Afterwards, platelets were permeabilized by addition of 50 µL 0.1% NP-40 in PBS and stained for 30 min with 20 µL of FITC-labeled anti-vWF, anti-P-selectin (12H10), anti-fibronectin, or anti-β1 integrin antibody, or FITC-labeled anti-fibrinogen Fab. Finally,

samples were analyzed on a BD FACSCalibur™ Flow Cytometer using Cell Quest™ software.

3.2.6.4 Inquiry of integrin recruitment and GP shedding

100 µL of blood were withdrawn from the retroorbital plexus of anesthetized mice with capillary pipettes into 300 µL heparin (20 U/mL), and 500 µL of Tyrode's buffer without Ca^{2+} were added. Samples were washed (5 min at 2,800 rpm) in 750 µL of Tyrode's buffer without Ca^{2+}, and resuspended in 950 µL of Tyrode's buffer containing 2 mM Ca^{2+}. 50 µL of washed blood were incubated for 15 min at 37 °C with 10 µL of FITC-labeled antibodies in the presence and in the absence of thrombin (0.1 U/mL). To stop the incubation period, 500 µL PBS were added, and samples were analyzed on a BD FACSCalibur™ Flow Cytometer using Cell Quest™ software. For all tested platelet surface molecules, the percentage change in surface abundance (activated compared to resting state) was calculated according to the following formula (MFI, mean fluorescence intensity):

$$\text{change in surface abundance } [\%] = \left(\frac{MFI_{\text{activated state}}}{MFI_{\text{resting state}}} - 1 \right) \times 100$$

3.2.6.5 Evaluation of β1 integrin activation

50 µL of washed platelets (0.3×10^6 platelets μL^{-1}) were incubated for 7 min at 37 °C followed by 7 min at RT with 10 µL of a 1:9 dilution of FITC-labeled 9EG7-antibody (directed against active β1 integrin) in the presence of appropriately diluted agonists (ADP, U46619, a combination of both, thrombin, CRP, and rhodocytin). The incubation was terminated by the addition of 400 µL of Tyrode's buffer containing 2 mM Ca^{2+}. Samples were measured on a BD FACSCalibur™ Flow Cytometer using Cell Quest™ software.

3.2.7 Measurement of basic blood parameters

Red and white blood cell count, platelet count, hematocrit (HCT), hemoglobin concentration (Hb), mean corpuscular volume (MCV), mean platelet volume (MPV), and platelet distribution width (PDW) were measured in heparinized whole blood on a Sysmex KX-21N automated hematology analyzer.

3.2.8 Spreading assays

3.2.8.1 Spreading on fibrinogen

Differential interference contrast microscopy

Rectangular glass slides (24 × 50 mm) were coated overnight at 4 °C with 100 µg/mL human fibrinogen in sterile PBS in a humid chamber. The next day, the slides were blocked for 1 h at RT with 3% BSA in sterile PBS, rinsed with sterile PBS, and incubated for ~20 min with 300 µL of Tyrode's buffer containing 2 mM Ca^{2+}. 30–50 µL of washed platelets (0.3×10^6 platelets μL^{-1}) were mixed with 50–70 µL of Tyrode's buffer containing 2 mM Ca^{2+}, activated with thrombin (0.01 U/mL), and pipetted onto the fibrinogen matrix. After three different time periods (5, 15, and 30 min), the spreading process was terminated by the addition of 300 µL 4% PFA in PBS. The samples were covered with coverslips prior to examination by differential interference contrast (DIC) microscopy, employing a Zeiss Axiovert 200 M inverted microscope (Carl Zeiss Microscopy, Göttingen, Germany) with a 100x 1.4 oil objective. Pictures were taken with a CoolSNAP EZ camera (Photometrics, Tucson, AZ, USA) and analyzed with ImageJ software (National Institutes of Health, Bethesda, MD, USA). Phase abundances of four different spreading stages were determined (**Fig. 5**).

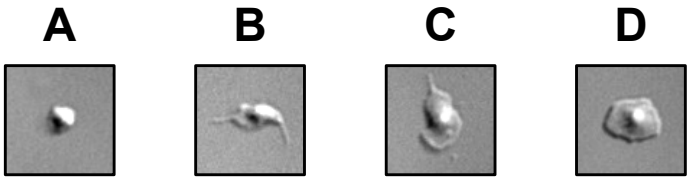

Fig. 5: Definition of four different platelet spreading stages

Platelet spreading on a fibrinogen matrix (100 µg/mL) was divided into four stages: roundish **(A)**, only filopodia **(B)**, filopodia and lamellipodia **(C)**, and fully spread **(D)**.

Confocal microscopy

Immunofluorescence specimens for confocal microscopy were prepared in collaboration with Dr. Simon Stritt. Platelets were activated with thrombin (0.01 U/mL), allowed to spread on fibrinogen for 0 min (resting control) or 15 min, and subsequently fixed and permeabilized for 20 min at 4 °C in PHEM complete buffer. After blocking for 2 h at 37 °C with 5% BSA in sterile PBS, the samples were incubated with appropriate primary and fluorophore-labeled secondary antibodies (the respective fluorophore is denoted in brackets below) directed against β3 integrin (Cy3), talin (Alexa Fluor® 488), and an Alexa Fluor® 488-conjugated anti-α-tubulin primary antibody. Filamentous actin was visualized with ATTO 647N-labeled phalloidin. Samples were mounted with Fluoroshield™ and investigated on a Leica TCS SP5 confocal microscope, using an HCX PL APO CS 100x 1.4 oil objective (both from Leica Microsystems, Wetzlar, Germany). Finally, pictures were evaluated and processed with ImageJ software.

3.2.8.2 Spreading on von Willebrand factor

Rectangular glass slides (24 × 50 mm) were coated overnight at 4 °C with 200 µL of a 1:500 dilution of a polyclonal rabbit anti-human vWF antibody in coating buffer. The next day, the slides were rinsed with sterile PBS and blocked for 1 h at 37 °C with 200 µL 3% BSA in sterile PBS. During this incubation period, mouse plasma was prepared.

For this purpose, anesthetized mice were bled from their retroorbital plexus up to 1 mL into 300 µL heparin (20 U/mL). Blood samples were centrifuged for 10 min at 2,800 rpm, the supernatant was collected into a new tube and centrifuged for 10 min at 14,000 rpm. The supernatant (mouse plasma) was transferred into a new tube and subsequently used for spreading experiments on vWF.

Glass slides were rinsed twice with 300 µL sterile PBS and incubated for 2 h at 37 °C with 100 µL of mouse plasma. Afterwards, glass slides were rinsed again and incubated for ~20 min with 300 µL of Tyrode's buffer containing 2 mM Ca^{2+}. Then, 50 µL of washed platelets (0.3×10^6 platelets μL^{-1}) were mixed with an equal volume of Tyrode's buffer with Ca^{2+}, treated with eptifibatide (40 µg/mL) and botrocetin (2 µg/mL), and allowed to spread on the vWF matrix for 15 min. Spreading was terminated by the addition of 300 µL 4% PFA in PBS. The specimen slides were covered with coverslips and microscopy and photography were performed as outlined in **3.2.8.1**. Pictures were evaluated with ImageJ software, dividing platelets into three categories, depending on the number of formed filopodia (**Fig. 6**). Finally, the percentage value of each category was calculated.

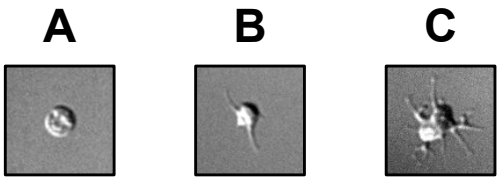

Fig. 6: Definition of three different filopodia categories

Platelets spreading on a von Willebrand factor matrix (1:500) were divided into three different filopodia categories: no filopodia **(A)**, 1–3 filopodia **(B)**, and >3 filopodia per platelet **(C)**.

3.2.9 Histology

3.2.9.1 Preparation of paraffin sections

Heart, lung, liver, kidney, spleen, thymus, lymph nodes, and femora of WT and orph mice were dissected and fixed overnight at 4 °C in 4% PFA in PBS. Prior to further processing, femora were decalcified at 4 °C for 14 days in decalcification buffer (consumed buffer was substituted every other day). All organs were dehydrated in a Leica ASP200 S tissue processor (Leica Biosystems, Nussloch, Germany) and subsequently embedded in paraffin. 3-µm thin sections of the paraffin-embedded organs were generated on an HM 355 rotary microtome (MICROM, Walldorf, Germany), mounted on microscope slides (25 × 75 mm; Gerhard Menzel GmbH, Braunschweig, Germany), and dried overnight at 37 °C.

Hematoxylin and eosin stain

Paraffin-embedded histology sections were deparaffinized in xylene (2 × 10 min) and rehydrated, using a descending ethanol series (100%, 90%, 80%, and 70% ethanol; each step for 2 min) and a final step in deionized water (2 min). Subsequently, the slides were stained with hematoxylin solution for 10 s and allowed to rest in a constant flow of tap water for 5 min. Afterwards, the counterstaining was performed, applying a freshly prepared 0.05% eosin solution for 2 min. Sections were shortly washed in deionized water prior to dehydration in an ascending ethanol series (70%, 80%, 90%, and 100% ethanol; each step for 2 min) and reparaffinization in xylene (2 × 3 min). Samples were permitted to dry and finally mounted, using Eukitt® mounting medium and coverslips. Hematoxylin and eosin (H&E) stained organ sections were examined on a Leica DMI4000 B inverted microscope (Leica Microsystems, Wetzlar, Germany). Images were taken and further processed with ImageJ software.

Reticulin silver staining

For the detection of reticular fibers in BM sections, a reticulin silver plating kit according to Gordon & Sweets (courtesy of Dr. Carsten Deppermann) was used. BM sections were deparaffinized in xylene (2 × 10 min), rehydrated in a descending ethanol series (100%, 90%, 80%, and 70% ethanol; each step for 2 min), and transferred into deionized water (2 min). Initially, samples were treated with a solution of potassium permanganate and sulfuric acid for 5 min. Thereafter, solutions of oxalic acid, ammonium iron(III) sulfate, silver nitrate, formaldehyde, gold chloride, and sodium thiosulfate were applied (each reagent for 2 min). Finally, slides were washed in deionized water, dehydrated in an ascending ethanol series (70%, 80%, 90%, and 100% ethanol; each step for 2 min), and reparaffinized in xylene (2 × 3 min). Sections were allowed to dry and subsequently mounted with Eukitt® mounting medium and coverslips. The presence of reticular fibers was determined on a Leica DMI4000 B inverted microscope. Pictures were taken and edited with ImageJ software.

3.2.9.2 Preparation of whole femora cryosections

Whole femora cryosections were kindly generated by Dr. Simon Stritt. Briefly, femora of WT and orph mice were isolated and fixed with 4% PFA containing 5 mM sucrose. Prior to embedding in Cryo-Gel®, samples were transferred into 10% sucrose in PBS and dehydrated in an ascending sucrose series. Finally, samples were quick-frozen in liquid nitrogen and stored at -80°C until the preparation of 7-µm thin cryosections on a CryoJane® tape-transfer system (Leica Biosystems, Nussloch, Germany).

Immunofluorescence stain

Whole femora cryosections were treated with Alexa Fluor® 488-labeled 7A9 antibody directed against GPIb on MKs and platelets, and Alexa Fluor® 647-labeled anti-CD105 antibody to visualize endothelial cells. Nuclei were

stained with DAPI and samples were analyzed on a Leica TCS SP5 confocal microscope with an HCX PL APO CS 40x 1.25 oil objective (Leica Microsystems, Wetzlar, Germany). Pictures were examined and edited with ImageJ software.

3.2.9.3 Preparation of blood smears

3 µL of heparinized blood were pipetted onto one end of a glass slide (25 × 75 mm), hereon referred to as the specimen slide. A second glass slide, the spreader slide, was held at a 45° angle and moved into the proximity of the blood drop, gently touching it. After the blood had distributed along its width, the spreader slide was rapidly pushed forward, dispersing the blood over the length of the specimen slide. Prior to staining, specimen slides were allowed to air-dry.

Pappenheim stain

Air-dried blood smears were stained for 7 min in May–Grünwald's solution prior to counterstaining for 10 min in Giemsa working solution (1:20 dilution of Giemsa stock solution in phosphate buffer according to Sörensen). Then, samples were rinsed with phosphate buffer according to Sörensen, permitted to dry, and analyzed on a Leica DMI4000 B inverted microscope. Finally, images were taken and evaluated with ImageJ software.

3.2.9.4 Transmission electron microscopy of platelet samples

PRP was prepared, collected into a tube previously supplied with apyrase (0.02 U/mL) and PGI_2 (0.1 µg/mL), allowed to rest for 20 min at 37 °C, mixed with 1 volume of 5% glutaraldehyde in PBS, and incubated for 1 h at 37 °C. Thereafter, samples were centrifuged for 5 min at 1,500 g, supernatants were removed, and platelet pellets were washed thrice in 0.1 M cacodylate buffer (pH 7.2). After addition of 1% osmium tetroxide in cacodylate buffer and incubation for 1 h at RT, the samples were washed twice in cacodylate buffer and deionized water. Then, 2% uranyl acetate in deionized water were

added (1 h at 4 °C) before samples were dehydrated using an ascending ethanol series (3 × 5 min in 70% ethanol, 3 × 15 min in 95% ethanol, and 3 × 15 min in 100% ethanol). Subsequently, samples were incubated in propylene oxide (2 × 10 min) and placed into a 1:1 mixture of the epoxy resin EMbed 812 and propylene oxide for 1 h under rotation. EMbed 812 was added two times and platelet samples were incubated overnight and for 2 h on the following day at RT under rotation. Prior to the preparation of ultrathin sections and staining in 2% uranyl acetate (in ethanol) and lead citrate (in deionized water), samples were kept at 60 °C for 2 d to achieve setting of the epoxy resin. Finally, sections were analyzed on a Zeiss EM900 transmission electron microscope.

3.2.10 Statistical analysis

The results are displayed as mean ± standard deviation (SD). For analysis of differences between two groups, the Student's t-test was applied. Results demonstrating a p-value < 0.05 were considered as statistically significant and labeled with a single asterisk (*); $p < 0.01$ and $p < 0.001$ were labeled with two (**) and three asterisks (***), respectively. Results with a p-value ≥ 0.05 were regarded as statistically not significant (NS).

4 Results

4.1 Investigation of platelet function in CAP2-deficient mice

CAPs are evolutionarily highly conserved actin monomer-binding proteins that play a decisive role in the regulation of actin dynamics.[33] The reorganization of the actin cytoskeleton is of paramount importance for both platelet biogenesis in the BM[11] as well as for proper platelet function in the circulation.[25] In association with Dr. Vivek Peche (Institute for Biochemistry I, University of Cologne, Germany) we capitalized on mice constitutively lacking CAP2 (*Cap2*$^{gt/gt}$) and investigated the function of CAP2 in thrombopoiesis and platelet function. In these mice, the *Cap2* gene on chromosome 13 has been targeted by a gene-trap approach, abolishing its expression.[37] *Cap2*$^{gt/gt}$ mice were viable, fertile, and born in the expected Mendelian ratios. *Cap2*$^{+/+}$ littermates were used as controls for all experiments described in this study.

4.1.1 Murine platelets contain both CAP1 and CAP2

In order to investigate the presence of CAP isoforms in murine platelets, platelet lysates were prepared, separated by SDS-PAGE, and analyzed by immunoblotting. The applied anti-CAP2 antibody revealed three separate bands in WT samples (**Fig. 7**), a strong central band at a molecular weight of approximately 56 kDa surrounded by two fainter bands. This finding is in accordance with a study by Bertling *et al.* who identified three distinct CAP2 splice variants in mouse heart, brain, skeletal muscle, and testis by Northern blot analysis.[70] Consequently, at least three different CAP2 proteins appear to exist in murine platelets. The knockout (KO) strategy worked most effectively for the central and most abundant CAP2 protein which was completely absent in platelets from *Cap2*$^{gt/gt}$ mice. The expression of both the weak

upper and lower CAP2 band, however, seemed to be largely unaffected by the insertion of the *Cap2*^{gt} allele.

Further isoform expression profiling also revealed the presence of the CAP1 isoform in mouse platelets. Interestingly, platelets represent a cell type that co-expresses both mammalian CAP isoforms.

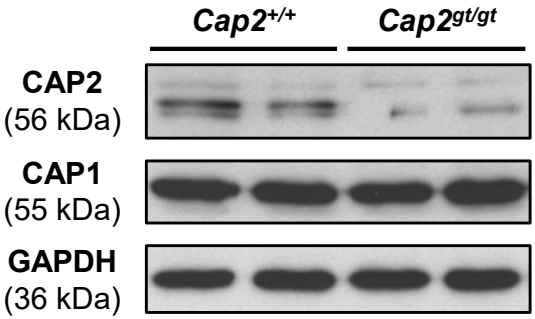

Fig. 7: Murine platelets express both mammalian CAP isoforms

Platelet lysates from wild-type (*Cap2*$^{+/+}$) and knockout (*Cap2*$^{gt/gt}$) mice were separated by SDS-PAGE and immunoblotted with anti-CAP2 and anti-CAP1 antibody. Glyceraldehyde 3-phosphate dehydrogenase (GAPDH) was detected as loading control.

4.1.2 Increased platelet size in *Cap2*$^{gt/gt}$ mice

Platelet count and size as well as the expression levels of prominent platelet surface molecules were determined by flow cytometry in *Cap2*$^{+/+}$ and *Cap2*$^{gt/gt}$ mice by incubating heparinized whole blood with saturating amounts of fluorophore-labeled antibodies. Whereas the platelet count in *Cap2*$^{gt/gt}$ mice was unaltered (**Fig. 8 A**), their platelet size was significantly increased by 15–20% compared to WT controls (**Fig. 8 B**). Accordingly, the expression levels of certain surface molecules such as GPV, GPIX, or GPIIbIIIa (αIIbβ3 integrin) were slightly elevated on CAP2-deficient platelets (**Fig. 8 C**).

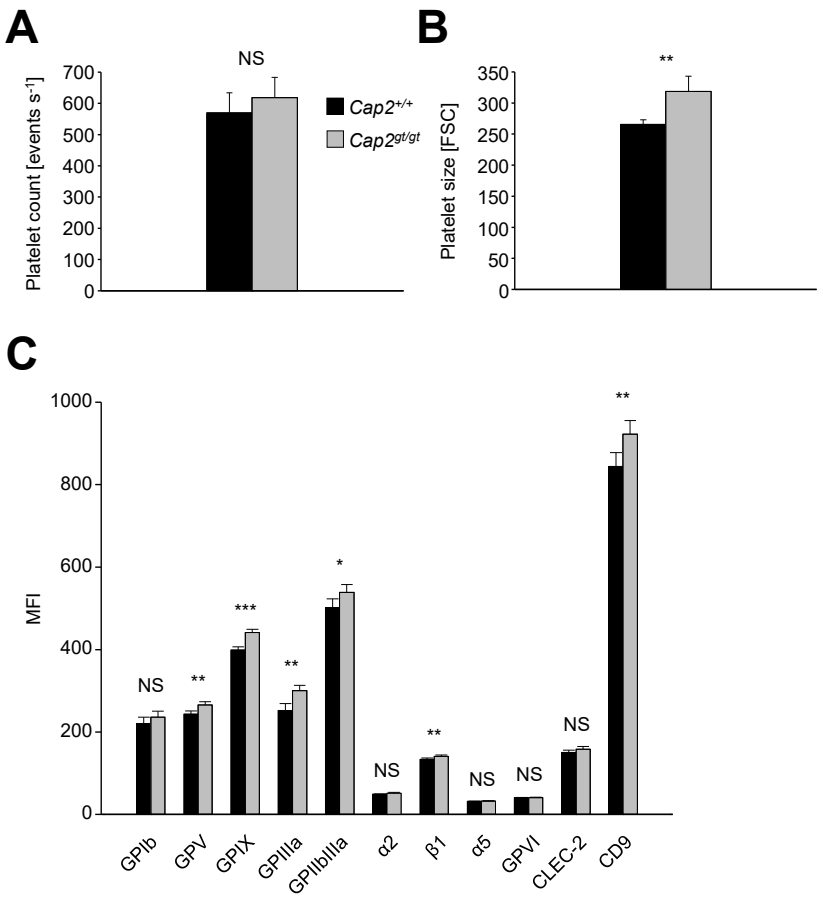

Fig. 8: Increased platelet size in *Cap2$^{gt/gt}$* mice

Platelet count **(A)**, platelet size **(B)**, and expression levels of prominent platelet surface molecules **(C)** of *Cap2$^{gt/gt}$* mice and the respective WT littermates were measured by flow cytometry. Results are displayed as mean ± SD of 5 mice per group. FSC, forward scatter; MFI, mean fluorescence intensity; Student's t-test: *, $p < 0.05$; **, $p < 0.01$; ***, $p < 0.001$; NS, not significant

4.1.3 CAP2-deficient platelets are hyperresponsive towards (hem)ITAM-specific agonists

Platelet signaling following treatment with various agonists was studied by flow cytometry. Blood from *Cap2$^{+/+}$* and *Cap2$^{gt/gt}$* mice was highly diluted to prevent the accumulation of second wave mediators and to allow the

selective detection of primary platelet signaling responses. The applied agonists can be divided into two categories: on the one hand, ADP, the stable TXA_2 analog U46619, and thrombin activate platelets through GPCRs;[26] on the other hand, CRP and the snake venom toxin rhodocytin stimulate platelets via GPVI and CLEC-2, respectively, thereby inducing (hem)ITAM signaling.[71]

Platelet activation responses were measured with two separate markers: first, the activation of GPIIbIIIa was detected with PE-conjugated JON/A antibody specifically directed against the active conformation of GPIIbIIIa; second, platelet α-granule release was determined with a FITC-labeled anti-P-selectin antibody.

CAP2-deficient platelets displayed normal activation responses following treatment with the GPCR agonists ADP, U46619, a combination of both, and thrombin (**Fig. 9 A, B**). Occasionally, minor differences between CAP2 WT and KO platelets were seen for GPCR agonists such as an elevated P-selectin exposure of KO platelets in response to an intermediate (0.01 U/mL) thrombin concentration (**Fig. 9 B**). Yet, these differences were not consistent throughout all performed experiments and therefore interpreted as statistical fluctuations rather than meaningful observations. In contrast to the overall normal activation pattern for GPCR agonists, GPIIbIIIa activation and P-selectin exposure in response to CRP which stimulates the ITAM-coupled collagen receptor GPVI, and rhodocytin which signals through the hemITAM-bearing receptor CLEC-2,[71] were markedly increased in CAP2-deficient platelets. Interestingly, CAP2-deficient platelets showed an elevated mean fluorescence intensity (MFI) for active GPIIbIIIa in the resting state, which is most likely explained by an increased GPIIbIIIa surface expression of CAP2-deficient platelets in the first place (**Fig. 8 C**).

In conclusion, CAP2 deficiency resulted in a pronounced hyperresponsiveness of platelets towards (hem)ITAM-specific agonists.

4.1.4 CAP2-deficient platelets spread normally on fibrinogen

Occupation of the platelet surface receptor GPIIbIIIa by its ligand fibrinogen initiates outside-in signaling which leads to platelet shape change, a process that highly depends on the reorganization of the actin cytoskeleton.[23]

In order to address the role of CAP2 in cytoskeletal dynamics, platelets from *Cap2*$^{+/+}$ and *Cap2*$^{gt/gt}$ mice were stimulated with a low concentration of thrombin (0.01 U/mL), and allowed to spread on a fibrinogen matrix for three different time periods (5, 15, and 30 min). However, we could not observe a significant difference in the spreading behavior between CAP2 WT and KO platelets after all tested time points (**Fig. 10**).

In summary, CAP2-null mice have larger platelets in peripheral blood than WT littermates. Platelet counts in *Cap2*$^{+/+}$ and *Cap2*$^{gt/gt}$ mice, on the other hand, are comparable. While CAP2-deficient platelets display a selective hyperresponsiveness towards (hem)ITAM-stimulating agonists, their spreading behavior on fibrinogen is unaltered.

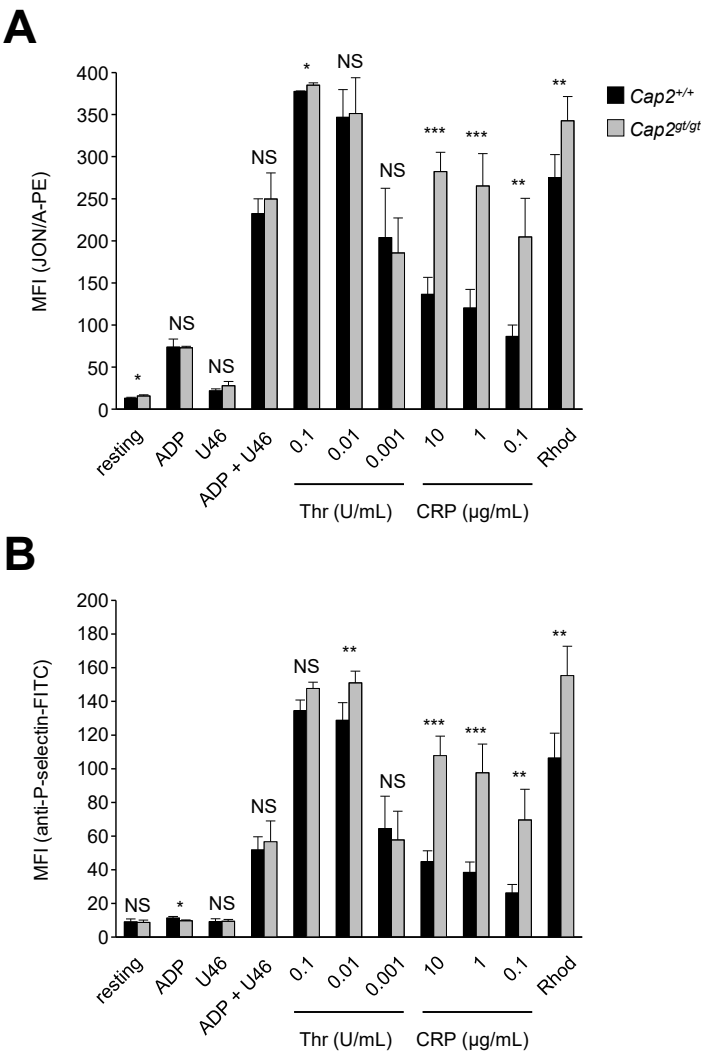

Fig. 9: GPIIbIIIa activation and P-selectin exposure are increased in CAP2-deficient platelets upon treatment with (hem)ITAM-specific agonists

GPIIbIIIa activation **(A)** and P-selectin exposure **(B)** in response to treatment with the indicated agonists were investigated in platelets from *Cap2*$^{+/+}$ and *Cap2*$^{gt/gt}$ mice by flow cytometry. The final concentrations of thrombin and CRP are depicted; ADP: 10 µM; U46: 1 µM; Rhod: 1 µg/mL. Results are mean ± SD of at least 5 mice per group. MFI, mean fluorescence intensity; U46, U46619; Rhod, rhodocytin; Student's t-test: *, $p < 0.05$; **, $p < 0.01$; ***, $p < 0.001$; NS, not significant

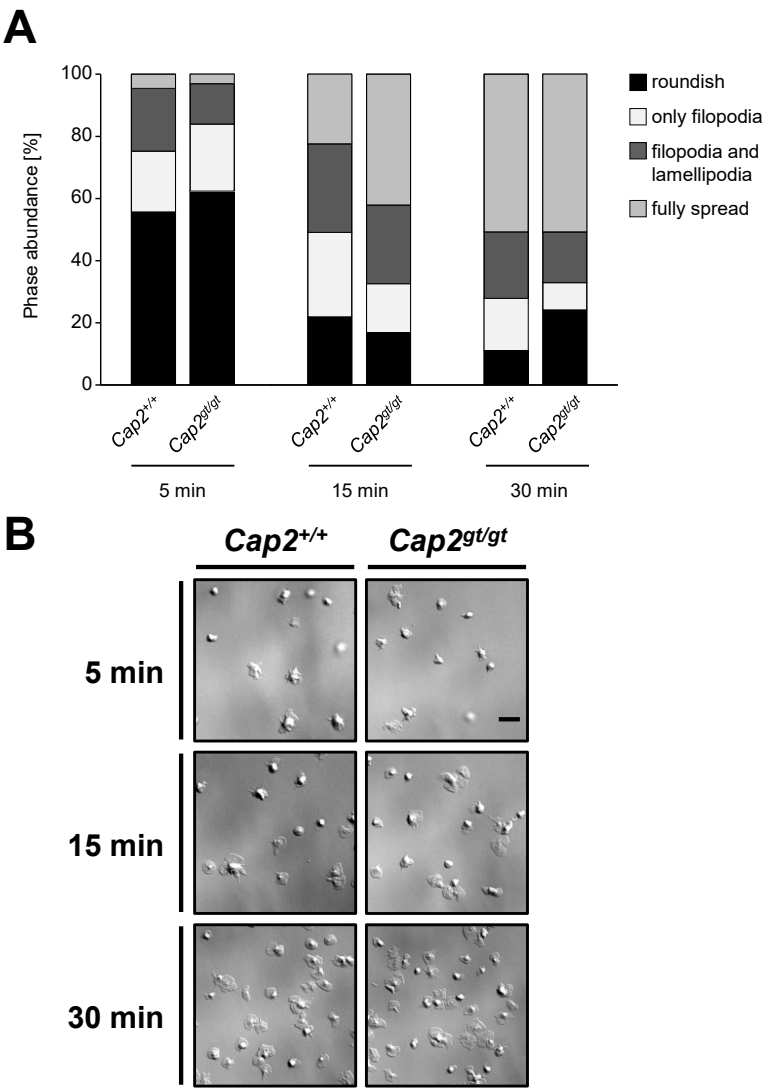

Fig. 10: Spreading of CAP2-deficient platelets on fibrinogen is unaltered

Washed platelets from *Cap2*$^{+/+}$ and *Cap2*$^{gt/gt}$ mice (n = 3 mice per group) were stimulated with thrombin (0.01 U/mL), allowed to spread on a fibrinogen matrix (100 µg/mL) for three different time intervals (5, 15, and 30 min), and analyzed by DIC microscopy. Phase abundances of four spreading stages (see **Fig. 5** for definition) **(A)** and representative DIC images **(B)** are shown. Scale bar, 5 µm

4.2 Description of an inherited macrothrombocytopenia

During the flow cytometry studies on CAP2, mice from both the *Cap2*$^{+/+}$ and *Cap2*$^{gt/gt}$ group occasionally showed a drastic reduction in platelet count combined with a massive increase in platelet size (FSC). This observation has been confirmed by independent investigators.

Therefore, mice displaying a dramatically lowered platelet count in conjunction with an increased platelet size — henceforth preliminarily referred to as orph mice — were backcrossed on a *Cap2*$^{+/+}$ background (C57BL/6J) to exclude any influence of the *Cap2*^{gt} allele.

4.2.1 CAPs and Rho-GTPases are present in orph platelets

Prior to further experiments, it was mandatory to ascertain the independence of the phenotype of orph mice from CAP2 deficiency. To this end, the expression levels of different cytoskeleton-associated proteins were analyzed by immunoblotting in platelet lysates of WT, *Cap2*$^{gt/gt}$, and orph mice. CAP1 as well as the Rho-GTPases Cdc42 and Rac1 were present in all tested platelet samples. Three CAP2 bands could be detected in WT and in orph platelets, whereas the most prominent central band was missing in CAP2-deficient platelets (**Fig. 11**), in accordance with previous results,[37] thus clearly indicating that the phenotype of orph mice is independent of CAP2 deficiency.

4.2.2 Orph mice show a severe macrothrombocytopenia

Flow cytometric analysis of 10 WT vs. 10 orph mice revealed a marked reduction in platelet counts of ~90% compared to WT controls (**Fig. 12 A**) as well as a doubled platelet size (**Fig. 12 B**), a constellation clinically reflecting a severe macrothrombocytopenia.

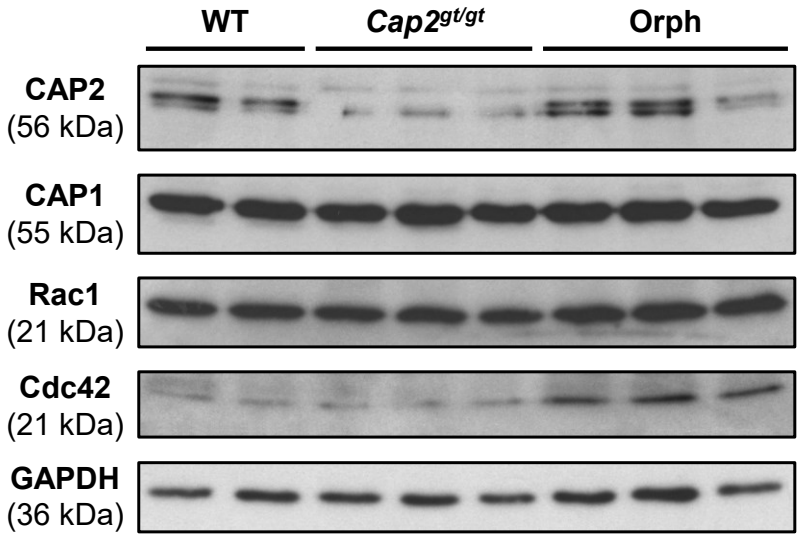

Fig. 11: Orph platelets express both CAP isoforms as well as the Rho-GTPases Rac1 and Cdc42

Platelet lysates from wild-type (WT), CAP2 knockout (*Cap2*$^{gt/gt}$), and orphan (orph) mice were separated by SDS-PAGE and immunoblotted with anti-CAP2, anti-CAP1, anti-Rac1, and anti-Cdc42 antibody. GAPDH was detected as loading control.

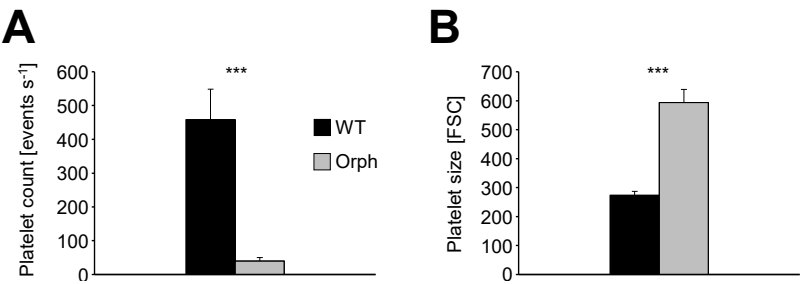

Fig. 12: Orph mice show a severe macrothrombocytopenia

Platelet count **(A)** and size **(B)** of wild-type (WT) and orphan (orph) mice were determined by flow cytometry. Results are displayed as mean ± SD of 10 mice per group. FSC, forward scatter; Student's t-test: ***, $p < 0.001$

4.2.3 Orph mice display a heterogeneous platelet size and a mild normocytic anemia

The severe macrothrombocytopenia of orph mice raised the question if other hematologic cell lines were affected as well. To address this question, basic

blood parameters of WT and orph mice were assessed on an automated hematology analyzer.

In agreement with the flow cytometric dataset, a pronounced macrothrombocytopenia was observed in orph mice (**Fig. 13 A, B**). The platelet distribution width (PDW) reflects the uniformity of individual platelet sizes in a given sample. The elevated PDW in orph mice indicated that their platelets varied more in size than those of their WT littermate controls (**Fig. 13 C**).

In addition to the low platelet count in orph mice, their red blood cell numbers were reduced as well (**Fig. 14 B**). This finding pointed to a general hematopoietic defect, exceeding platelet production.

Next, three important red blood cell parameters were evaluated. While hematocrit (HCT) — the volume percentage of erythrocytes in blood (**Fig. 15 A**) — and hemoglobin concentration (Hb) were significantly reduced (**Fig. 15 B**), the mean corpuscular volume (MCV) — a marker for the average volume of a red blood cell — was unaltered in orph mice (**Fig. 15 C**). This constellation of reduced HCT and Hb together with a normal MCV clinically represented a mild normocytic anemia, further suggesting a generalized hematopoietic defect or excessive bleeding.

A normal MCV, however, does not preclude *per se* pathologic changes in red blood cell morphology (termed poikilocytosis) or an abnormally large variation of individual cell sizes (anisocytosis). Hence, blood smears were prepared, stained according to Pappenheim (May–Grünwald–Giemsa staining), and studied by light microscopy. WT erythrocytes displayed the characteristic biconcave shape of red blood cells (**Fig. 16**). The appearance of orph erythrocytes was comparable, ruling out the possibility of poikilo- or anisocytosis.

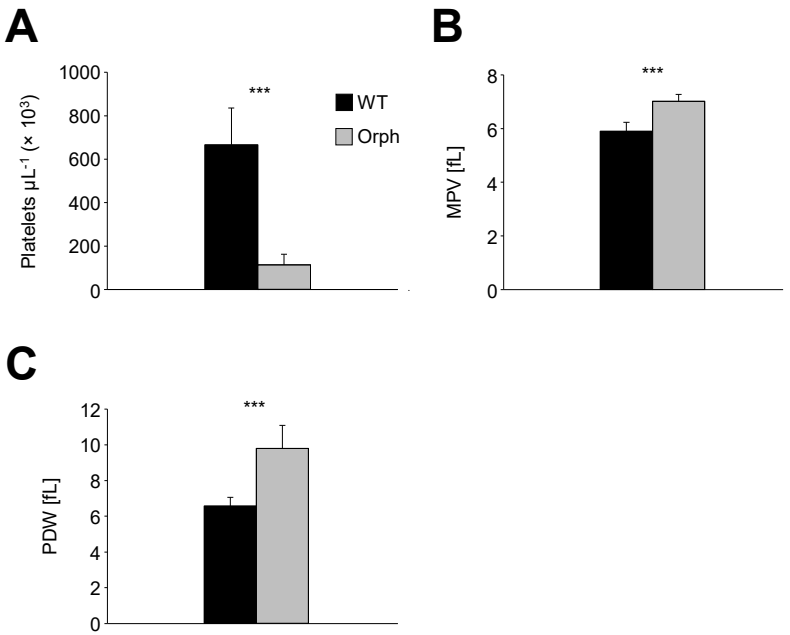

Fig. 13: Macrothrombocytopenia in orph mice is characterized by a heterogeneous platelet size

Platelet count **(A)**, mean platelet volume **(B)**, and platelet distribution width **(C)** were measured in heparinized whole blood from wild-type (WT) and orphan (orph) mice on an automated blood cell analyzer. Results are displayed as mean ± SD of 8 mice per group. MPV, mean platelet volume; PDW, platelet distribution width; Student's t-test: ***, $p < 0.001$

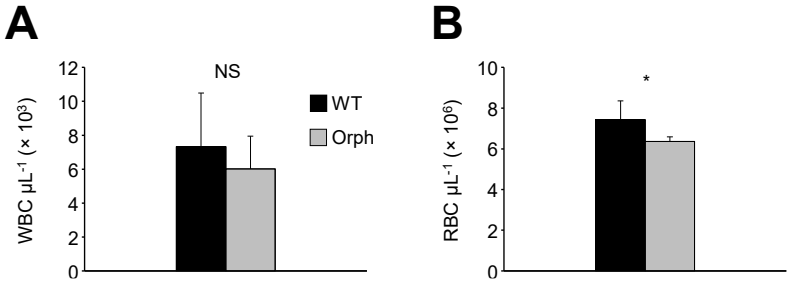

Fig. 14: Erythrocytopenia in orph mice

White **(A)** and red blood cell numbers **(B)** were assessed in heparinized whole blood from wild-type (WT) and orphan (orph) mice on an automated blood cell analyzer. Results are displayed as mean ± SD of 8 mice per group. WBC, white blood cells; RBC, red blood cells; Student's t-test: *, $p < 0.05$; NS, not significant

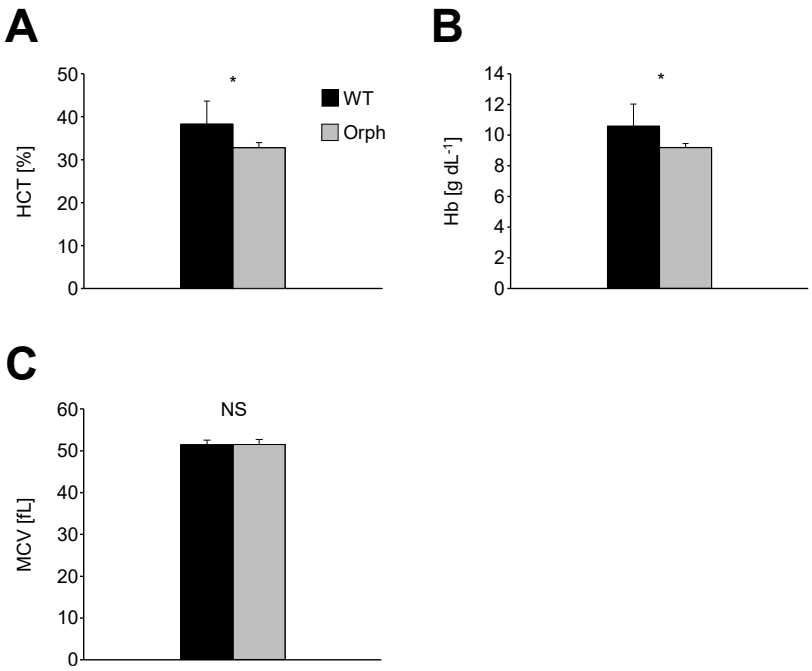

Fig. 15: Orph mice display a mild normocytic anemia

Hematocrit **(A)**, hemoglobin concentration **(B)**, and mean corpuscular volume **(C)** were determined in heparinized whole blood from wild-type (WT) and orphan (orph) mice on an automated blood cell analyzer. Results are displayed as mean ± SD of 8 mice per group. HCT, hematocrit; Hb, hemoglobin concentration; MCV, mean corpuscular volume; Student's t-test: *, $p < 0.05$; NS, not significant

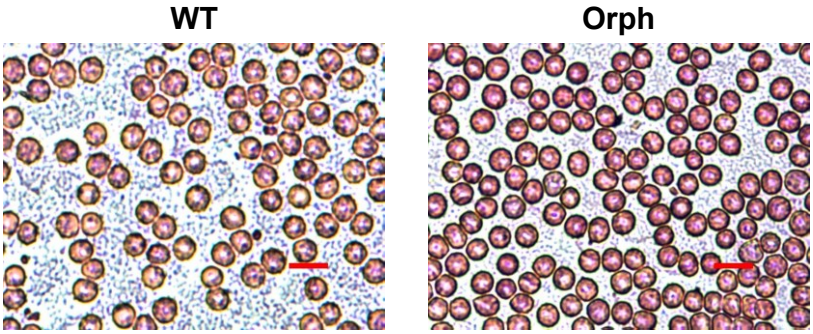

Fig. 16: Unaltered red blood cell morphology in orph mice

Smears of heparinized whole blood from wild-type (WT) and orphan (orph) mice were generated, stained according to May–Grünwald, and counterstained with Giemsa (Pappenheim's panoptic staining). Analysis was performed on a light microscope. Scale bar, 10 µm

4.2.4 Fibrosis of and increased MK numbers in the BM of orph mice

In order to study the underlying cause of the severe thrombocytopenia in orph mice, the BM — as primary hematopoietic site — was histologically analyzed on H&E-stained paraffin sections of femora. Light microscopic examination revealed a uniform morphology of WT MKs; in contrast, MK morphology in orph mice was strikingly heterogeneous (**Fig. 17 A**; **arrows**).

Additionally, indications of fibrosis were observed in H&E-stained BM sections of orph mice. To confirm this observation, a silver staining according to Gordon & Sweets, which is more sensitive in the detection of reticular fibers than the conventional H&E stain, was performed. In agreement with the initial observation, an increased presence of reticular fibers was found in the BM of orph mice (**Fig. 17 B**), especially in the epi- and metaphyses, indicating that BM fibrosis might account for the severe macrothrombocytopenia in orph mice. Of note, the diaphyses of orph femora were mostly spared from fibrosis.

Due to the altered morphology of orph MKs, whole femora cryosections of WT and orph mice were generated, immunostained, and BM MK numbers and morpholgy were further characterized by confocal microscopic analysis. Interestingly, orph mice displayed ~70% more MKs per visual field than their WT littermates (WT: 10.9 ± 2.4 MKs per visual field; orph: 18.4 ± 1.0 MKs per visual field; **Fig. 18 A**), reflecting the increased platelet need.

Moreover, close-up views of the BM cryosections were taken in order to study MK morphology in more detail. The appearance of WT MKs was homogeneous and they were located adjacent to BM sinusoids (**Fig. 19 A**). Occasionally, WT MKs extending proplatelets into the sinusoidal lumen could be found (**Fig. 19 A**; **arrowhead**). Orph MKs, on the other hand, displayed an aberrant and heterogeneous morphology, yet also formed proplatelets.

These elongations, however, appeared to occur randomly and not directed since they did not extend into the direction of adjacent vessel lumina but instead pointed into the BM cavity (**Fig. 19 B**; **solid arrows**). In line with this observation, signs of a premature platelet release into the BM were detected (**Fig. 19 B**; **dashed arrow**). The non-directed proplatelet formation together with the premature platelet release into the BM may contribute to the severe thrombocytopenia in orph mice.

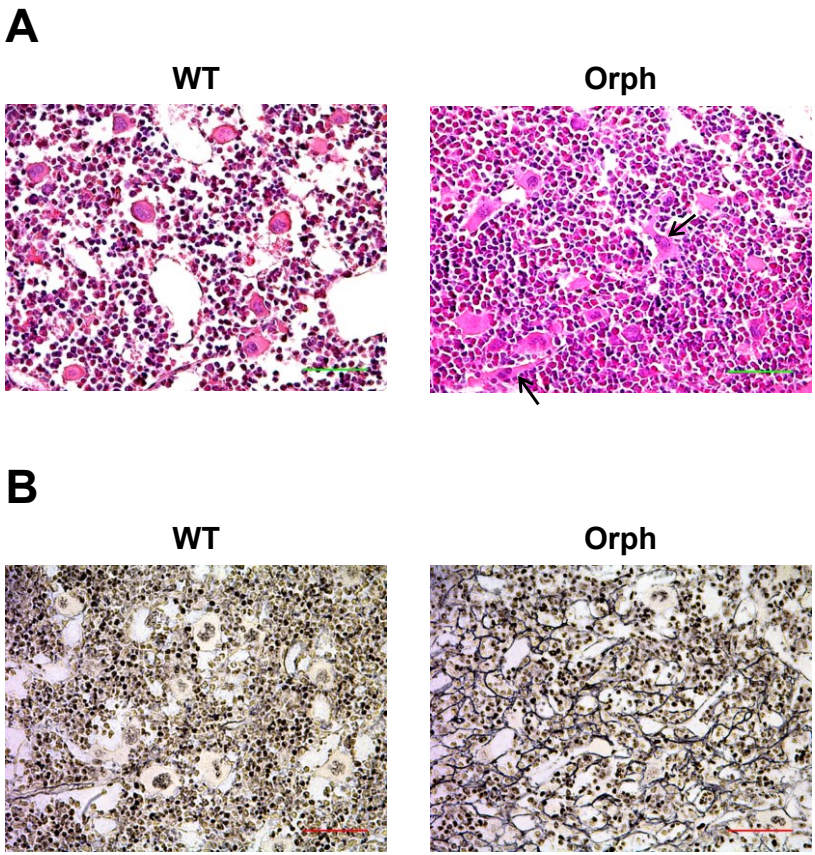

Fig. 17: Orph mice display a heterogeneous MK morphology and develop BM fibrosis

Representative light microscopy images of H&E **(A)** or silver stained (according to Gordon & Sweets) BM sections **(B)** of wild-type (WT) and orphan (orph) mice (n = 4 mice per group) are shown. Arrows indicate aberrantly shaped MKs. Scale bar, 50 µm

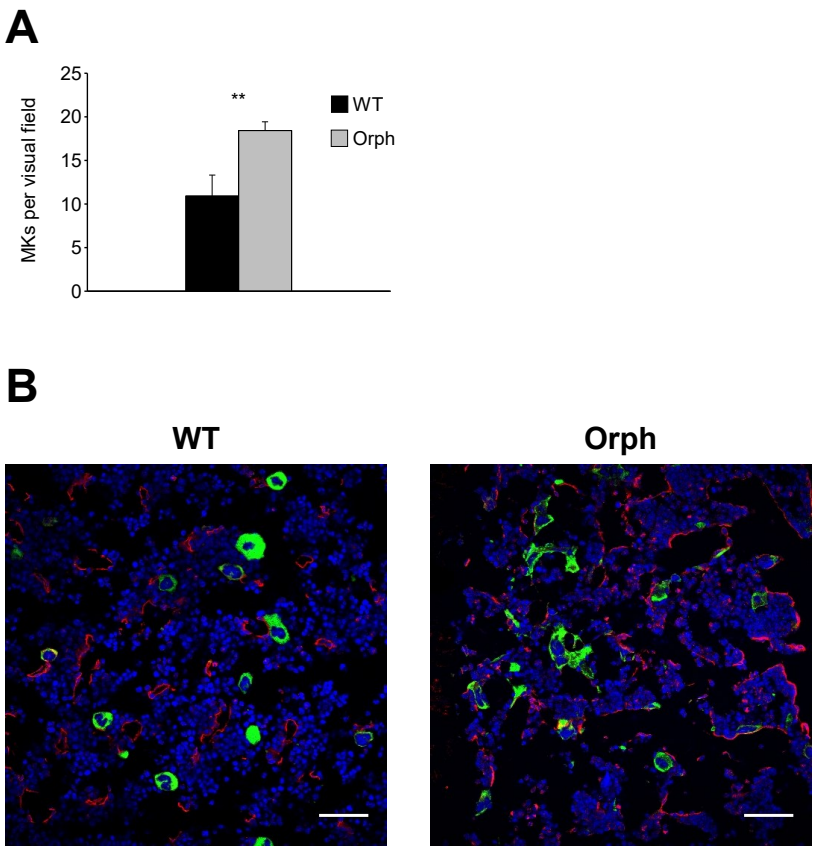

Fig. 18: Increased MK numbers in the BM of orph mice

Whole femora cryosections were stained with fluorophore-conjugated antibodies directed against GPIb (green) and CD105 (red) to specifically label MKs/platelets and endothelial cells, respectively. Nuclei were visualized with DAPI (blue). Specimens were investigated by confocal microscopy and the number of MKs per visual field (387.5 × 387.5 µm) was determined. A comparison of MK numbers between wild-type (WT) and orphan (orph) BM **(A)** and representative images **(B)** are shown. Results are displayed as mean ± SD of 4 mice per group. Student's t-test: **, $p < 0.01$. Scale bar, 50 µm

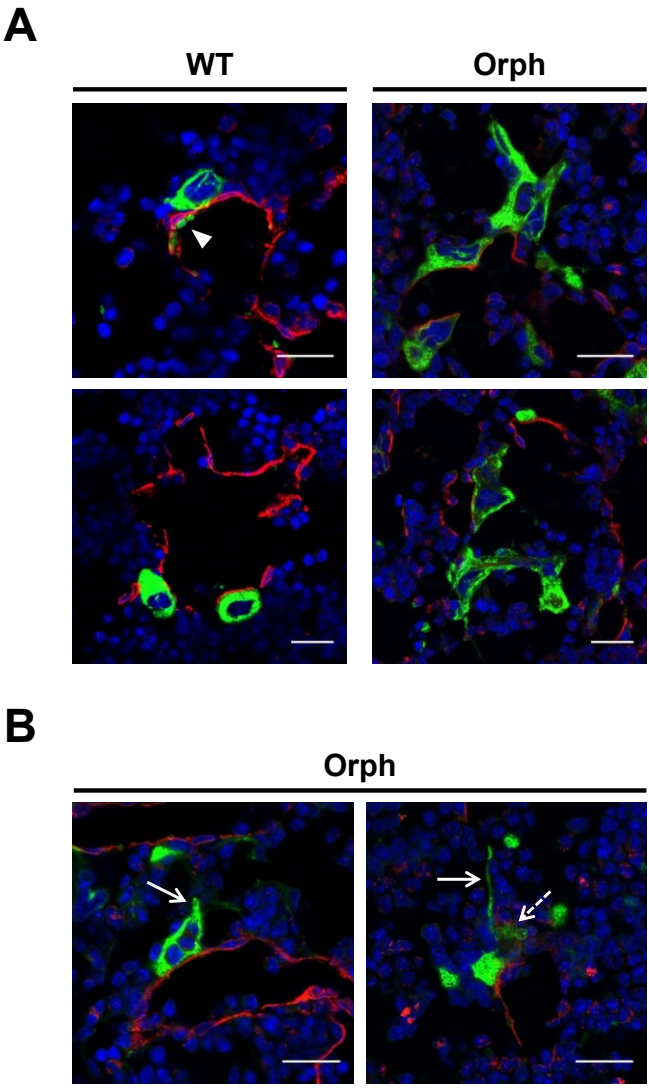

Fig. 19: Orph MKs have an altered morphology and appear to extend aberrant protrusions

A morphologic comparison between wild-type (WT) and orphan (orph) MKs on immunostained cryosections of femora **(A)** and examples of abnormal extensions formed by orph MKs **(B)** are depicted. The arrowhead indicates physiologic proplatelet formation whereas the solid arrows highlight aberrant MK protrusions. The dashed arrow refers to signs of premature platelet release into the BM cavity. Scale bar, 20 µm

4.2.5 Extramedullary hematopoiesis in orph mice

Hematologic disorders are often accompanied by splenomegaly, an increase in spleen size and weight.[72] Therefore, body and spleen weights of WT and orph mice were measured and the spleen-to-body weight ratio was calculated. Remarkably, the spleen-to-body weight ratio was nearly doubled in orph mice compared to WT controls (**Fig. 20 A**, **B**).

Splenomegaly as a symptom of BM pathologies in both humans and mice may be elicited by extramedullary hematopoiesis. In states of thrombocytopenia, for example, MKs in the spleen proliferate, thus (partially) compensating for the platelet production deficit of the BM.[73,74] To investigate this further, spleen sections of WT and orph mice were prepared, stained with H&E, and the abundance of MKs was assessed. Orph mice displayed a non-significant trend ($p = 0.0502$) towards elevated numbers of splenic MKs (**Fig. 20 C**, **D**).

In order to test if other organs also showed pathologic alterations, H&E-stained paraffin sections of heart, lung, liver, kidney, thymus, and lymph nodes were analyzed; yet, no striking histologic abnormalities were observed (**Fig. 21**), hence restricting the phenotype of orph mice to the hematopoietic system and to the circulation for the present.

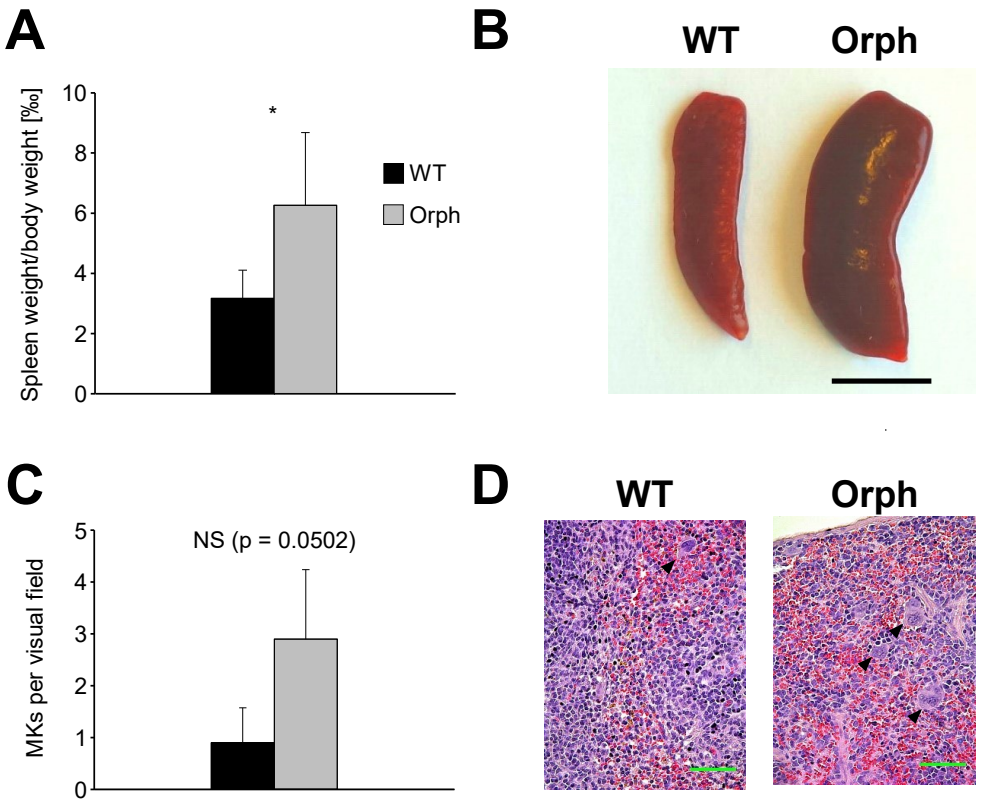

Fig. 20: Orph mice show an increased spleen-to-body weight ratio

Assessment of the spleen-to-body weight ratio (n = 7 mice per group) **(A)**, a representative photo of spleens from wild-type (WT) and orphan (orph) mice **(B)**, a comparison of splenic MK numbers (n = 4 mice per group; 294 × 221 µm) **(C)**, and representative histological images **(D)** are shown. Arrowheads point at MKs. Results are displayed as mean ± SD. Student's t-test: *, $p < 0.05$; NS, not significant. Black scale bar, 5 mm; green scale bar, 50 µm

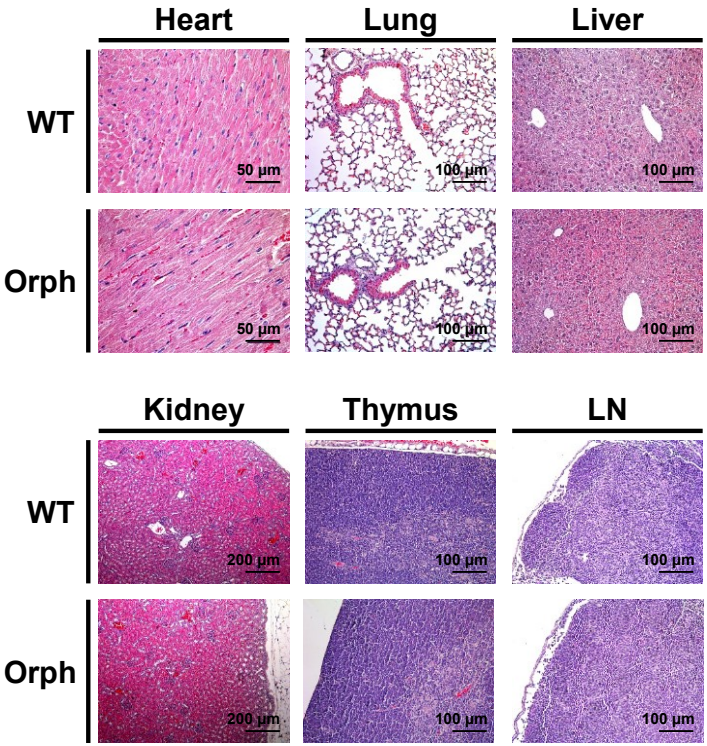

Fig. 21: Normal histology of the heart, lung, liver, kidney, thymus, and lymph nodes in orph mice

Paraffin sections of heart, lung, liver, kidney, thymus, and lymph nodes (LN) of wild-type (WT) and orphan (orph) mice (n = 4 mice per group) were stained with H&E and studied on a light microscope.

4.2.6 GPVI expression is halved in orph platelets

Since a platelet production defect may also lead to impaired platelet function, a detailed functional characterization of orph platelets was performed. First of all, expression levels of prominent platelet surface molecules were determined. While the expression levels of GPIX, GPIIbIIIa, or α2 integrin were increased in orph platelets compared to WT controls (**Fig. 22**), concordant with the increased platelet size, expression levels of GPIb, β1 integrin, or CD9 were reduced. Most strikingly, the surface prevalence of GPVI on orph platelets was decreased by ~50% as compared with WT controls.

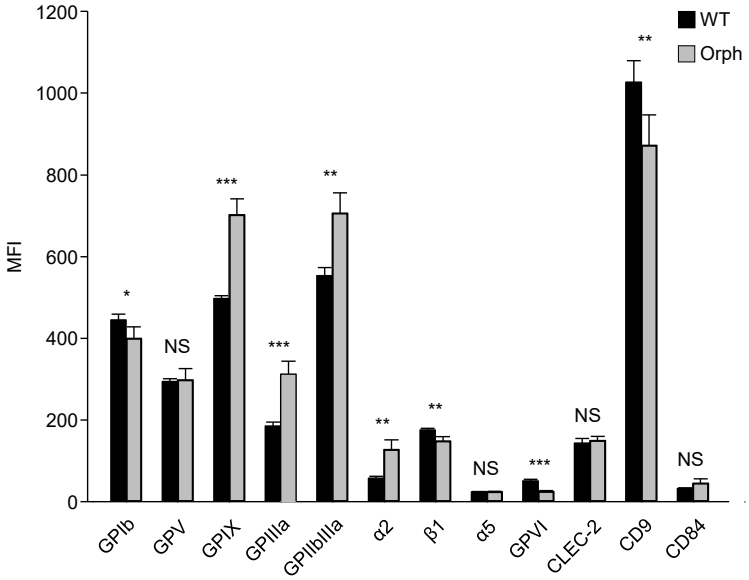

Fig. 22: GPVI levels are halved in orph platelets

Expression levels of prominent surface molecules of wild-type (WT) and orphan (orph) platelets were assessed by flow cytometry. Results are displayed as mean ± SD of 4 mice per group. MFI, mean fluorescence intensity; Student's t-test: *, $p < 0.05$; **, $p < 0.01$; ***, $p < 0.001$; NS, not significant

4.2.7 Orph platelets display a degranulation and integrin activation defect

Next, platelet signaling was investigated, evaluating two platelet activation parameters: transition of GPIIbIIIa from resting to active state and recruitment of P-selectin to the cell membrane, serving as a measure of α-granule release. In contrast to WT controls, GPIIbIIIa activation upon stimulation with the GPVI agonist CRP was severely reduced at all tested concentrations in orph platelets (**Fig. 23 A**). This observation may be explained by the reduced receptor density of GPVI (**Fig. 22**) or by a generalized ITAM-specific signaling defect in orph platelets. Furthermore, assessment of P-selectin exposure revealed an overall impaired α-granule release in response to all tested agonists (**Fig. 23 B**).

4.2.8 Orph platelets show a reduced β1 integrin activation upon stimulation with CRP or thrombin

In order to determine whether the observed activation defect of integrins in response to ITAM stimulation is restricted to GPIIbIIIa, β1 integrin activation was analyzed. Platelets from WT and orph mice were incubated with FITC-labeled 9EG7 antibody directed against active β1 integrin, stimulated with different agonists, and examined by flow cytometry. Orph platelets showed a reduced β1 integrin activation upon stimulation with high and intermediate concentrations of CRP or thrombin as compared with WT controls (**Fig. 24**). Of note, the surface abundance of active β1 integrin under resting conditions was higher in orph platelets than in WT controls. Taken together, these findings suggest a generalized ITAM-specific signaling defect in orph platelets.

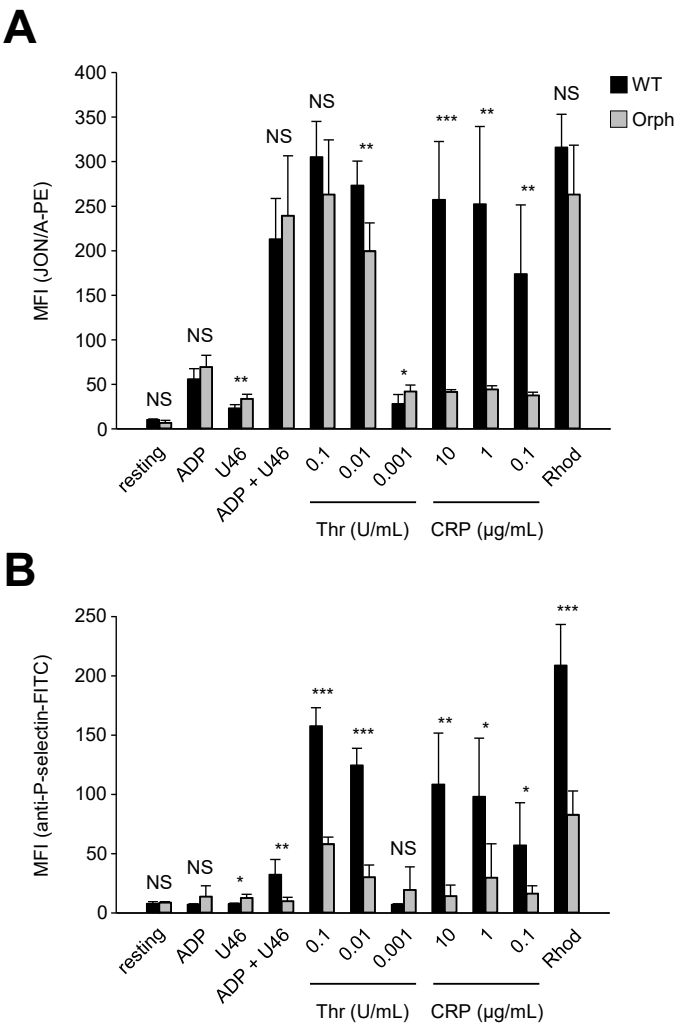

Fig. 23: Orph platelets display marked activation defects

GPIIbIIIa activation **(A)** and P-selectin exposure **(B)** of wild-type (WT) and orphan (orph) platelets following stimulation with the indicated agonists were assessed by flow cytometry. The final concentrations of thrombin and CRP are depicted; ADP: 10 µM; U46: 1 µM; Rhod: 1 µg/mL. Results are mean ± SD of 4 mice per group. MFI, mean fluorescence intensity; U46, U46619; Rhod, rhodocytin; Student's t-test: *, $p < 0.05$; **, $p < 0.01$; ***, $p < 0.001$; NS, not significant

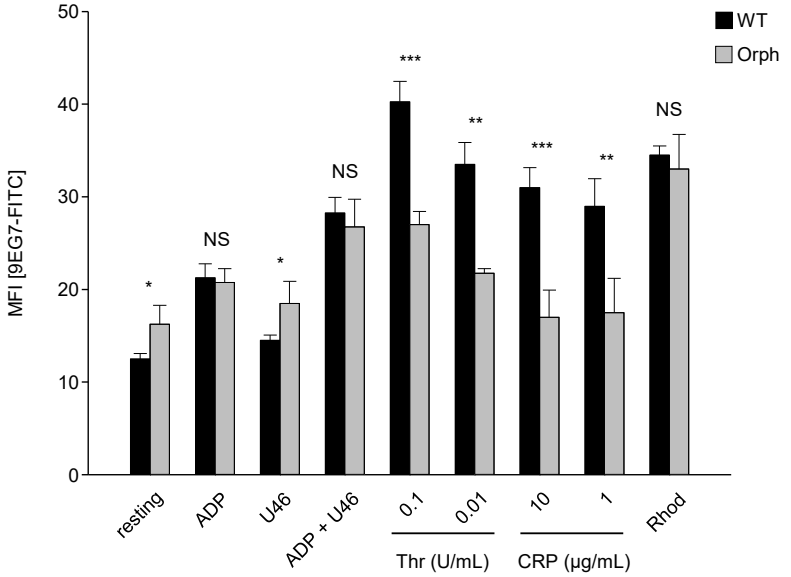

Fig. 24: Altered activation of β1 integrin in orph platelets

Washed platelets from wild-type (WT) and orphan (orph) mice were incubated with FITC-labeled 9EG7 antibody, stimulated with the indicated agonists, and investigated by flow cytometry. The final concentrations of thrombin and CRP are depicted; ADP: 10 µM; U46: 1 µM; Rhod: 1 µg/mL. Results are mean ± SD of 4 mice per group. MFI, mean fluorescence intensity; U46, U46619; Rhod, rhodocytin; Student's t-test: *, $p < 0.05$; **, $p < 0.01$; ***, $p < 0.001$; NS, not significant

4.2.9 Impaired α-granule release might account for the hyporesponsiveness of orph platelets

The defective P-selectin exposure observed in orph platelets (**Fig. 23**) could either be due to impaired α-granule release or to *a priori* diminished contents of recruitable P-selectin therein.

To test this, the prevalence of the α-granular proteins vWF, P-selectin, fibrinogen, fibronectin, and β1 integrin in WT and orph platelets was determined. Surprisingly, despite the significantly increased platelet size, the content of the tested proteins was unaltered in orph platelets (**Fig. 25**).

Furthermore, analysis of platelet samples by transmission electron microscopy (TEM) allowed the direct visualization of α-granules in both WT and

orph platelets (**Fig. 26**). These findings clearly demonstrate that a defective granule release accounts for the impaired P-selectin exposure in orph platelets.

Besides P-selectin, various other membrane proteins are stored in α-granules and become exposed on the platelet surface upon stimulation.[17] If orph platelets indeed manifested impaired α-granule secretion, recruitment of α-granular proteins other than P-selectin during platelet activation should be minimized, too. To test this hypothesis, platelets from WT and orph mice remained resting or were stimulated with 0.1 U/mL thrombin, incubated with fluorophore-labeled antibodies directed against integrins α2, α5, β1, and GPIIbIIIa, and the ratios between surface abundance in activated versus resting platelets were determined by flow cytometry. For all tested molecules except for GPIIbIIIa, the rise in surface expression was significantly lower in orph platelets than in WT controls (**Fig. 27 A**), thus corroborating the impaired α-granule release.

In contrast to the aforementioned proteins, the GPIb–IX–V receptor complex is downregulated by proteolysis or by receptor internalization upon platelet stimulation. While GPIbα is predominantly shed by A Disintegrin And Metalloproteinase (ADAM)17, GPV is cleaved by ADAM10, ADAM17, and thrombin.[75] To test whether ectodomain shedding contributes to the altered surface expression of different GPs, downregulation of GPIb and GPV was investigated by flow cytometry. Of note, a markedly reduced downregulation of GPIb and a slightly reduced downregulation of GPV were observed in orph platelets (**Fig. 27 B**).

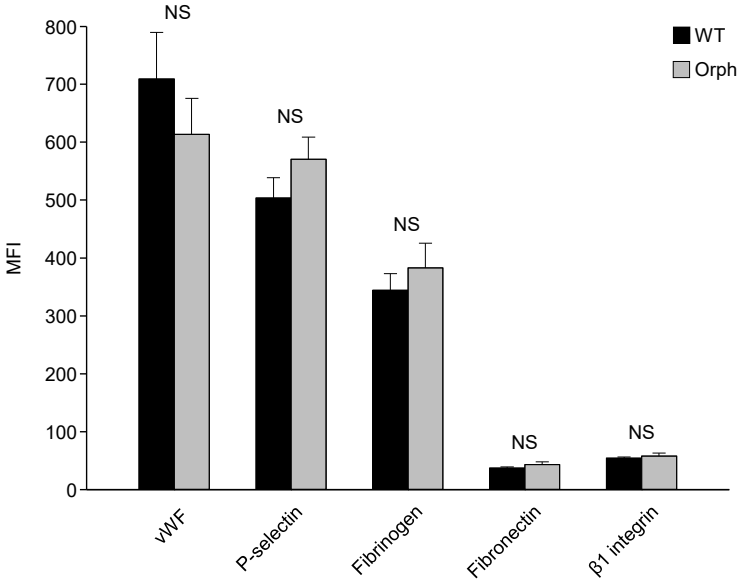

Fig. 25: Unaltered content of α-granular proteins in orph platelets

Washed wild-type (WT) and orphan (orph) platelets were fixed, permeabilized, stained with FITC-labeled antibodies directed against the indicated molecules, and the respective MFI values were determined by flow cytometry. Results are displayed as mean ± SD of at least 4 mice per group. MFI, mean fluorescence intensity; Student's t-test: NS, not significant

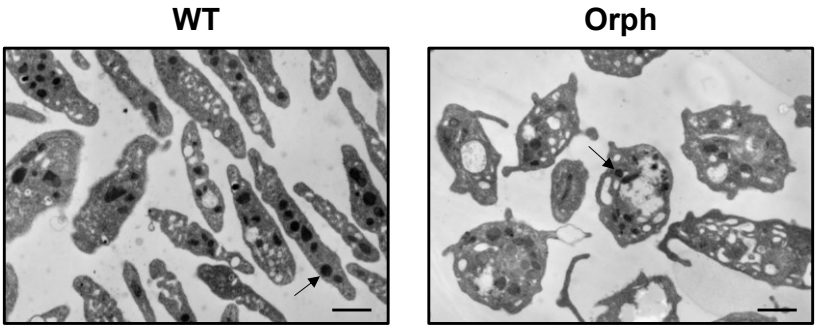

Fig. 26: Orph platelets contain α-granules

Ultrathin sections of platelet samples from wild-type (WT) and orphan (orph) mice (n = 3 mice per group) were prepared, stained with uranyl acetate and lead citrate, and analyzed on a transmission electron microscope. Arrows indicate platelet α-granules. Scale bar, 1 µm

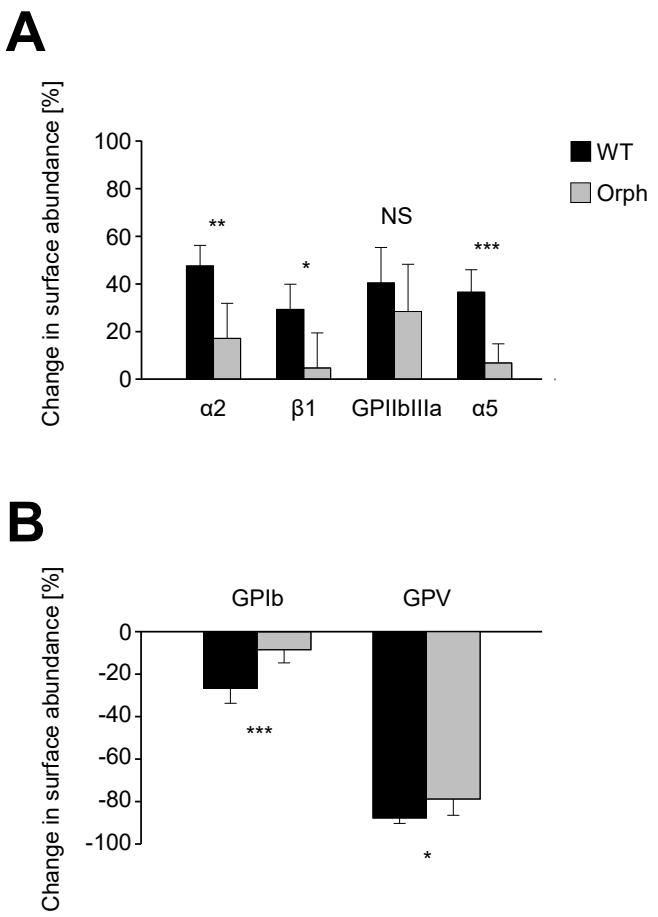

Fig. 27: Thrombin-induced surface recruitment and shedding of GPs are diminished in orph platelets

Platelets from wild-type (WT) and orphan (orph) mice were incubated with FITC-labeled antibodies directed against the indicated proteins in the presence or absence of 0.1 U/mL thrombin, and analyzed by flow cytometry. Mean fluorescence intensities of the target proteins were measured under resting and activating conditions, and the change in surface abundance was calculated according to the formula depicted in **3.2.6.4**. Increases in surface abundance correspond to protein recruitment from α-granules to the cell surface **(A)**, while decreases reflect GP ectodomain shedding by thrombin **(B)**. Results are mean ± SD of 6 mice per group. Student's t-test: *, $p < 0.05$; **, $p < 0.01$; ***, $p < 0.001$; NS, not significant

4.2.10 Spreading of orph platelets on fibrinogen is severely delayed

To test whether platelet outside-in signaling was also affected, WT and orph platelets were allowed to spread on fibrinogen-coated glass slides for three different time intervals (5, 15, and 30 min). After 5 min, the percentage of filopodia-forming platelets was significantly increased among orph platelets compared to WT controls (**Fig. 28**; WT: 32 ± 6%; orph: 47 ± 2%; p = 0.0355). At the 15-min time point, however, the abundances of advanced spreading stages (formation of both filo- and lamellipodia and full spreading) were dramatically reduced among orph platelets. This observation could be confirmed after 30 min: while 41 ± 8% of WT platelets had fully spread, only 7 ± 4% of orph platelets had proceeded to the final spreading stage (p = 0.0076). In conclusion, spreading of orph platelets on fibrinogen was severely delayed. Moreover, orph platelets appeared to form more and longer filopodia than WT controls at all time points investigated, resulting in a generally "spikier" appearance (**Fig. 29**).

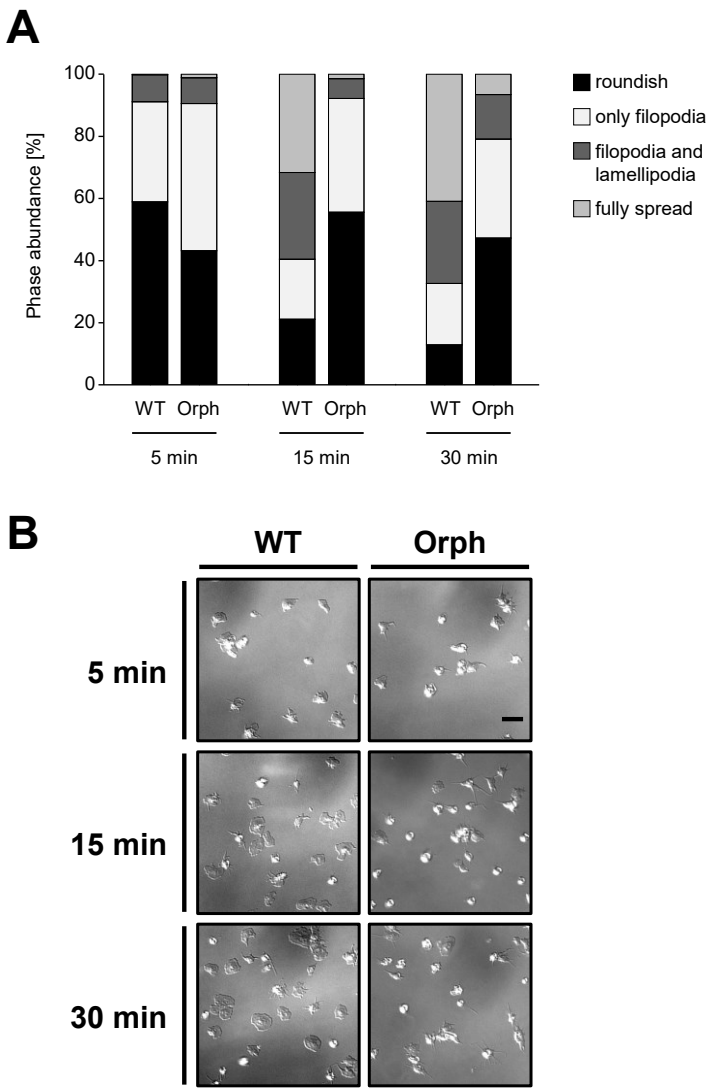

Fig. 28: Spreading of orph platelets on fibrinogen is dramatically delayed

Washed wild-type (WT) and orphan (orph) platelets (n = 3 mice per group) were stimulated with thrombin (0.01 U/mL), allowed to spread on a fibrinogen matrix (100 µg/mL) for three different time periods (5, 15, and 30 min), and analyzed by DIC microscopy. Phase abundances of four spreading stages **(A)** and representative DIC images **(B)** are shown. Scale bar, 5 µm

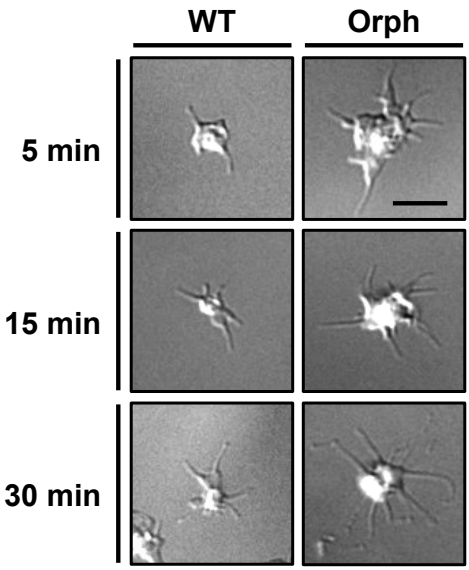

Fig. 29: Orph platelets appear to form more and longer filopodia than WT controls when spreading on fibrinogen

Spreading of wild-type (WT) and orphan (orph) platelets on a fibrinogen matrix was carried out as described in **Fig. 28**. General platelet morphology was studied by DIC microscopy. Scale bar, 2 µm

4.2.11 Unaltered filopodia formation of orph platelets on von Willebrand factor

Due to the spiky morphology of orph platelets upon spreading on fibrinogen, filopodia formation was specifically examined in a spreading assay on a vWF matrix. To this end, platelet integrins were blocked with eptifibatide (integrilin®) prior to induction of GPIb clustering by botrocetin, a viper venom protein from *Bothrops jararaca*. While eptifibatide reversibly inhibits GPIIbIIIa,[28] botrocetin enables clustering and binding of GPIbα to vWF under static conditions.[23] Platelets were then allowed to spread on vWF-coated cover slips for 15 min. The subsequent analysis was performed by DIC microscopy, dividing platelets into three categories depending on the number of filopodia they each formed: no filopodia, 1–3 filopodia, or more than 3 filopodia per platelet (see also **Fig. 6**). This experiment allowed a specific investigation of

Cdc42-mediated filopodia formation in response to GPIb–IX–V receptor signaling. A slight, yet non-significant, trend towards elevated numbers of filopodia was observed among orph platelets (**Fig. 30**), indicating that the high number of filopodia in orph platelets upon spreading on fibrinogen was not due to increased Cdc42 signaling.

4.2.12 Perturbed cytoskeletal architecture in orph platelets

In order to study cytoskeletal rearrangements, WT and orph platelets remained resting or were allowed to spread on fibrinogen, were fixed, stained for different cytoskeletal components, and analyzed by confocal microscopy.

First, filamentous actin and microtubules were stained with fluorophore-conjugated phalloidin and an anti-α-tubulin antibody, respectively, and general platelet morphology was compared between WT and orph samples. Under resting conditions, both WT and orph platelets displayed the characteristic discoid shape (**Fig. 31 A**). Some orph platelets, however, were more ellipsoid than WT controls. In contrast, upon spreading for 15 min, the majority of WT platelets had proceeded to advanced spreading stages and many had already fully spread (**Fig. 31 B**), whereas most of the orph platelets still maintained filopodia, indicative of delayed spreading and supporting the findings obtained by DIC microscopy in **4.2.10**.

The analysis of the cytoskeletal architecture revealed three major differences between WT and orph platelets: first, microtubules in resting and spread orph platelets were not arranged into the typical ring underlying the cell periphery — the so-called marginal band — but were instead distributed throughout the cytoplasm in a disorganized, convoluted manner (**Fig. 31** and **Fig. 32 A**). Second, numerous accumulations of filamentous actin were present in orph platelets, presumably actin nodules, while they could exceedingly rarely be detected in WT controls (**Fig. 32 B**). Additionally, in orph platelets F-actin

was assembled into a massive ring located between the platelet center and the cell periphery (**Fig. 33**). Third, orph platelets frequently displayed a spiky, filopodia-rich morphology (**Fig. 32 C**).

β3 integrin is a constituent of two important platelet ECM receptors, αIIbβ3 and αvβ3.[23] Talin, on the other hand, is an adaptor protein that links αIIbβ3 to the actin cytoskeleton. Binding of talin to the tail of β3 integrins has been demonstrated to be a prerequisite for integrin activation.[76] To test whether talin recruitment is altered and hence accounts for the impaired integrin activation in orph platelets (**Fig. 23 A** and **Fig. 24**), spread platelets were stained for talin and β3 integrins and analyzed by confocal microscopy.

In agreement with previous reports,[76] talin and β3 integrin co-localized particularly at the leading edge of WT platelets (**Fig. 33**). A similar cortical co-localization of talin and β3 integrin was observed in orph platelets; however, in contrast to WT platelets, talin and β3 integrin also strongly accumulated in the center of orph platelets. Together, these results suggest that impaired trafficking of talin and β3 integrins may underlie the integrin activation defect observed in orph platelets.

In summary, the cytoskeleton of orph platelets was characterized by disorganized microtubules and accumulations of F-actin, presumably in actin nodules, in numerous filopodia, and in a massive ring-shaped structure.

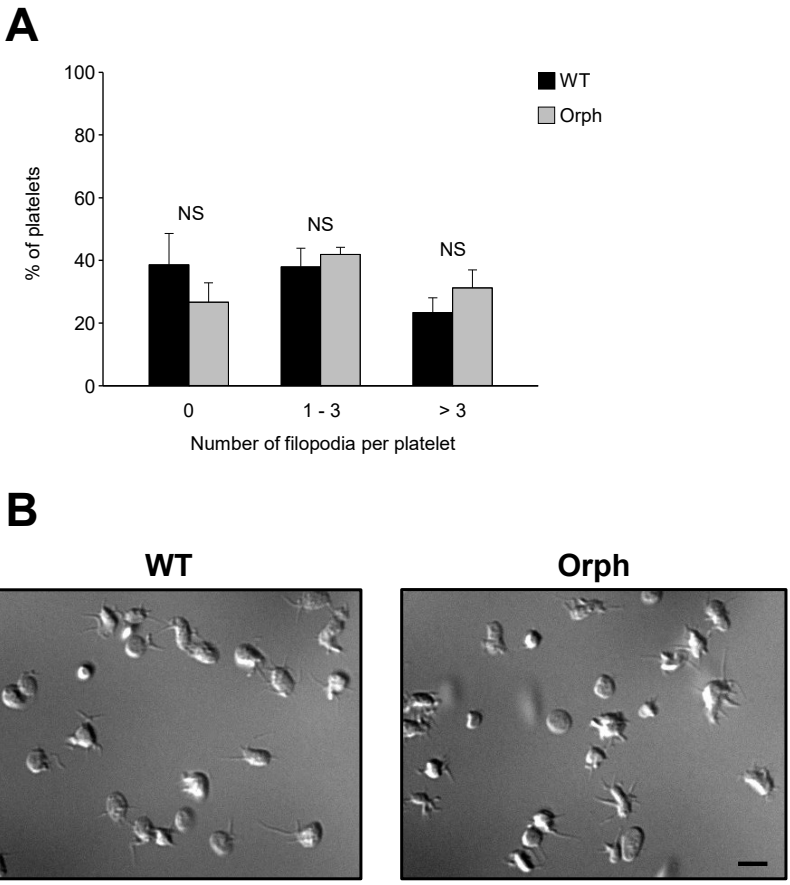

Fig. 30: Unaltered spreading of orph platelets on vWF

Washed wild-type (WT) and orphan (orph) platelets (n = 3 mice per group) were treated with eptifibatide (40 µg/mL) and botrocetin (2 µg/mL), allowed to spread on a vWF matrix for 15 min, and analyzed by DIC microscopy. Platelets were divided into three categories depending on the number of formed filopodia (0, 1–3, or >3 filopodia per platelet; **Fig. 6**), and the percentage value of each category was calculated. An evaluation of the spreading assay **(A)** and representative DIC images **(B)** are shown. Student's t-test: NS, not significant. Scale bar, 2 µm

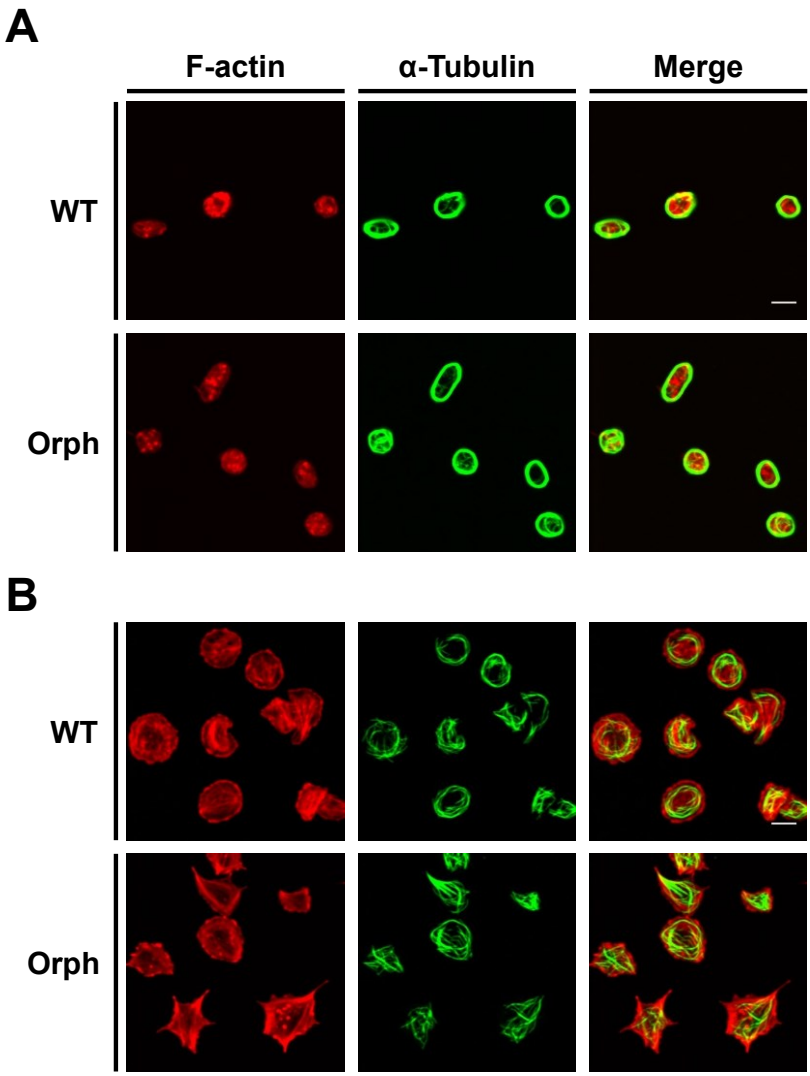

Fig. 31: Delayed spreading of orph platelets on fibrinogen

Washed platelets from wild-type (WT) and orphan (orph) mice either remained resting and were allowed to adhere to poly-L-lysine-coated cover slips **(A)** or were stimulated with thrombin (0.01 U/mL) and allowed to spread on a fibrinogen matrix (100 µg/mL) for 15 min **(B)**. F-actin (red) and α-tubulin (green) were visualized with ATTO 647N-labeled phalloidin and Alexa Fluor® 488-conjugated anti-α-tubulin antibody, respectively. Samples were analyzed by confocal microscopy. Scale bars, 3 µm

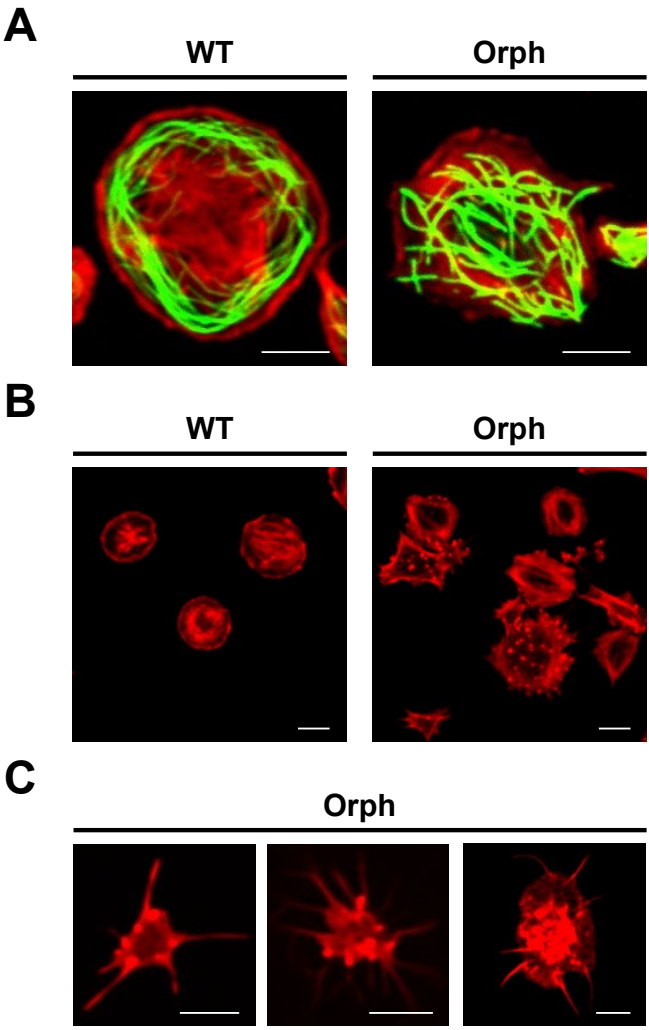

Fig. 32: Orph platelets display an aberrant cytoskeletal organization

Wild-type (WT) and orphan (orph) platelets were prepared for confocal microscopy and analyzed as delineated in **Fig. 31**. F-actin and α-tubulin are displayed in red and green, respectively. A comparison of microtubule organization **(A)**, presence of actin nodules **(B)**, and examples of filopodia-extending orph platelets **(C)** are shown. Scale bars, 3 µm

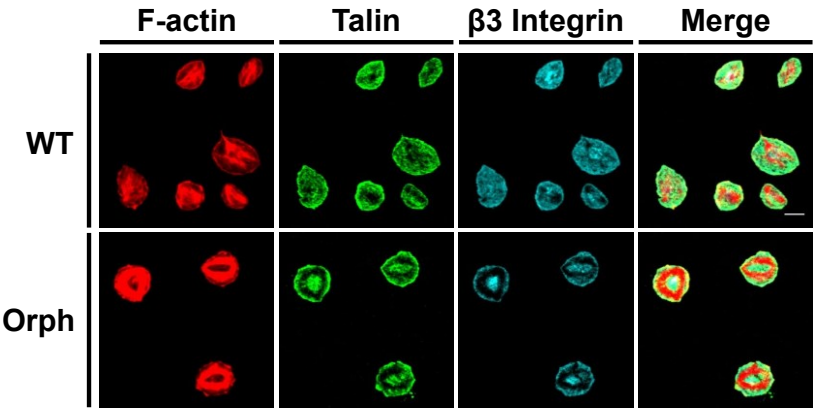

Fig. 33: Altered recruitment of β3 integrins to the leading edge of spread orph platelets

Washed platelets from wild-type (WT) and orphan (orph) mice were allowed to spread on a fibrinogen matrix (100 µg/mL) for 15 min. F-actin (red) was labeled with ATTO 647N-conjugated phalloidin while talin (green) and β3 integrin (cyan) were labeled using primary and fluorophore-conjugated secondary antibodies. Samples were visualized by confocal microscopy. Scale bar, 3 µm

5 Discussion

5.1 The role of CAP2 in platelets

Cyclase-associated proteins are evolutionarily highly conserved actin-binding proteins which exert important roles in a myriad of cellular processes such as endocytosis, determination of cell size, polarity, cytokinesis, and development.[33,36] Mammalian cells express two CAP isoforms, CAP1 and CAP2. In mice, CAP1 is expressed ubiquitously (except for skeletal muscle), while CAP2 has so far only been detected in brain, heart, skeletal muscle, skin, and testis.[41] To date, ASP-56 is the sole CAP isoform identified in pig platelets. ASP-56 was discovered in 1992 by Gieselmann and Mann who described its actin-sequestering properties.[51] Sequence analyses later confirmed that ASP-56 is equal to porcine CAP1.[36] Of note, the expression of a second mammalian CAP isoform, CAP2, in MKs/platelets has not yet been proven. To investigate the presence and putative function(s) of CAP2 in murine platelets, genetically modified mice constitutively lacking CAP2 (*Cap2*$^{gt/gt}$) and their wild-type littermates (*Cap2*$^{+/+}$) were analyzed in the course of this thesis.

Immunoblot experiments with platelet lysates revealed the presence of both isoforms, CAP1 and CAP2, in murine WT platelets (**Fig. 7**). Remarkably, the applied anti-CAP2 antibody detected three separate bands, of which only the most prominent was missing in CAP2-deficient platelets. This result is in agreement with a previous report by Bertling *et al.* who identified three distinct CAP2 splice variants in mouse heart, brain, skeletal muscle, and testis by Northern blot analysis.[70] However, we cannot confirm that the two faint additional bands detected by the anti-CAP2 antibody do indeed represent splice variants of CAP2 since they could merely represent proteins structurally related to CAP2 (or even structurally unrelated proteins), and not

CAP2 itself. In order to determine the identity of these additional bands, mass spectrometric analyses need to be performed. It has been demonstrated by Kosmas *et al.* that CAP1 is upregulated in skin lysates of CAP2-deficient mice.[44] In platelets, however, no upregulation of CAP1 in the absence of CAP2 could be detected (**Fig. 11**).

While platelet counts in peripheral blood were comparable in *Cap2*$^{gt/gt}$ and *Cap2*$^{+/+}$ mice, CAP2-deficient platelets were slightly larger than those of WT controls (**Fig. 8**). This observation is in line with previous findings in *Saccharomyces cerevisiae*[77,78] and the slime mold *Dictyostelium discoideum*[79] where CAP deficiency also led to increased cell sizes.

Bertling and colleagues have suggested that mammalian actin-binding proteins exist in a muscle and a nonmuscle isoform since actin turnover in myocytes is much slower than in nonmuscle cell types, and, therefore, might require different regulatory proteins.[80] While this rationale applies to the actin-binding proteins ADF/cofilin,[81] twinfilin,[82] and capping protein,[83] it currently remains elusive whether it is also true for mammalian CAP. Evidence in favor of this hypothesis comes from studies in the nematode (roundworm) *Caenorhabditis elegans* which possesses a muscle-specific CAP (CAS-1)[84] and a nonmuscle CAP (CAS-2).[36,85] In mice, ablation of CAP2 severely perturbs the well-orchestrated actin–myosin organization present in sarcomeres, the basic contractile units of striated muscle cells, thereby evoking a serious heart disease (dilated cardiomyopathy) which leads to premature death.[37] Sarcomeres are composed primarily of thick myosin and thin actin filaments that slide past each other to generate force. Sarcomeric F-actin undergoes little turnover and is tightly coiled with nebulin filaments to provide for stability during repetitive cycles of muscle contraction and relaxation.[86] According to a model proposed by Peche *et al.*, CAP2 localizes to the M-band of the sarcomere where it regulates the length of actin filaments through its F-actin-

severing activity.[37] In the *Cap2*$^{gt/gt}$ mouse model, CAP1 cannot compensate for the loss of CAP2, suggesting the possibility that CAP2 is the predominant isoform in cell types with slow actin dynamics such as (cardio)myocytes. Conversely, CAP1 could represent the nonmuscle isoform required in cell types with higher actin turnover velocities, e.g. platelets. In support of this notion, the expression level of CAP1 in hematopoietic cells is more than 100 times higher than that of CAP2 (biogps.org).

In contrast to muscle cells which reversibly change their length in the course of contraction and relaxation but maintain their overall morphology, platelets fundamentally and irrevocably alter their shape from non-adhesive "disks" when circulating in the bloodstream to sticky spiny "spheres" upon contact with the thrombogenic extracellular matrix. Platelet shape change is highly dependent on the rapid remodeling of the actin cytoskeleton. From this perspective, the postulated nonmuscle CAP isoform, CAP1, might be of greater functional importance to platelets than CAP2.

The results presented in this thesis provide experimental evidence for this hypothesis. Even though the flow cytometric analysis showed a selective hyperresponsiveness of CAP2-deficient platelets upon stimulation with the (hem)ITAM-specific agonists CRP and rhodocytin (**Fig. 9**), the spreading behavior of CAP2 WT and KO platelets on a fibrinogen matrix was comparable (**Fig. 10**), indicating that CAP2-deficient platelets were, overall, functionally intact. Therefore, CAP1 might represent the functionally predominant CAP isoform during platelet spreading on fibrinogen, while CAP2's role would largely be confined to the signaling pathway downstream of the surface receptors GPVI and CLEC-2. Here, CAP2 might act as a molecular brake on actin dynamics, decelerating actin remodeling in a twofold manner: first, by sequestration of G-actin from the G-/F-actin equilibrium (analogous to the role of ASP-56 in porcine platelets[51]); and second, by fragmentation of

preexisting actin filaments as shown *in vitro* by Peche *et al.*.[37] If this were indeed the case, abolition of CAP2 would disinhibit actin dynamics and consequently cause platelet hyperresponsiveness. This hypothesis should be experimentally addressed by comparing the spreading behavior of CAP2 WT and KO platelets on a collagen I or CRP matrix.

In order to finally elucidate the role of CAPs for platelet function, *Cap1* single as well as *Cap1*/*Cap2* double knockout animals need to be generated and analyzed in the future. These studies will further decipher the role of CAPs in thrombopoiesis and platelet function.

5.2 Description of an inherited macrothrombocytopenia in mice

The knowledge about the genetic and molecular pathomechanisms underlying inherited macrothrombocytopenias has vastly expanded over the recent years, particularly due to considerable advances in next-generation sequencing techniques.[87] Nevertheless, the precise genetic alterations still remain elusive in at least 40% of IMT patients.[58,63]

In the course of this thesis a subpopulation of the *Cap2*$^{gt/gt}$ and *Cap2*$^{+/+}$ mice was observed that exhibited a severe form of macrothrombocytopenia of unknown genetic origin, a trait which was preliminarily termed orphan (orph). By crossing the respective mice to C57BL/6J wild-type mice, the phenotype of orph mice could be uncoupled from the targeted *Cap2* allele. Thereby, an autosomal recessive inheritance of the severe macrothrombocytopenia was identified. Detailed studies proved that the phenotype of orph mice occurred independently of the most common targeting constructs, as no neomycin, lacZ, or Cre transgene could be found in the mutant animals.

Orph mice displayed severely reduced platelet counts in peripheral blood, an increased platelet size as well as platelet anisocytosis, evidenced by an elevated PDW (**Fig. 13**). Moreover, their red blood cell count, HCT, and Hb were also decreased (**Fig. 14** and **Fig. 15**), suggesting a general hematopoietic defect that exceeds platelet production. In the BM of orph mice, an increased presence of reticular fibers — an indication of BM fibrosis — was detected (**Fig. 17**). Additionally, orph BM MKs showed an aberrant and heterogeneous morphology, and appeared to extend abnormal, non-directed proplatelet protrusions. Signs of ectopic platelet release into the BM cavity were also observed (**Fig. 19**), suggesting that impaired platelet production, likely due to BM failure, contributes to or even accounts for the observed macrothrombocytopenia. However, since our BM analysis was performed on two-dimensional images only, we may have missed important 3D information about (pro)platelet formation in orph mice. In support of BM failure, orph mice developed splenomegaly which could reflect extramedullary hematopoiesis. Additionally, a (non-significant) trend towards higher numbers of splenic MKs in orph mice was observed (**Fig. 20**). Besides platelet production, an accelerated clearance of aberrant platelets might also contribute to the decreased numbers of circulating platelets. To test this, platelet life span as well as production after anti-GPIbα antibody-mediated platelet depletion should be assessed. In addition to platelet production, platelet function was also affected in orph mice. Remarkably, orph platelets exhibited a generalized ITAM-specific integrin activation defect (**Fig. 23** and **Fig. 24**) as well as an impaired α-granule release (**Fig. 23**). Furthermore, spreading of orph platelets on fibrinogen was dramatically delayed (**Fig. 28**), suggesting defective platelet integrin outside-in signaling or impaired cytoskeletal rearrangements. In support of the latter, the cytoskeleton of orph platelets was characterized by disorganized microtubules, numerous actin-rich nodules (**Fig. 32**), and a

massive ring-shaped accumulation of filamentous actin which may have hindered the transport of β3 integrins and talin to the leading edge during platelet activation, confining them to the platelet center (**Fig. 33**). In order to exclude impaired platelet outside-in signaling, clot retraction and aggregate formation under flow should be assessed in orph platelets.

In humans, myosin heavy chain (MYH)9-related diseases (MYH9-RDs) constitute the commonest (prevalence ≥ 1/100,000) form of IMT. MYH9-RDs are elicited by mutations in the gene *MYH9* which encodes the motor protein nonmuscle myosin heavy chain IIA (NMMHC IIA)/MYH9, an important regulator of cell locomotion, cytokinesis, and morphology.[62,80] Neutrophil granulocytes from MYH9-RD patients characteristically exhibit Döhle body-like inclusions (cytoplasmic aggregates consisting of mutant NMMHC IIA protein, MYH9 mRNA, and ribosomes), structures we could not detect in neutrophils from orph mice when studying May–Grünwald–Giemsa stained peripheral blood smears. However, since there are some technical limitations, the absence of NMMHC IIA aggregates in orph neutrophils should be confirmed by an immunofluorescence (IF) analysis.[58,63] The future examination of blood smears from orph mice with this IF technique will be of paramount importance because the demonstration that orph neutrophils lack inclusion bodies could reliably exclude an MYH9-RD etiology as the cause of the observed phenotype.[88] Moreover, since MYH9-RDs are autosomal dominantly inherited disorders,[61] it is rather unlikely that variants therein account for the macrothrombocytopenia in orph mice whose phenotype is transmitted autosomal recessively.

Mutations in the murine genes *Tubb1* or *Actn1*, encoding β1-tubulin and α-actinin 1, respectively, are also candidates for evoking the phenotype of orph mice. In mammals, the expression of β1-tubulin is limited to mature MKs and platelets. Humans with mutant β1-tubulin display aberrantly shaped MKs

with perturbed proplatelet extension and platelet release,[61] concurring with observations made in our study (**Fig. 19**). Moreover, we found the microtubules of orph platelets spreading on fibrinogen to be severely disrupted (**Fig. 32**), possibly reflecting an impaired interaction between α- and β-tubulin in tubulin heterodimers, a pathomechanism proposed by Kunishima *et al.*.[89]

α-actinin 1, on the other hand, is an important regulator of the actin cytoskeleton in MKs, stabilizing F-actin meshworks by crosslinking actin filaments into bundles.[61] In humans, mutations in α-actinin 1 lead to defective F-actin assembly followed by the disruption of the megakaryocytic actin cytoskeleton. Affected MKs extend reduced numbers of abnormally large proplatelets, resulting in macrothrombocytopenia accompanied by red blood cell anisocytosis.[90] One might speculate that the alterations of the actin cytoskeleton in orph platelets (**Fig. 32** and **Fig. 33**) might trace back to mutations in α-actinin 1. In contrast to humans, however, orph mice did not display red blood cell anisocytosis (**Fig. 16**). Besides, mutations in β1-tubulin and in α-actinin 1 are transmitted in an autosomal dominant fashion;[61] therefore, variants therein also appear rather unlikely to cause the macrothrombocytopenia in orph mice.

In humans, mutations in the genes *ABCG5* or *ABCG8* which code for ATP-binding cassette (ABC) transporters in gut and liver cause an autosomal recessive IMT termed sitosterolemia which is characterized by increased plasma sterol concentrations (including phytosterols), hemolysis, and stomatocytosis (the presence of erythrocytes with a central pale, mouth-shaped area).[58,62] Although blood smears from orph mice did not show stomatocytes (**Fig. 16**), plasma sterol levels in orph vs. WT mice should be compared in order to reliably exclude sitosterolemia in orph mice.

Gray platelet syndrome (GPS) is a predominantly autosomal recessive IMT evoked by mutations in *NBEAL2* which codes for the BEACH (beige and

Chediak–Higashi syndrome) domain-containing neurobeachin-like protein 2 (NBEAL2).[91] While GPS patients develop BM fibrosis and splenomegaly[63] in a similar fashion to orph mice, their platelets lack α-granules, a feature we did not observe in orph mice, in whom the content of α-granular proteins was unaltered (**Fig. 25**). In addition, the presence of platelet α-granules has been confirmed by TEM (**Fig. 26**). Therefore, mutations in *Nbeal2* appear unlikely to cause the phenotype of orph mice.

Growth factor-independent 1B (GFI1B) and GATA-1 are hematopoietic system-specific transcription factors whose mutation in humans causes macrothrombocytopenia. Mutations of GFI1B stall erythroid and megakaryocytic development at the bipotent erythro–megakaryocytic progenitor stage, leading to red blood cell anisopoikilocytosis (a combination of unequally sized and abnormally shaped erythrocytes), platelet α-granule deficiency, and a defective expression of several platelet-specific proteins including GPIbα, fibrinogen, and P-selectin.[61,92] In orph mice, however, none of these features could be observed: orph erythrocytes display an unaltered morphology (**Fig. 16**), the amount of fibrinogen and P-selectin (which are both stored in α-granules) is normal in orph platelets (**Fig. 25**), and orph platelets contain α-granules (**Fig. 26**), making mutations in the murine gene *Gfi1b* unlikely as the cause of the phenotype of orph mice.

Individuals affected by mutations in GATA-1, by contrast, clinically resemble orph mice to a much higher degree, since they display a mild anemia and dysplastic BM MKs. Additionally, platelet adhesion and thrombus formation on collagen are reduced in these patients.[58] On the other hand, mutations in GATA-1 lead to a reduced expression of the *GP1BA*, *GP1BB*, *GP9*, and *GP5* genes, thereby reducing the protein level as well as the functionality of the GPIb–IX–V complex,[63] a feature which we did not observe in orph mice (**Fig. 22** and **Fig. 30**).

Bernard–Soulier syndrome (BSS) is an autosomal recessive bleeding disorder originally described in 1948 by Jean Bernard and Jean Pierre Soulier.[93] Mutations in the *GP1BA*, *GP1BB*, or *GP9* genes encoding the platelet surface receptors GPIbα, GPIbβ, and GPIX, respectively, lead to quantitative or qualitative abnormalities of the GPIb–IX–V complex. Macrothrombocytopenia in BSS patients has been ascribed to perturbed proplatelet formation due to a missing link between mutant/absent GPIbα and the actin cytoskeleton via filamin A.[61] Since neither the expression level of the GPIb–IX–V complex on orph platelets (**Fig. 22**) nor their spreading behavior on vWF were altered (**Fig. 30**), a BSS etiology including the involvement of downstream effectors appears unlikely as the cause of the phenotype of orph mice.

Similarly, Glanzmann thrombasthenia (GT), an autosomal recessive platelet disorder characterized by quantitative and/or qualitative deficiencies of αIIbβ3 integrin/GPIIbIIIa on the platelet surface which abrogate fibrinogen bridging of neighboring platelets during thrombus formation, can be excluded as cause for the phenotype of orph mice. Whereas patients suffering from classic GT display a normal platelet count, volume, and morphology, monoallelic variants of GT have been described that are associated with macrothrombocytopenia. These monoallelic GT variants are elicited by mutations in the *ITGA2B* or *ITGB3* genes which encode the integrins αIIb and β3, respectively, and lead to reductions of varying degree in αIIbβ3 expression on the platelet surface.[94] Although orph platelets did not exhibit reduced αIIbβ3 expression levels (**Fig. 22**), orph mice showed some striking similarities to patients with mutations in *ITGA2B*/*ITGB3*. Jayo *et al.* have described the case of a Spanish woman with a heterozygous L718P mutation in the cytoplasmic membrane-proximal region of β3 integrin causing platelet anisocytosis and severe hemorrhages.[95] Orph mice also displayed platelet anisocytosis (**Fig. 13**); however, their tail bleeding time has not yet been assessed,

so a statement about bleeding tendency cannot be made at this point. At least, so far there is no evidence that orph mice suffer from spontaneous bleeding. While the Spanish patient described above displayed decreased platelet aggregation in response to ADP, arachidonic acid, epinephrine, and collagen, reflecting a broad platelet activation defect which comprises both GPCR- and ITAM-signaling pathways, orph mice showed an ITAM-specific integrin activation defect (**Fig. 23** and **Fig. 24**). Ristocetin-induced platelet aggregation (RIPA), by contrast, was unaltered in the Spanish woman. Ristocetin is an antibiotic from the bacterium *Amycolatopsis lurida* that mediates binding of vWF to GPIbα under static conditions.[96] In a similar fashion to RIPA, botrocetin-induced platelet spreading on vWF was normal in orph mice (**Fig. 30**). Strikingly, the Spanish patient displayed a degranulation defect with diminished surface expression of both P-selectin and CD63 upon stimulation with thrombin receptor-activating peptide (TRAP). P-selectin and CD63/granulophysin are typically stored in α-granules and lysosomes, respectively, and become exposed on the plasma membrane upon platelet activation. Of note, lysosome degranulation requires stronger stimuli than α-granule release.[19] Based on the postulated α-granule secretion defect as the responsible mechanism for the hyporesponsiveness of orph platelets (**4.2.9**), it will be exciting to elucidate whether such a degranulation defect also applies to orph lysosomes. Preliminary data obtained from a flow cytometric analysis of the surface abundance of CD63 in resting and activated platelets showed that CD63 exposure upon treatment with CRP or thrombin was reduced in orph mice compared to WT controls, pointing to a generalized degranulation defect in orph mice. A well-established signaling pathway for platelet granule secretion is initiated by ligation of GPVI with collagen (or with CRP under laboratory conditions) and subsequent activation of protein kinase (PK)C.[23] One possibility to distinguish between general secretory defects of platelets and exocytosis defects arising from impaired

signaling is to treat platelets with phorbol 12-myristate 13-acetate (PMA). PMA is a direct activator of PKC and provokes strong P-selectin exposure and GPIIbIIIa activation.[97] If orph platelets showed a normal response to PMA, the reason for the observed degranulation defect would be due to defects in the signaling pathway upstream of PKC. By contrast, if platelets failed to respond to PMA, a more general secretory defect, likely due to altered Ca^{2+} store content/mobilization, could be responsible. Further experiments such as PMA stimulation of platelets and Ca^{2+} signaling studies are required to better characterize the molecular mechanisms underlying the granule secretion defect in orph platelets. Interestingly, platelets from the Spanish patient with the heterozygous L718P mutation in the cytoplasmic membrane-proximal domain of integrin β3 described by Jayo and colleagues exhibited perturbed spreading and hampered lamellipodia formation on a fibrinogen-coated surface,[95] reminiscent of the spreading defects of orph platelets (**Fig. 28**). The bleeding diathesis in all forms of GT originates from a compromised ability (of varying degree) of αIIbβ3 to bind fibrinogen, and, consequently, a failure to establish firm platelet aggregates. Under physiological circumstances, this final step of platelet aggregation is critical for thrombus growth and stability.[94] It is tempting to assume that orph mice are able to form thrombi upon vascular injury (because of the apparently functional vWF–GPIbα interaction which is necessary for initial tethering of platelets to the exposed subendothelium), but that these thrombi are small and unstable (since the αIIbβ3–fibrinogen axis might be defective). To test this hypothesis, *in vitro* flow chamber analyses as well as *in vivo* thrombosis models and tail bleeding assays of WT vs. orph animals should be performed. While flow chamber experiments monitor platelet adhesion to collagen-bound vWF and subsequent thrombus formation under different shear conditions,[98] murine thrombosis models — by artificially inducing vessel wall injuries, e.g. mechanically (firm compression of vessels with a forceps) or chemically (injection

of ferric chloride ($FeCl_3$))[16] — allow the *in vivo* observation of (primary) hemostasis. The tail bleeding assay, finally, compares the mean duration until cessation of bleeding after cutting a small piece of distal mouse tail, thus delivering information about the integrity of the clotting cascade.[97]

Paris–Trousseau thrombocytopenia (TCPT) and Jacobsen syndrome (JBS) are two partially overlapping genetic diseases elicited by a heterozygous 11q23 deletion which includes *FLI1*, the gene encoding the homonymous transcription factor, a critical regulator of megakaryopoiesis and platelet GP expression. On the one hand, FLI1 pushes thrombopoiesis by transactivation of several genes linked to MK maturation, e.g. *MPL*, *GP9*, *GP1BA*, *ITGA2*, and *PF4*. On the other hand, FLI1 downregulates the expression of *MYH10*, the gene for nonmuscle myosin heavy chain IIB (NMMHC IIB)/MYH10. Silencing of NMMHC IIB is a critical step in MK development as it represents the molecular switch from mitosis to endomitosis and subsequent polyploidization. Consequently, loss of FLI1 causes an abnormal persistence of NMMHC IIB in MKs and hinders their transition to polyploid states, leading to an increased presence of immature, hypolobulated, and dystrophic MKs in the BM of affected individuals.[61] Exclusion of a persistent NMMHC IIB expression in orph platelets (by Western blotting) as well as the determination of the MK ploidy profile in orph mice (by fluorescence-activated cell sorting (FACS)) may represent elegant approaches to indirectly rule out mutations in the murine gene *Fli1*.

Moreover, mutations in another transcription factor, RUNX1, also lead to abrogated downregulation of *MYH10* and persistence of NMMHC IIB, triggering familial platelet disorder with predisposition to acute myeloid leukemia (FPD/AML). The thrombocytopenia in FPD/AML, however, is associated with normal-sized platelets;[61] therefore, mutations in *Runx1* are unlikely to cause the phenotype of orph mice.

Filamin A is a cytoskeletal protein that cross-links actin filaments and tethers the intracellular domain of the platelet surface receptor GPIbα to the underlying actin cytoskeleton, a pivotal mechanism for proper platelet sizing.[62] Accordingly, mutations in *FLNA* cause IMT in humans,[58] and murine filamin A-null MKs have been reported to show defective platelet biogenesis, prematurely releasing large and fragile platelets that are rapidly cleared from the circulation.[99] Interestingly, filamin A-null platelets display impaired signaling responses downstream of the (hem)ITAM receptors GPVI and CLEC-2, leading to a reduced α-granule secretion and integrin αIIbβ3 activation upon platelet stimulation,[97] similar to the defects observed in orph mice (**Fig. 23**). However, since the *FLNA*/*Flna* gene is located on chromosome X in both humans and mice, mutations therein are unlikely to account for the phenotype of orph mice.

Recently, a novel homozygous *PRKACG* mutation has been described in members of a consanguineous family which causes an autosomal recessive IMT associated with pronounced platelet activation defects such as poor GPIb–IX–V downregulation, abrogated recruitment of integrin αIIbβ3 and P-selectin to the platelet surface as well as an impaired Ca^{2+} mobilization from internal stores. *PRKACG* encodes the γ isoform of the catalytic subunit (Cγ) of cAMP-dependent protein kinase A (PKA) which phosphorylates a wide variety of target proteins in platelets, e.g. GPIbβ and filamin A. Furthermore, individuals affected by the reported homozygous c.222C>G mutation display defective proplatelet formation, a heterogeneous platelet size, an increased cAMP concentration in platelets as well as an almost absent expression of filamin A in MKs/platelets.[100] Hence, mutations in the murine catalytic subunits Cα or Cβ of PKA (mice do not express Cγ[101]) might represent potential causes of the phenotype of orph mice. Ca^{2+} measurements,

an assessment of filamin A expression by immunoblotting as well as the analysis of cAMP levels in orph platelets may shed light on this idea.

Moreover, a TEM investigation of BM MKs and the determination of platelet life span[60] will be helpful to elucidate whether the thrombocytopenia in orph mice is due to MK development/maturation defects, ectopic release of platelets into the BM, or increased peripheral clearing of platelets (e.g. in the spleen). Thereby, together with the experiments delineated above, evidence for or against the described mutations/platelet disorders can be collected. A firm "diagnosis", however, may only be established on the basis of genetic testing. Next-generation sequencing which encompasses whole-genome, whole-exome, and RNA sequencing has recently been successfully applied to discover the causative mutations in IMTs.[58,87] Preparation of appropriate DNA samples from orph mice and ensuing molecular genetic investigations will hopefully identify the mutation underlying the phenotype of orph mice.

In humans, the precise molecular origin in nearly half of all IMT cases still remains unknown.[58,63] Therefore, it is likely that the so far unrevealed mutation in orph mice and a possible human equivalent will belong to this large group of undescribed mutations. If this were indeed the case, screening of the (postulated) orph gene locus might be included in routine testing of IMTs, and IMT patients previously classified as "idiopathic" could be provided with a clearer diagnosis. In case of a human equivalent, family trees of affected individuals could be analyzed to verify the inheritance, and, based on those collected epidemiologic data, prevalence and incidence of a human orph analog may be estimated. Notably, it will be crucial to compare the responsible gene in humans and mice: where are the similarities and where are the differences? This last aspect, among others, will be essential to establish possible therapeutic approaches for the treatment of patients with variants in the orph gene.

Nowadays, the management of inherited platelet disorders encompasses preventive measures, symptomatic treatment of acute hemorrhages, pathogenetically oriented therapies (THPO mimetics), and, to a much lesser extent (due to potentially severe adverse effects), curative approaches (hematopoietic stem cell transplantation (HSCT)).

Besides patient education and enrollment in specialized centers, preventive measures in patients suffering from inherited platelet disorders include vaccination against hepatitis B, iron supplementation in cases of concomitant anemia (target hemoglobin level > 10 g/dL), avoidance of contact sports and non-steroidal antiinflammatory drugs (NSAIDs), preservation of dental hygiene to prevent gingival bleeding, and oral contraceptives in females to minimize blood loss during menstruation. Acute hemorrhages can be countered by tough compression (e.g. anterior or posterior packing in epistaxis), topical application of antifibrinolytic agents (e.g. tranexamic acid) or fibrin sealants to bleeding wounds, and intravenous administration of desmopressin, recombinant factor VIIa (rFVIIa), or platelet concentrates. Treatment of patients with THPO mimetics such as romiplostim or eltrombopag aims at stimulating thrombopoiesis via activation of the THPO receptor c-Mpl on MKs, thereby increasing peripheral platelet counts. Finally, HSCT has been performed as a curative therapy in a small number of GT, WAS, and BSS cases. However, many of these drugs/therapeutic interventions bear the risk of substantial side effects. While desmopressin and rFVIIa are linked to cardiovascular complications such as myocardial infarction and ischemic stroke, platelet transfusions can lead to alloimmunization against human leukocyte antigens (HLA) and/or platelet GPs. THPO mimetics are generally well-tolerated; nevertheless, a rebound deterioration of thrombocytopenia upon cessation of treatment as well as an increased blast formation in the BM have been reported. Last but not least, HSCT may be accompanied by severe

graft-versus-host disease (GvHD) and recurrent, potentially life-threatening infections as a consequence of immunosuppression.[102-104]

Despite recent therapeutical advances, the paucity of modern, pathophysiologically and molecularly tailored therapies in the treatment of inherited platelet disorders still persists. The feasibility of such strategies in hematology has been impressively demonstrated by the advent of tyrosine kinase inhibitors (e.g. imatinib) in the treatment of chronic myeloid leukemia (CML).[105] Hopefully, the discovery and investigation of the phenotype of orph mice as a new form of inherited macrothrombocytopenia will contribute to the understanding of both normal thrombopoiesis and its deviations in genetic platelet disorders. Elucidation of the (patho)physiological processes underlying platelet biogenesis will be vital to envision future therapeutic strategies that may one day improve the life of affected individuals.

6 Summary

Cyclase-associated protein (CAP)2 is an evolutionarily highly conserved actin-binding protein implicated in striated muscle development, carcinogenesis, and wound healing in mammals. To date, the presence as well as the putative role(s) of CAP2 in platelets, however, remain unknown. Therefore, mice constitutively lacking CAP2 (*Cap2*$^{gt/gt}$ mice) were examined for platelet function. These studies confirmed the presence of both mammalian CAP isoforms, CAP1 and CAP2, in platelets. CAP2-deficient platelets were slightly larger than WT controls and displayed increased GPIIbIIIa activation and P-selection recruitment in response to the (hem)ITAM-specific agonists collagen-related peptide and rhodocytin. However, spreading of CAP2-deficient platelets on a fibrinogen matrix was unaltered. In conclusion, the functionally redundant CAP1 isoform may compensate for the lack of CAP2 in murine platelets.

Moreover, the studies presented in this thesis unveiled a severe macrothrombocytopenia that occurred independently of the targeted *Cap2* allele and which was preliminarily termed orphan (orph). Crossing of the respective mice to C57BL/6J wild-type animals revealed an autosomal recessive inheritance. Orph mice were anemic and developed splenomegaly as well as BM fibrosis, suggesting a general hematopoietic defect. Strikingly, BM MKs of orph mice demonstrated an aberrant morphology and appeared to release platelets ectopically into the BM cavity, thus pointing to defective thrombopoiesis as cause for the low platelet counts. Orph platelets exhibited marked activation defects and spread poorly on fibrinogen. The unaltered protein content strongly suggested a defective α-granule release to account for the observed hyporesponsiveness. In addition, the cytoskeleton of orph platelets

was characterized by disorganized microtubules and accumulations of filamentous actin. However, further experiments are required to elucidate the activation defects and cytoskeletal abnormalities in orph platelets. Above all, the gene mutation responsible for the phenotype of orph mice needs to be determined by next-generation sequencing in order to shed light on the underlying genetic and mechanistic cause.

Zusammenfassung

Cyclase-associated protein 2 (CAP)2 ist ein evolutionär hoch konserviertes Aktin-bindendes Protein, welches in der Entwicklung der quergestreiften Muskulatur, der Krebsentstehung und der Wundheilung von Säugetieren eine Rolle spielt. Bis heute sind jedoch das Vorhandensein sowie die mutmaßliche(n) Funktion(en) von CAP2 in Thrombozyten unbekannt. Aus diesem Grund wurden Mäuse, denen konstitutiv CAP2 fehlt (*Cap2*$^{gt/gt}$-Mäuse), im Hinblick auf ihre Thrombozytenfunktion untersucht. Diese Untersuchungen bestätigten die Anwesenheit beider Säugetierisoforme von CAP, CAP1 und CAP2, in Thrombozyten. CAP2-defiziente Thrombozyten waren geringfügig größer als WT-Kontrollen und zeigten eine erhöhte GPIIbIIIa-Aktivierung und P-Selektin-Rekrutierung nach Stimulation durch die (hem)ITAM-spezifischen Agonisten *collagen-related peptide* und Rhodozytin. Demgegenüber verlief die Adhäsion (sog. *spreading*) CAP2-defizienter Thrombozyten auf einer Fibrinogen-Matrix unverändert. Dies legt den Schluss nahe, dass die funktionell redundante CAP1-Isoform in der Lage ist, den Mangel an CAP2 in Mäusethrombozyten zu kompensieren.

Darüber hinaus offenbarten die in dieser Dissertation präsentierten Untersuchungen eine schwere Makrothrombozytopenie, welche unabhängig von dem veränderten *Cap2*-Allel auftrat und welche vorläufig als orphan (orph) bezeichnet wurde. Das Kreuzen der entsprechenden Mäuse mit C57BL/6J-Wildtyp-Tieren enthüllte einen autosomal rezessiven Erbgang. Orph-Mäuse waren anämisch und entwickelten eine Milzvergrößerung sowie eine Knochenmarkfibrose, was einen generellen hämatopoetischen Defekt nahelegte. Bemerkenswerterweise waren Knochenmarksmegakaryozten von orph-Mäusen morphologisch auffällig und gaben allem Anschein nach Thrombozyten ektop in das Knochenmarkstroma ab, was auf eine defekte Thrombopoese als Ursache für die niedrigen Thrombozytenzahlen hindeutet. Orph-

Thrombozyten zeigten ausgesprochene Aktivierungsdefekte und adhärierten kaum auf Fibrinogen. Der unveränderte Gehalt an Proteinen lenkte den Verdacht auf eine defekte Exozytose von α-Granula als Ursache der Mindererregbarkeit. Des Weiteren war das Zytoskelett von orph-Thrombozyten durch unorganisierte Mikrotubuli und Akkumulationen von filamentösem Aktin charakterisiert. Weitere Experimente sind jedoch notwendig, um die Aktivierungsdefekte und die Zytoskelettveränderungen aufzuklären. Vor allem aber muss die Genmutation, welche für den Phänotyp der orph-Mäuse verantwortlich ist, mittels Sequenziermethoden der nächsten Generation (*next-generation sequencing*) aufgeklärt werden um Aufschluss über die zugrunde liegende genetische und mechanistische Ursache zu geben.

7 References

1. Thon J, Italiano J. Platelets: Production, Morphology and Ultrastructure. In: Gresele P, Born GVR, Patrono C, Page CP eds, Antiplatelet Agents: Springer Berlin Heidelberg; 2012:3-22
2. Long MW, Williams N, Ebbe S. Immature megakaryocytes in the mouse: physical characteristics, cell cycle status, and in vitro responsiveness to thrombopoietic stimulatory factor. Blood 1982;59(3):569-575
3. Ogawa M. Differentiation and proliferation of hematopoietic stem cells. Blood 1993;81(11):2844-2853
4. Bunting S, Widmer R, Lipari T, et al. Normal platelets and megakaryocytes are produced in vivo in the absence of thrombopoietin. Blood 1997;90(9):3423-3429
5. Bartley TD, Bogenberger J, Hunt P, et al. Identification and cloning of a megakaryocyte growth and development factor that is a ligand for the cytokine receptor Mpl. Cell 1994;77(7):1117-1124
6. Kaushansky K. The molecular mechanisms that control thrombopoiesis. J Clin Invest 2005;115(12):3339-3347
7. Zimmet J, Ravid K. Polyploidy: occurrence in nature, mechanisms, and significance for the megakaryocyte-platelet system. Exp Hematol 2000;28(1):3-16
8. Machlus KR, Italiano JE, Jr. The incredible journey: From megakaryocyte development to platelet formation. J Cell Biol 2013;201(6):785-796
9. Stegner D, vanEeuwijk JMM, Angay O, et al. Thrombopoiesis is spatially regulated by the bone marrow vasculature. Nat Commun 2017;8(1):127
10. Schachtner H, Calaminus SD, Sinclair A, et al. Megakaryocytes assemble podosomes that degrade matrix and protrude through basement membrane. Blood 2013;121(13):2542-2552
11. French DL. Megakaryocytes put a foot through the door. Blood 2013;121(13):2379-2380
12. Stritt S, Thielmann I, Dutting S, Stegner D, Nieswandt B. Phospholipase D is a central regulator of collagen I-induced cytoskeletal rearrangement and podosome formation in megakaryocytes. J Thromb Haemost 2014;12(8):1364-1371
13. Thon JN, Montalvo A, Patel-Hett S, et al. Cytoskeletal mechanics of proplatelet maturation and platelet release. J Cell Biol 2010;191(4):861-874
14. Bender M, Thon JN, Ehrlicher AJ, et al. Microtubule sliding drives proplatelet elongation and is dependent on cytoplasmic dynein. Blood 2015;125(5):860-868
15. Machlus KR, Thon JN, Italiano JE, Jr. Interpreting the developmental dance of the megakaryocyte: a review of the cellular and molecular processes mediating platelet formation. Br J Haematol 2014;165(2):227-236

16. Sachs UJ, Nieswandt B. In vivo thrombus formation in murine models. Circ Res 2007;100(7):979-991
17. Blair P, Flaumenhaft R. Platelet alpha-granules: basic biology and clinical correlates. Blood Rev 2009;23(4):177-189
18. McNicol A, Israels SJ. Platelet dense granules: structure, function and implications for haemostasis. Thromb Res 1999;95(1):1-18
19. Rumbaut RE, Thiagarajan P. Platelet-Vessel Wall Interactions in Hemostasis and Thrombosis. Colloquium Series on Integrated Systems Physiology: From Molecule to Function 2010;2(1):1-75
20. Ruiz FA, Lea CR, Oldfield E, Docampo R. Human platelet dense granules contain polyphosphate and are similar to acidocalcisomes of bacteria and unicellular eukaryotes. J Biol Chem 2004;279(43):44250-44257
21. White JG. Chapter 3 - Platelet structure. In: Michelson AD ed, Platelets (Second Edition). Burlington: Academic Press; 2007:45-73
22. Thon JN, Peters CG, Machlus KR, et al. T granules in human platelets function in TLR9 organization and signaling. J Cell Biol 2012;198(4):561-574
23. Varga-Szabo D, Pleines I, Nieswandt B. Cell adhesion mechanisms in platelets. Arterioscler Thromb Vasc Biol 2008;28(3):403-412
24. Savage B, Almus-Jacobs F, Ruggeri ZM. Specific synergy of multiple substrate-receptor interactions in platelet thrombus formation under flow. Cell 1998;94(5):657-666
25. Bearer EL, Prakash JM, Li Z. Actin dynamics in platelets. Int Rev Cytol 2002;217:137-182
26. Offermanns S. Activation of platelet function through G protein-coupled receptors. Circ Res 2006;99(12):1293-1304
27. May F, Hagedorn I, Pleines I, et al. CLEC-2 is an essential platelet-activating receptor in hemostasis and thrombosis. Blood 2009;114(16):3464-3472
28. Jackson SP. Arterial thrombosis--insidious, unpredictable and deadly. Nat Med 2011;17(11):1423-1436
29. Pollard TD, Cooper JA. Actin, a central player in cell shape and movement. Science 2009;326(5957):1208-1212
30. Erickson HP. Evolution of the cytoskeleton. Bioessays 2007;29(7):668-677
31. Fox JE. Cytoskeletal proteins and platelet signaling. Thromb Haemost 2001;86(1):198-213
32. Hubberstey AV, Mottillo EP. Cyclase-associated proteins: CAPacity for linking signal transduction and actin polymerization. FASEB J 2002;16(6):487-499
33. Paavilainen VO, Bertling E, Falck S, Lappalainen P. Regulation of cytoskeletal dynamics by actin-monomer-binding proteins. Trends Cell Biol 2004;14(7):386-394

34. Field J, Vojtek A, Ballester R, et al. Cloning and characterization of CAP, the S. cerevisiae gene encoding the 70 kd adenylyl cyclase-associated protein. Cell 1990;61(2):319-327

35. Fedor-Chaiken M, Deschenes RJ, Broach JR. SRV2, a gene required for RAS activation of adenylate cyclase in yeast. Cell 1990;61(2):329-340

36. Ono S. The role of cyclase-associated protein in regulating actin filament dynamics - more than a monomer-sequestration factor. J Cell Sci 2013;126(Pt 15):3249-3258

37. Peche VS, Holak TA, Burgute BD, et al. Ablation of cyclase-associated protein 2 (CAP2) leads to cardiomyopathy. Cell Mol Life Sci 2013;70(3):527-543

38. Chaudhry F, Breitsprecher D, Little K, et al. Srv2/cyclase-associated protein forms hexameric shurikens that directly catalyze actin filament severing by cofilin. Mol Biol Cell 2013;24(1):31-41

39. Chaudhry F, Guerin C, von Witsch M, Blanchoin L, Staiger CJ. Identification of Arabidopsis cyclase-associated protein 1 as the first nucleotide exchange factor for plant actin. Mol Biol Cell 2007;18(8):3002-3014

40. Cauwe B, Martens E, Van den Steen PE, et al. Adenylyl cyclase-associated protein-1/CAP1 as a biological target substrate of gelatinase B/MMP-9. Exp Cell Res 2008;314(15):2739-2749

41. Peche V, Shekar S, Leichter M, et al. CAP2, cyclase-associated protein 2, is a dual compartment protein. Cell Mol Life Sci 2007;64(19-20):2702-2715

42. Effendi K, Yamazaki K, Mori T, et al. Involvement of hepatocellular carcinoma biomarker, cyclase-associated protein 2 in zebrafish body development and cancer progression. Exp Cell Res 2013;319(1):35-44

43. Wang C, Zhou GL, Vedantam S, Li P, Field J. Mitochondrial shuttling of CAP1 promotes actin- and cofilin-dependent apoptosis. J Cell Sci 2008;121(Pt 17):2913-2920

44. Kosmas K, Eskandarnaz A, Khorsandi AB, et al. CAP2 is a regulator of the actin cytoskeleton and its absence changes infiltration of inflammatory cells and contraction of wounds. Eur J Cell Biol 2015;94(1):32-45

45. Shibata R, Mori T, Du W, et al. Overexpression of cyclase-associated protein 2 in multistage hepatocarcinogenesis. Clin Cancer Res 2006;12(18):5363-5368

46. Chereau D, Kerff F, Graceffa P, et al. Actin-bound structures of Wiskott-Aldrich syndrome protein (WASP)-homology domain 2 and the implications for filament assembly. Proc Natl Acad Sci U S A 2005;102(46):16644-16649

47. Czisch M, Schleicher M, Horger S, Voelter W, Holak TA. Conformation of thymosin beta 4 in water determined by NMR spectroscopy. Eur J Biochem 1993;218(2):335-344

48. Thierry-Mieg D, Thierry-Mieg J. AceView: a comprehensive cDNA-supported gene and transcripts annotation. Genome Biol 2006;7 Suppl 1:S12 11-14

49. Wolanski M, Khosrowshahian F, Jerant L, et al. Expression of CAP2 during early Xenopus embryogenesis. Int J Dev Biol 2009;53(7):1063-1067
50. Pollard TD. Rate constants for the reactions of ATP- and ADP-actin with the ends of actin filaments. J Cell Biol 1986;103(6 Pt 2):2747-2754
51. Gieselmann R, Mann K. ASP-56, a new actin sequestering protein from pig platelets with homology to CAP, an adenylate cyclase-associated protein from yeast. FEBS Lett 1992;298(2-3):149-153
52. Nurden P, Debili N, Coupry I, et al. Thrombocytopenia resulting from mutations in filamin A can be expressed as an isolated syndrome. Blood 2011;118(22):5928-5937
53. Li Z, Kim ES, Bearer EL. Arp2/3 complex is required for actin polymerization during platelet shape change. Blood 2002;99(12):4466-4474
54. Machesky LM, Gould KL. The Arp2/3 complex: a multifunctional actin organizer. Curr Opin Cell Biol 1999;11(1):117-121
55. Svitkina TM, Borisy GG. Arp2/3 complex and actin depolymerizing factor/cofilin in dendritic organization and treadmilling of actin filament array in lamellipodia. J Cell Biol 1999;145(5):1009-1026
56. Fox JE, Phillips DR. Inhibition of actin polymerization in blood platelets by cytochalasins. Nature 1981;292(5824):650-652
57. Otey CA, Pavalko FM, Burridge K. An interaction between alpha-actinin and the beta 1 integrin subunit in vitro. J Cell Biol 1990;111(2):721-729
58. Favier R, Raslova H. Progress in understanding the diagnosis and molecular genetics of macrothrombocytopenias. Br J Haematol 2015;170(5):626-639
59. Gauer RL, Braun MM. Thrombocytopenia. Am Fam Physician 2012;85(6):612-622
60. Bender M, Stritt S, Nurden P, et al. Megakaryocyte-specific Profilin1-deficiency alters microtubule stability and causes a Wiskott-Aldrich syndrome-like platelet defect. Nat Commun 2014;5:4746
61. Pecci A, Balduini CL. Lessons in platelet production from inherited thrombocytopenias. Br J Haematol 2014;165(2):179-192
62. Rabbolini DJ, Morel-Kopp MC, Stevenson W, Ward CM. Inherited macrothrombocytopenias. Semin Thromb Hemost 2014;40(7):774-784
63. Kunishima S, Saito H. Congenital macrothrombocytopenias. Blood Rev 2006;20(2):111-121
64. Nieswandt B, Bergmeier W, Rackebrandt K, Gessner JE, Zirngibl H. Identification of critical antigen-specific mechanisms in the development of immune thrombocytopenic purpura in mice. Blood 2000;96(7):2520-2527
65. Nieswandt B, Echtenacher B, Wachs FP, et al. Acute systemic reaction and lung alterations induced by an antiplatelet integrin gpIIb/IIIa antibody in mice. Blood 1999;94(2):684-693

66. Stritt S, Wolf K, Lorenz V, et al. Rap1-GTP-interacting adaptor molecule (RIAM) is dispensable for platelet integrin activation and function in mice. Blood 2015;125(2):219-222

67. Nieswandt B, Schulte V, Bergmeier W, et al. Long-term antithrombotic protection by in vivo depletion of platelet glycoprotein VI in mice. J Exp Med 2001;193(4):459-469

68. Hofmann S, Vogtle T, Bender M, Rose-John S, Nieswandt B. The SLAM family member CD84 is regulated by ADAM10 and calpain in platelets. J Thromb Haemost 2012;10(12):2581-2592

69. Bergmeier W, Schulte V, Brockhoff G, et al. Flow cytometric detection of activated mouse integrin alphaIIbbeta3 with a novel monoclonal antibody. Cytometry 2002;48(2):80-86

70. Bertling E, Hotulainen P, Mattila PK, et al. Cyclase-associated protein 1 (CAP1) promotes cofilin-induced actin dynamics in mammalian nonmuscle cells. Mol Biol Cell 2004;15(5):2324-2334

71. Stegner D, Haining EJ, Nieswandt B. Targeting glycoprotein VI and the immunoreceptor tyrosine-based activation motif signaling pathway. Arterioscler Thromb Vasc Biol 2014;34(8):1615-1620

72. Pozo AL, Godfrey EM, Bowles KM. Splenomegaly: investigation, diagnosis and management. Blood Rev 2009;23(3):105-111

73. O'Malley DP, Kim YS, Perkins SL, et al. Morphologic and immunohistochemical evaluation of splenic hematopoietic proliferations in neoplastic and benign disorders. Mod Pathol 2005;18(12):1550-1561

74. Bauer W, Rauner M, Haase M, et al. Osteomyelosclerosis, anemia and extramedullary hematopoiesis in mice lacking the transcription factor NFATc2. Haematologica 2011;96(11):1580-1588

75. Gardiner EE, Andrews RK. Platelet receptor expression and shedding: glycoprotein Ib-IX-V and glycoprotein VI. Transfus Med Rev 2014;28(2):56-60

76. Nieswandt B, Moser M, Pleines I, et al. Loss of talin1 in platelets abrogates integrin activation, platelet aggregation, and thrombus formation in vitro and in vivo. J Exp Med 2007;204(13):3113-3118

77. Gerst JE, Ferguson K, Vojtek A, Wigler M, Field J. CAP is a bifunctional component of the Saccharomyces cerevisiae adenylyl cyclase complex. Mol Cell Biol 1991;11(3):1248-1257

78. Vojtek A, Haarer B, Field J, et al. Evidence for a functional link between profilin and CAP in the yeast S. cerevisiae. Cell 1991;66(3):497-505

79. Noegel AA, Rivero F, Albrecht R, et al. Assessing the role of the ASP56/CAP homologue of Dictyostelium discoideum and the requirements for subcellular localization. J Cell Sci 1999;112 (Pt 19):3195-3203

80. Althaus K, Greinacher A. MYH9-related platelet disorders. Semin Thromb Hemost 2009;35(2):189-203

81. Ono S, Minami N, Abe H, Obinata T. Characterization of a novel cofilin isoform that is predominantly expressed in mammalian skeletal muscle. J Biol Chem 1994;269(21):15280-15286

82. Vartiainen MK, Sarkkinen EM, Matilainen T, Salminen M, Lappalainen P. Mammals have two twinfilin isoforms whose subcellular localizations and tissue distributions are differentially regulated. J Biol Chem 2003;278(36):34347-34355

83. Schafer DA, Korshunova YO, Schroer TA, Cooper JA. Differential localization and sequence analysis of capping protein beta-subunit isoforms of vertebrates. J Cell Biol 1994;127(2):453-465

84. Nomura K, Ono K, Ono S. CAS-1, a C. elegans cyclase-associated protein, is required for sarcomeric actin assembly in striated muscle. J Cell Sci 2012;125(Pt 17):4077-4089

85. Nomura K, Ono S. ATP-dependent regulation of actin monomer-filament equilibrium by cyclase-associated protein and ADF/cofilin. Biochem J 2013;453(2):249-259

86. Ottenheijm CA, Granzier H. Lifting the nebula: novel insights into skeletal muscle contractility. Physiology (Bethesda) 2010;25(5):304-310

87. Simeoni I, Stephens JC, Hu F, et al. A high-throughput sequencing test for diagnosing inherited bleeding, thrombotic, and platelet disorders. Blood 2016;127(23):2791-2803

88. Savoia A, De Rocco D, Panza E, et al. Heavy chain myosin 9-related disease (MYH9 -RD): neutrophil inclusions of myosin-9 as a pathognomonic sign of the disorder. Thromb Haemost 2010;103(4):826-832

89. Kunishima S, Kobayashi R, Itoh TJ, Hamaguchi M, Saito H. Mutation of the beta1-tubulin gene associated with congenital macrothrombocytopenia affecting microtubule assembly. Blood 2009;113(2):458-461

90. Kunishima S, Okuno Y, Yoshida K, et al. ACTN1 mutations cause congenital macrothrombocytopenia. Am J Hum Genet 2013;92(3):431-438

91. Deppermann C, Cherpokova D, Nurden P, et al. Gray platelet syndrome and defective thrombo-inflammation in Nbeal2-deficient mice. J Clin Invest 2013

92. Randrianarison-Huetz V, Laurent B, Bardet V, et al. Gfi-1B controls human erythroid and megakaryocytic differentiation by regulating TGF-beta signaling at the bipotent erythro-megakaryocytic progenitor stage. Blood 2010;115(14):2784-2795

93. Bernard J, Soulier JP. Sur une nouvelle variété de dystrophie thrombocytaire hémorragipare congénitale. Sem Hop Paris 1948;24(Spec. No.):3217-3223

94. Nurden AT, Pillois X, Fiore M, Heilig R, Nurden P. Glanzmann thrombasthenia-like syndromes associated with Macrothrombocytopenias and mutations in the genes encoding the alphaIIbbeta3 integrin. Semin Thromb Hemost 2011;37(6):698-706

95. Jayo A, Conde I, Lastres P, et al. L718P mutation in the membrane-proximal cytoplasmic tail of beta 3 promotes abnormal alpha IIb beta 3 clustering and lipid microdomain coalescence, and associates with a thrombasthenia-like phenotype. Haematologica 2010;95(7):1158-1166

96. Weiss HJ, Rogers J, Brand H. Defective ristocetin-induced platelet aggregation in von Willebrand's disease and its correction by factor VIII. J Clin Invest 1973;52(11):2697-2707

97. Falet H, Pollitt AY, Begonja AJ, et al. A novel interaction between FlnA and Syk regulates platelet ITAM-mediated receptor signaling and function. J Exp Med 2010;207(9):1967-1979

98. Ruggeri ZM, Mendolicchio GL. Adhesion mechanisms in platelet function. Circ Res 2007;100(12):1673-1685

99. Jurak Begonja A, Hoffmeister KM, Hartwig JH, Falet H. FlnA-null megakaryocytes prematurely release large and fragile platelets that circulate poorly. Blood 2011;118(8):2285-2295

100. Manchev VT, Hilpert M, Berrou E, et al. A new form of macrothrombocytopenia induced by a germ-line mutation in the PRKACG gene. Blood 2014;124(16):2554-2563

101. Kirschner LS, Yin Z, Jones GN, Mahoney E. Mouse models of altered protein kinase A signaling. Endocr Relat Cancer 2009;16(3):773-793

102. Bolton-Maggs PH, Chalmers EA, Collins PW, et al. A review of inherited platelet disorders with guidelines for their management on behalf of the UKHCDO. Br J Haematol 2006;135(5):603-633

103. Seligsohn U. Treatment of inherited platelet disorders. Haemophilia 2012;18 Suppl 4:161-165

104. Kuter DJ. Thrombopoietin and thrombopoietin mimetics in the treatment of thrombocytopenia. Annu Rev Med 2009;60:193-206

105. Stegmeier F, Warmuth M, Sellers WR, Dorsch M. Targeted cancer therapies in the twenty-first century: lessons from imatinib. Clin Pharmacol Ther 2010;87(5):543-552

Acknowledgments

First and foremost, I owe my sincere gratitude to my supervisor Prof. Dr. Bernhard Nieswandt for providing me with the opportunity to accomplish my medical doctoral (MD) thesis in his group at the Chair of Experimental Biomedicine, University Hospital Würzburg and Rudolf Virchow Center. I would like to thank Prof. Nieswandt for his critical input into the project, his extraordinary support, and encouragement. Moreover, I am heartily thankful to the members of my thesis committee, Prof. Dr. Harald Schulze and Prof. Dr. Carsten Hoffmann, for their outstanding advice and inspiration throughout all stages of my dissertation.

I am earnestly indebted to Dr. Simon Stritt for introducing me to various laboratory techniques including confocal microscopy, for his precious and critical input into my thesis, the fruitful discussions, and for proofreading of the manuscript.

Additionally, I would like to express my deep gratitude to our collaborators Prof. Dr. Angelika Noegel and Dr. Vivek Peche for generously providing the *Cap2*$^{gt/gt}$ mice, Dr. Carsten Deppermann for sharing his reticulin silver plating kit, Dr. Katrin Heinze for access to the confocal microscope at the Bio-Imaging Center and Sylvia Hengst, Birgit Midloch, and Jonas Müller for their excellent technical support in daily lab routine.

I am particularly obliged to the Faculty for Medicine and the Graduate School of Life Sciences (GSLS), Würzburg, for granting me an MD researcher stipend, for organizing the transferable skills program and the annual "Eureka!" international symposium as well as for the financial support.

Furthermore, I would like to cordially thank my friends Rabih El-Merahbi, Jonathan Trujillo, Michelle Mittnacht, and Marius Eisert for proofreading of

the manuscript and for the exceptional social support throughout the entire period of my MD project.

Finally, my honest thanks go to all current and former members of the Nieswandt lab for the inspirational, constructive, and excitatory atmosphere both at and besides work.

Publications

Profilin 1-mediated cytoskeletal rearrangements regulate integrin function in mouse platelets (Simon Stritt, Inga Birkholz, Sarah Beck, Simona Sorrentino, K. Tanuj Sapra, Julien Viaud, Johannes Heck, Frédérique Gaits-Iacovoni, Harald Schulze, Xiaoping Du, John H. Hartwig, Attila Braun, Markus Bender, Ohad Medalia and Bernhard Nieswandt; Blood Advances, Volume 2, Issue 9, 2018)

Curriculum vitae

Affidavit

I hereby confirm that my thesis entitled *Role of cyclase-associated protein 2 in platelet function and description of an inherited macrothrombocytopenia* is the result of my own work. I did not receive any help or support from commercial consultants. All sources and/or materials applied are listed and specified in the thesis.

Furthermore, I confirm that this thesis has not yet been submitted as part of another examination process neither in identical nor in similar form.

.....

Würzburg, 14 June 2018 Johannes Heck

Eidesstattliche Erklärung

Hiermit erkläre ich an Eides statt, die Dissertation *Rolle von cyclase-associated protein 2 in der Thrombozytenfunktion und Beschreibung einer erblich bedingten Makrothrombozytopenie* eigenständig, d.h. insbesondere selbstständig und ohne Hilfe eines kommerziellen Promotionsberaters angefertigt und keine anderen als die von mir angegebenen Quellen und Hilfsmittel verwendet zu haben.

Ich erkläre außerdem, dass die Dissertation weder in gleicher noch in ähnlicher Form bereits in einem anderen Prüfungsverfahren vorgelegen hat.

.....

Würzburg, 14 June 2018 Johannes Heck